The Influence of Inert Anode Material and Electrolyte Composition on the Electrochemical Production of Oxygen from Molten Oxides

by

Andrew J. Gmitter

B.S. Ceramic and Materials Engineering
Rutgers, the State University of New Jersey, 2005

Submitted to the Department of Materials Science and Engineering
in Partial Fulfillment of the Requirements for the Degree of
Master of Science in Materials Science and Engineering

at the

Massachusetts Institute of Technology

February 2008

Signature of Author: _____
Department of Materials Science and Engineering
December 18, 2007

Certified by: _____
Donald R. Sadoway
John F. Elliot Professor of Materials Chemistry
Thesis Supervisor

Accepted by: _____
Samuel M. Allen
POSCO Professor of Physical Metallurgy
Chair, Department Committee on Graduate Students

The Influence of Inert Anode Material and Electrolyte Composition on the Electrochemical Production of Oxygen from Molten Oxides

by

Andrew J. Gmitter

Submitted to the Department of Materials Science and Engineering
on December 18, 2007 in Partial Fulfillment of the
Requirements for the Degree of Master of Science in
Materials Science and Engineering

ABSTRACT

Shifts in global and political climates have led industries worldwide to search for more environmentally sound processes that are still economically viable. The steel industry is studying the feasibility of molten oxide electrolysis, a novel process by which molten iron and gaseous oxygen are the products; no carbon dioxide is produced at the site of the electrolysis cell. The research presented in this thesis focuses on the anodic reaction and the preliminary development of an inert anode, as well as investigations into the mechanism of the oxygen evolution reaction.

Various elements have been considered with the platinum group metals possessing the best combination of physical properties to serve as the inert anode. Cyclic voltammetry at 1575°C was used to compare the candidates. Iridium yielded the highest current density at a given overpotential followed by rhodium and platinum regardless of the composition of the electrolyte. Speculation as to metal oxide intermediate phases formed and mechanisms for the oxygen evolution reaction are discussed.

Notably, the basicity of the molten aluminosilicate electrolyte was found to greatly influence the rate of oxygen gas evolution as evidenced by the linear dependence of the current density on optical basicity. This is crucial for the design of a full-scale electrolysis cell as improved kinetics of the anodic reaction will yield higher throughput and/or enhanced power efficiency. Combining our finding of the relationship between current density and basicity with previous authors' contributions on the effect of partial pressure of oxygen, we argue that to a first approximation, the magnitude of the current density is governed by the concentration of free oxide ions and by the partial pressure of oxygen in the headspace above the melt.

Lastly, to, in part, address the disparate natures of the interests of steelmakers, glassmakers, geochemists, and electrochemists, the difficulties in performing electrochemical measurements at extremely high temperatures (~1600°C), and the absence of a comprehensive review of the last sixty years of work on oxygen evolution from molten silicates, this thesis is intended to serve as an essential guide for future work in this field.

Thesis Supervisor: Donald R. Sadoway
Title: John F. Elliot Professor of Materials Chemistry

BIOGRAPHICAL NOTE

Andrew J. Gmitter was born in New Jersey and grew up along the Jersey Shore. While an undergraduate student at Rutgers in the Dept. of Ceramic and Materials Engineering, he had opportunities to explore different applications of materials science. With the Energy Storage Research Group under the direction of Dr. Glenn G. Amatucci, he contributed to the processing and characterization of lithium manganese oxyfluoride spinels for enhanced cycling ability of rechargeable lithium batteries. Under the tutelage of Prof. James A. Harrington, a pioneer in the field of specialty fiber optics, Andrew worked with chalcogenide materials and hollow optical waveguides. Specifically, Andrew's senior research project concerned modeling and construction of low loss waveguides for THz radiation.

In 2005, Andrew received the Stephen Zudnak Award from the Ceramic Association of New Jersey and the Outstanding Engineering Scholar Award, acknowledging the student(s) with the highest cumulative GPA graduating from the School of Engineering. That fall at MIT, he was a teaching assistant in *3.091, Introduction to Solid State Chemistry*, where he was introduced to Prof. Donald R. Sadoway. In spring 2006, Andrew was a TA for the lab sections of *3.022, Microstructural Evolution in Materials* and *3.024 Electronic, Optical, and Magnetic Properties of Materials*. After successful completion of the written qualifying examination for doctoral studies, he began research with Prof. Sadoway who was influential in Andrew's success at MIT.

Andrew also enjoys pastimes of bowling, playing drums, and going to the beach as well as spending time with his family and friends.

PREVIOUS PUBLICATIONS

I. Plitz, A. DuPasquier, F. Badway, J. Gural, N. Pereira, A. Gmitter, and G.G. Amatucci, "The Design of Alternative Nonaqueous High Power Chemistries." *Applied Physics A-Materials Science & Processing*, **82**[4], 615-626 (2006)

J.A. Harrington, P. Pedersen, B.F. Bowden, A. Gmitter, and E. Mueller, "Hollow Cu-Coated Plastic Waveguides for the Delivery of THz Radiation." *Proceedings of SPIE-The International Society for Optical Engineering*, 5727 (Terahertz and Gigahertz Electronics and Photonics IV), 143-150 (2005)

PENDING PUBLICATIONS

D. Wang, A.J. Gmitter, and D.R. Sadoway, "An Inert Anode for the Production of Oxygen Gas by Electrochemical Decomposition of an Oxide Melt," manuscript written as of Dec. 3, 2007 for potential publication in *Nature*

ACKNOWLEDGMENTS

I thank the American Iron and Steel Institute (AISI) and the National Aeronautics and Space Administration (NASA) for their financial sponsorship.

I would like to thank each of the following individuals and groups who have aided in the completion of this thesis:

Prof. Sadoway, for giving a kid from Rutgers a shot after a rough first semester; the opportunity to work with you transformed my experiences at MIT and culminated with this thesis;

Dr. Aislinn H.C. Sirk for her careful edits and constructive criticism and for sharing her knowledge on the essentials of electrochemistry and trying to pinpoint the oxidation mechanism;

Prof. Dihua Wang, a visiting scientist from Wuhan University in China, for sharing his results with me;

Mr. Guenter Arndt, for his machining expertise and willingness to lend his tools;

Mr. Greg Meszaros (U.S. Steel) for information related to the IRSID model;

Prof. Digby D. MacDonald (Penn State) for information related to the Point Defect Model;

Mr. Mike Tarkanian, for allowing me to utilize his machine shop and teaching me about tooling;

The entire Sadoway Research Group who helped me recognize the global character of the scientific community;

Ms. Jessica L. Driscoll, with whom I spent countless hours on the phone sharing the highs and lows of my experiences at MIT, and who endured dreadfully long Greyhound trips to Boston;

And all those who came before us, upon whose shoulders we stand striving for something higher.

I dedicate this thesis to my parents, Thomas J. and Jeannette, my grandparents, Thomas V., Mathilde, and Josephine, and the rest of my family and close friends, who instilled ideals of diligence, devotion, patriotism, egalitarianism, and altruism. These values are essential for all as they lead to solutions resulting in the best outcomes for the most people.

I am glad to have had the opportunity to partake in this project as it has led me to a great deal of knowledge and insight, both professionally and personally. I have been able to contribute to something which may one day benefit mankind. It has been a privilege to attend MIT, and earning a degree from such an establishment binds me to the greatest accountability and prudence. I wish to work hard and reap the benefits of a rewarding career, and I pledge to never stray from doing what is in the best interest for society.

TABLE OF CONTENTS

LIST OF FIGURES

LIST OF TABLES

CHAPTER 1: INTRODUCTION

1.1 MOTIVATION

For every ton of pig iron produced, two tons of carbon dioxide are emitted[1]. Considering the emissions from the 858 million metric tons of pig iron generated worldwide in 2006[2], as well as some portion of coal mining activities, metallurgical coke production, and carbon monoxide and carbon dioxide emissions from the basic oxygen process, the global steel industry accounted for roughly 7 percent of the anthropogenic contribution to greenhouse gases[3].

A recent article from the American Iron and Steel Institute (AISI) reported that the US steel industry has reduced its energy usage per ton of steel shipped by approximately 28 percent since 1990 and that the industry's aggregate carbon dioxide (CO_2) emissions per ton of steel shipped was reduced by 17 percent[4]. Progress has not come easily as the industry spent over $60 billion since 1975 on new technologies to improve energy efficiency and productivity[4]. Over the past two decades, recycling of steel scrap has been a principal reason for the enhanced energy efficiency. "In addition to the economic benefits, recycling conserves energy, landfill space, and natural resources. Recovery of 1 metric ton of steel from scrap conserves an estimated 1,130 kg of iron ore, 635 kg of coal, and 54 kg of limestone[5]".

Although the American iron and steel industry has made great strides, even outperforming targets established in the Kyoto Protocol, "[it] must do more[6]." Newer, technologically advanced production methods must be made available to mitigate greenhouse gas pollution, especially abroad. Lawrence W. Kavanaugh, AISI's VP of Manufacturing and Technology, acknowledges "it will require radical approaches to future steelmaking processes to achieve the reductions in energy use[6]."

Four *breakthrough* technologies are presently sponsored by the AISI to achieve dramatic reductions in carbon dioxide emissions[7]. Two proposals rely on carbon sequestration; however this is an interim solution because it fails to prevent carbon dioxide emissions, and there are still negative impacts associated with strip mining coal to produce metallurgical coke. Two proposals rely on electrolysis, which would yield significantly greener steel assuming the electricity

required was generated from greener methods. The first operates by producing hydrogen gas from the electrolysis of water which is then used to reduce concentrated iron ore. In a final, radically different approach, iron oxide is dissolved in a molten silicate and then reduced directly by passing current through the cell. Therefore, if one were willing to invest roughly 1V for the indirect hydrogen reduction process, why not attempt to reduce the iron ***directly*** using molten oxide electrolysis?

Not only is the steel industry interested in reducing greenhouse gas emissions, but the National Aeronautics and Space Administration has considered molten oxide electrolysis for producing oxygen from lunar or Martian regolith[8-10]. Because of our moon's substantially lower gravity well, launching expeditions from it would be easier than from Earth[8]. The regolith can be a source of useful products for space exploration, including oxygen for fuel, oxygen to sustain life, structural metals, and silicon[9]. Molten oxide electrolysis would not require additional reagents from Earth and is adaptable to different oxide compositions encountered, adding to its appeal[8,9]. On Earth, molten oxide electrolysis may also be suitable for the remediation of metallurgical and chemical waste[11].

1.2 Molten Oxide Electrolysis and the Concept of an Inert Anode

Molten oxide electrolysis is not a new concept. In fact, the idea was patented in 1906 by Aiken who outlined a continuous process for making iron metal by passing current through a molten bath of metal oxides more electropositive than iron[12]. It has not been until recent years that it has gained traction, notably by the efforts of Sadoway and as witnessed by sponsorship from AISI, NASA, the U.S. Army via Universal Technical Research Services (UTRS), and Companhia Vale do Rio Doce (CVRD). At the cathode, iron ions would be reduced to liquid iron metal, and at the anode, oxygen gas would be produced if, and only if, the anode was inert; Aiken's patent recommended carbon for the anode which would have yielded carbon dioxide. Due to the difference in densities of the liquid metal and molten oxides, the cell would become stratified. A schematic of an electrolysis cell is depicted in Fig. 1.1[13].

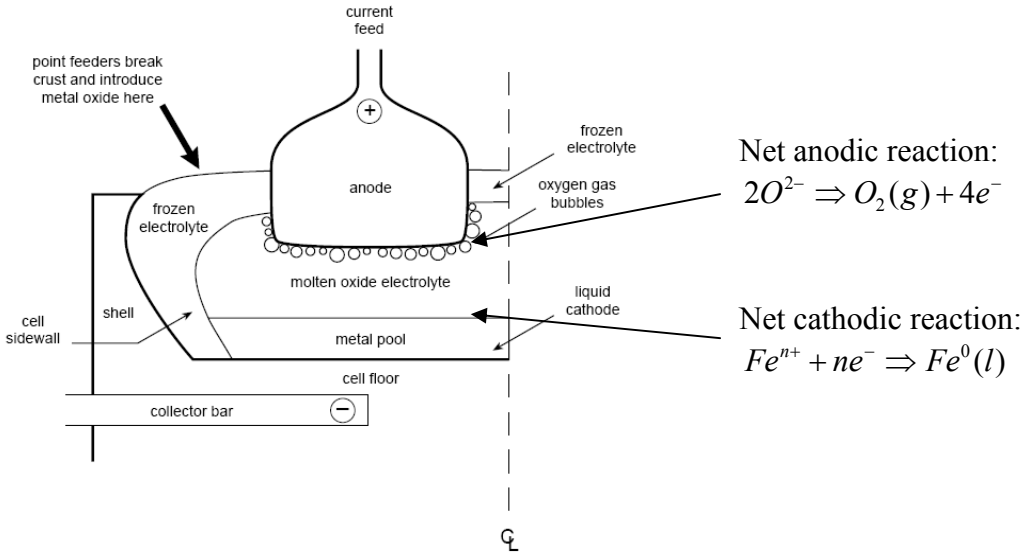

Figure 1.1 Electrolysis cell with primary reactions. Adapted from [13].

Development of such a cell poses many materials related challenges, especially when identifying a suitable anode. The anode should be inert to avoid costly maintenance shutdowns, preserve the optimal interelectrode spacing for power efficiency, and provide good returns on capital expenditures. Adapting several qualities key for inert anodes for aluminum electrowinning[14], and adding several parameters applicable to a molten oxide electrolysis system, such an anode must satisfy the following stringent requirements:

a) Operate at extremely high temperatures in excess of 1575°C
b) Possess high electronic conductivity
c) Resist corrosion / have low solubility in the molten silicate electrolyte
d) Withstand attack from oxygen
e) Intermediate phases must not be soluble nor electronically insulating
f) Exhibit low volatility of metal and metal oxides
g) As a corollary to (c) and (e), soluble phases must not contaminate the cathode product
h) Withstand anodic polarization without becoming oxidized
i) Possess sufficient wettability for intimate interfacial contact with electrolyte
j) Have robust mechanical properties including resistance to thermal shock and creep
k) Be simply manufactured and deployed
l) Not be cost prohibitive.

Further explanation for selecting candidate anodes is provided in 2.4 MATERIALS SELECTION.

Engineering an inert anode was not the primary focus of this thesis, but the results of the experiments are important considerations for future implementation and optimization of the anode and electrolysis cell. The main contributions of the research were the following:

- electrochemical experiments were designed that enabled discernment of features of different anode materials and different electrolytes
- a material was identified with superior properties for the inert anode
- altering the electrolyte composition affected the rate of oxygen evolution, i.e., a higher current density was achieved at a higher basicity
- a first approximation of the functionality of current density and basicity was made.

The following sections provide background information about electrochemistry in molten silicates with particular emphasis on anodic polarization and the Butler-Volmer equation. Afterwards, the concept of basicity of silicate melts is discussed and the chapters of the thesis are enumerated.

1.3 SURVEY OF ELECTROCHEMICAL MEASUREMENTS IN MOLTEN SILICATES

Depending on technologies available and the scope of their research, scientists have used many different electrochemical techniques to extract information on the thermodynamics, kinetics, and mechanism of a given reaction. Several fields of study relevant to molten silicates are summarized, but the main focus as it pertains to this thesis is 1.3.3 ANODIC REACTIONS. Bard and Faulkner[15] have provided an excellent overview of a variety of electrochemical techniques, albeit generally in room temperature aqueous solutions, and they have included many pertinent references.

1.3.1 Corrosion

The corrosion of metals and intermetallics for use as electrodes and bubblers for glass melting applications has been studied by monitoring corrosion potentials and polarization resistances[16-20]. Carton[16] et al analyzed the corrosion of pure chromium in borosilicates and found that above 1160°C, the chromium depassivated unless the glass was enriched with oxidizers. They also witnessed CrB formation. DiMartino[17,18] et al studied chromium and chromium superalloys and recommended anodically polarizing the metal to develop a coherent Cr_2O_3 film. Littner[19] et al investigated ruthenium additions to molybdenum disilicide and determined Ru did not improve the corrosion resistance of $MoSi_2$ despite Ru-rich compound formation at the surface. Interestingly, Sundaram and Speyer[20] polarized their Mo and $MoSi_2$ electrodes at +1V and -1V against open circuit potential, very high potentials considering corrosion tests are usually performed near open circuit. Mo performed poorly under anodic polarization due to formation of incoherent MoO_2, and $MoSi_2$ performed worse under cathodic polarization.

1.3.2 Redox Reactions

Multivalent elements are important in the manufacturing of glass. Redox constituents impose constraints on the refractories that can be used to contain the melt; they affect fining times, fining temperatures, and volatile losses; and they also determine optical, electrical, magnetic, and thermal properties of the melt and solidified glass[21,22]. The ability to monitor their behavior *in-situ* is desirable as it quickly provides information about the melt and resulting glass[23]. Thus, redox equilibria have been the focus of many electrochemical studies[21-32]. Redox equilibria are important to the molten oxide electrolysis cell because multivalent species such as ferrous and ferric ions may permit electronic conductivity via semiconduction or polaron hopping[33], resulting in decreased efficiency if the current was able to short across the cell. Additionally, higher valence cations would require more electrons for reduction to the metallic state.

Many electrochemical techniques have been utilized to probe the behavior of multivalent ions in molten silicates including, but not limited to, chronopotentiometry[27,34,35],

chronoamperometry[24], linear sweep voltammetry[29] (LSV), cyclic voltammetry[25-27,34,36] (CV), AC voltammetry[34] (ACV), normal pulse voltammetry[30,31] (NPV), differential pulse voltammetry[34] (DPV), square-wave voltammetry [21-23, 25-28,32,34,36,37] (SWV), and impedance spectroscopy[28]. Authors have used these methods primarily to extract information regarding redox equilibria[21-25,27,28,30,32] and diffusion coefficients[21,24,26,29,34-38].

SWV may be the best technique available because of its sensitivity when compared with other voltammetric techniques and short runtimes when compared with pulse methods[25,34]. [Consult Osteryoung and O'Dea[39] for a detailed description of the theory of SWV and relevant equations.] Data extracted from SWV is also quite versatile. LaFage and Taxil[27] were able to distinguish the half-wave potentials for Fe^{3+}/Fe^{2+} and Fe^{2+}/Fe^{0}. DeStrycker, Westbroek, and Temmerman[25] constructed a calibration plot of peak current vs. concentration for dilute concentrations of cobalt oxide. Additionally, they calculated the number of electrons transferred in the reduction of Co^{n+}. These were not possible using CV. Standard free enthalpies were obtained by Russel and Sprachmann[34].

There have been other notable contributions and unique experiments that did not utilize SWV. DeStrycker[24] et al performed chronoamperometry using a platinum rotating disc electrode in melts containing 10% Fe_2O_3 and found that the Levich equation was useful. Using impedance spectroscopy and modeling the results with equivalent circuits, Schirmer and Russel[28] concluded simple electron transfer for Fe^{3+}/Fe^{2+} that was controlled by diffusion. Vondrak[36] et al reported the double layer capacity on Pt at 900°C. Tilquin, Glibert, and Claes[31] delved into the merits of pulse techniques in order to avoid dc distortion factors; however, they concluded pulse techniques were time consuming when compared to voltammetric techniques. Takahashi and Miura[29] calculated equilibrium constants, *K*, for mutual interactions of various metal cations, e.g. $Fe^{2+} + Ce^{4+} \Leftrightarrow Fe^{3+} + Ce^{3+}$.

It is also worth mentioning that electrochemical techniques used in molten silicates can be extended to studies in molten borates. Morita, Yamashita, and Maekawa[40] studied the effect of electrolyte composition on Cr^{6+}/Cr^{3+} ratios. Suzumura, Kawamura, and Yokokawa[41]

performed CV in borate systems of varying basicity and developed an analogue to the Pourbaix diagram.

There are overarching trends when considering redox equilibria in molten silicates. Increasing the temperature causes a shift in the reduction potential to less negative values[22], and the electrolyte composition alters the redox ratio[23,30].

1.3.3 Anodic Reactions

1.3.3.1 Formation of Molecular Oxygen

Unlike the richness of the literature concerning redox reactions of metal cations, systematic studies under conditions of anodic polarization are sparse. What little information collected has been quite speculative with respect to the mechanism of oxygen evolution and the hypotheses have been incompatible. Much of the difficulty in elucidating the mechanism stems from the fact that the reactants are hosted in a solution, interact at an electrolyte/solid anode interface, and the products eventually leave the system as a gas. Since various phases are involved, simplistic schemes such as "diffusion of reduced species in a condensed phase/charge transfer/diffusion of oxidized species in the same condensed phase" cannot easily be applied. Adsorption, desorption, intermediate species, nucleation, and coalescence of gas bubbles must all be considered, resulting in complex, multi-step reaction schemes. Furthermore, running experiments at extremely high temperatures under controlled atmospheres precludes direct observation, and utilizing *in-situ* spectroscopy/microscopy techniques is extremely challenging.

The primary reaction at the anode involves the transfer of electrons from an anionic species and results in the formation of oxygen molecules. Ultimately, depending on the current density in controlled current techniques (or the applied overpotential in controlled potential techniques), oxygen would dissolve into the silicate or bubbles would evolve from the anode[42].

The identity of the anionic reactant species varied. In one of the earliest electrochemical studies in liquid silicates, Bockris, Kitchener, and Davies[43] speculated that gaseous oxygen was generated by the discharge of silicate polyanions. If they would have been able to separate the

cell into two compartments, the anolyte would have been richer in silica, and they believed they would have been able to determine the identity of the polyanion. It should be noted that regardless of their perceived difficulties, they did not consider a melt comprised of a distribution of silicate groups. Table 1.1 is adapted from [43] and lists the anion discharge reactions.

Table 1.1 Anion Discharge Reactions as Proposed by Bockris, Kitchener, and Davies[43]

ion type	equation	g equiv. O_2/Faraday	Mole SiO_2/Faraday
free oxygen ion	$O^{2-} \xrightarrow{-2e} \frac{1}{2}O_2$	1	-
orthosilicate	$SiO_4^{4-} \xrightarrow{-4e} SiO_2 + O_2$	1	$\frac{1}{4}$
pyrosilicate	$Si_2O_7^{6-} \xrightarrow{-6e} 2SiO_2 + \frac{2}{3}O_2$	1	$\frac{1}{3}$
rings/infinite chains	$(SiO_3)_n^{6n-} \xrightarrow{-2ne} nSiO_2 + \frac{n}{2}O_2$	1	$\frac{1}{2}$
chains	$(Si_4O_{11})_n^{6n-} \xrightarrow{-6ne} 4nSiO_2 + \frac{3n}{2}O_2$	1	$\frac{2}{3}$
sheets	$(Si_2O_5)_n^{2n-} \xrightarrow{-2ne} 2nSiO_2 + \frac{n}{2}O_2$	1	1

It was later suggested by Ghosh and King[42] in melts less basic than the orthosilicate composition, a polymerization reaction would occur locally to the surface of the anode such as

$$2SiO_4^{4-} \Rightarrow Si_2O_7^{6-} + O^{2-}. \quad (1a)$$

More generally, the chemical reaction might resemble[44]

$$2(Si_nO_{3n+1})^{-2n-2} \Rightarrow (Si_{2n}O_{6n+1})^{-4n-2} + O^{2-}. \quad (1b)$$

In moderately modified melts, orthosilicate units would combine to yield a pyrosilicate unit and a free oxide ion; the latter would then react at the anode[42,45]. One argument against this mechanism contended that since the mass transport of polymerized silicate units away from the electrolyte/electrode interface would be too slow, the anode would become enveloped in a passivating silica-rich layer over time, which was not observed[45].

Another mechanism is one in which the free oxide ion diffuses from the bulk to the anode and is consumed[45]. By the LeChatelier principle, the equilibrium concentration of free oxide ions would be maintained in the bulk electrolyte. This point of view was assumed in this work with more information related to free oxide ions presented in 1.5 BASICITY OF SILICATES.

There are many proposed schemes for the mechanisms of mass and charge transfer leading to the formation of molecular oxygen, some of which are discussed here in chronological order.

After reaction (1), Ghosh and King[42] presumed the following steps at 1350°C:

$O^{2-}(melt) \Rightarrow O(ads) + 2e^{-}$

$2O(ads) \Rightarrow O_2(g)$.

They also attempted to determine the rate determining step from Tafel slopes; however they were linear only at high current densities. The finer points of desorption and coalescence were not discussed. They attributed the rate determining step at low current densities to mass transfer, but at high current densities, they proposed passivation of the anode as a contributory factor.

Emi, Sakuraya, and Sanbongi[46] were interested in oxygen ion transfer in relation to steelmaking. Utilizing potential step methods, they suggested two possibilities for the rate determining step of oxygen evolution from 1200 to 1600°C, both involving two electrons.

$2O^{2-} \Rightarrow O_2^{2-} + 2e^{-}$ or $O_2^{2-} \Rightarrow 2O + 2e^{-}$

Note that while although not explicitly stated, the rate determining step should involve a *single* electron transfer[47]. The most noteworthy contributions of their work regarded exchange current densities and an estimation for the transfer coefficient around 0.5. [Consult Bockris, Reddy, and Galboa-Aldeco[47] for a thorough explanation of the Tafel slope, exchange current, and transfer coefficient. See also 1.4 A FUNDAMENTAL ELECTROCHEMICAL EQUATION.]

At low current densities at 1350°C, Suito and Ohtani[48] postulated a reaction sequence as follows:

$O^{2-}(melt) \Rightarrow O(ads) + 2e^{-}$

$O(ads) \Rightarrow O(melt)$

They did not witness either oxygen evolution or formation of an oxide film. Using galvanostatic methods, their potential-time curves yielded oxygen diffusivities. Their claim of monoatomic oxygen diffusing into the slag without further reaction was unusual as it is not expected that monoatomic oxygen would be stable.

In a lower range of temperatures from 900 to 1000°C, Maric, Brungs, and Skyllas-Kazacos[44] concluded that the mass transport of free oxide ions was rate limiting. CVs indicated a scan rate to the ½ power dependence of the peak current. They also proposed an oxidation mechanism that involved the formation of a thin surface film of platinum oxide followed by decomposition to yield oxygen.

$$2[Pt + O^{2-}(melt) \Rightarrow (Pt - O) + 2e^{-}]$$

$$2(Pt - O) \Rightarrow 2Pt + O_2(g)$$

It was also suggested that the thin surface film could undergo other reactions with the free oxide ions, resulting in the formation of a distinct platinum oxide phase and/or a return to platinum base metal accompanied with electron transfer.

$$(Pt - O) + O^{2-}(melt) \Rightarrow PtO_2 + 2e^{-}$$

and/or

$$(Pt - O) + O^{2-}(melt) \Rightarrow Pt + O_2(g) + 2e^{-}$$

Tilquin, Glibert, and Claes[45] studied binary sodium silicates at 1000°C. As in [44] their CVs indicated scan rate dependence of the peak current, and they concluded the diffusion of free oxide ions to be rate limiting. They believed the number of electrons transferred during the rate determining step was 2. Once again, this has not been shown for a well characterized system. They also witnessed a small peak prior to the main anodic peak in solutions richer in sodium oxide which they attributed to peroxide formation. Their primary process occurring in all melts was the following:

$$O^{2-}(melt) \Rightarrow O(ads) + 2e^{-}$$

$$O(ads) \Rightarrow O(melt)$$

$$2O(melt) \Rightarrow O_2(g)$$

In basic melts, concomitantly, peroxide ions were subsequently oxidized to yield molecular oxygen directly.

$$O^{2-}(ads) + O^{2-}(melt) \Rightarrow O_2^{2-}(ads) + 2e^{-}$$

$$O_2^{2-}(ads) \Rightarrow O_2(g) + 2e^{-}$$

It was remarkable that they did not expect any adsorption in acidic melts and that they believed in both desorption of monoatomic oxygen to combine in the bulk and direct transformation of peroxide to diatomic oxygen.

1.3.3.2 Reduction of Molecular Oxygen to Oxide Ions

To more firmly establish reaction mechanisms and rate determining steps using Tafel slopes, it is desirable to investigate the reverse reaction[47]. Only one reference discussed it. Kawakami and Goto[49] applied small potentials on a Pt electrode to reduce oxygen of varying partial pressures. Working in binary melts containing no transition metals, they found that physically dissolved diatomic oxygen was reduced.

$$\tfrac{1}{2}O_2(melt) + 2e^- \Rightarrow O^{2-}(melt)$$

1.3.3.3 Platinum Oxide Formation

When considering the generation of oxygen and/or the reaction of free oxide ions at elevated temperatures on metal surfaces, formation of passive or intermediate oxide films must not be neglected. As with evolution of molecular oxygen, there has been speculation from only a few authors. Further complicating the matter is the thermodynamic instability of platinum oxides at elevated temperatures[50]. Higgins performed a variety of studies on platinum electrodes under alternating current conditions[51], in different oxides including silicates, borates, and phosphates[52,53], and over a range of temperatures[51,53,54]. His oscillograms suggested that double layer charging occurred first, followed by formation of a monolayer of PtO_2, and finally, oxygen evolution[52,54]. Notably, oxide film formation was suspected at low current densities and high temperatures, but never at high current densities[54]. Higgins also found that the charge passed for oxygen evolution was independent of changes of current density but dependent on reactions occurring on the anode prior to oxygen evolution[53].

Maric, Brungs, and Skyllas-Kazacos[44] believed formation of platinum oxide was a necessary preliminary step for evolution of gaseous oxygen, and $O_2(g)$ was the byproduct of platinum oxide decomposition. The film thickness was related to its formation/decomposition rate. They

believed their relationship of i_p vs. $v^{1/2}$ was governed by mass transfer of free oxide ions and not due to passivation.

Miura and Takahashi[55] performed anodic tests at 900°C to very high switching potentials to 5V. At roughly 1V vs. the Pt quasi-reference electrode, they obtained significant peaks on nickel, cobalt, and chromium electrodes and found that passivation indeed occurred to produce a thin film of roughly 100% coverage of the electrode. Perhaps a similar analysis can be performed on CVs recorded by Maric, Brungs, and Skyllas-Kazacos[44] to confirm oxide film formation on platinum. Rather than a diffusion-limited peak for the mass transport of free oxide ions, perhaps they witnessed passivation of platinum.

In complete contrast, Tilquin, Glibert, and Claes[45] disputed the formation of any platinum-oxide phases during electrolysis. They witnessed no colloidal platinum near the anode, nor any black deposit on their working electrode.

1.3.3.4 Parasitic Anode Reactions

Since the molten oxide cell will contain transition metal oxides, particularly iron oxide, there is a possibility of oxidizing ferrous ions to ferric ions at the anode, thus resulting in less oxygen generation and a lower current efficiency[10,56]. A similar concern was raised by Maric, Brungs, and Skyllas-Kazacos[44], but originated from a different reaction. Rather than directly oxidize ferrous iron to ferric iron in its own electrochemical process, they believed that at low current densities, the oxygen generated on the anode would be chemically soluble into the molten silicate, promoting oxidation of Fe^{2+} to Fe^{3+}. In either case, the current efficiency for the electrolysis cell would be lower.

As was presented in 1.3.3 Anodic Reactions, the literature review has yielded a variety of possible mechanisms, rate determining steps, and kinetic parameters for anodic polarization experiments outlined in the literature. The proposed mechanisms are often contradictory, and due to difficulties in observing and controlling reactions in challenging experimental conditions, quite speculative. None of the schemes are supported by enough evidence to be conclusive, but

they do provide a useful starting point for discussion. While the primary focus was on the electrode material and electrolyte composition, it was partially the aim of this study to more firmly explain the mechanisms of oxygen evolution and describe how platinum group metal oxides behave on polarized anodes.

1.4 A Fundamental Electrochemical Equation

When mass transfer is not limiting the current, or when the applied current is low such that the concentration of the electroactive species near the anode is similar to the bulk, the Butler-Volmer equation is valid[15]. Charge transfer is rate limiting, and in potential sweep methods, the scan rate has no influence on the current generated. In its most general form for multistep reactions in which electron transfer may be occurring in steps other than the rate determining step, the Butler-Volmer equation is written as

$$i = i_0\left(e^{\alpha_f F\eta/RT} - e^{-\alpha_b F\eta/RT}\right)$$

where i is the current in A, i_0 is the exchange current in A, α is the transfer coefficient [no units], F is Faraday's constant, η is the overpotential in V, R is the universal gas constant in J/mol·K, and T is the temperature on the Kelvin scale[47]. The subscripts f and b denote the forward and back reactions, with forward being anodic throughout this thesis.

$$2O^{2-} \xrightarrow{f} O_2 + 4e^-$$

$$2O^{2-} \xleftarrow[b]{} O_2 + 4e^-$$

A positive value for η will be used to describe the overpotential for an anodic reaction. Thus, at high anodic overpotentials, the net current is positive.

The exchange current density, i_0, has been further defined by Bard and Faulkner[15] as

$$i_0 = FAk^0 C_R^{*\alpha_f} C_O^{*\alpha_b}$$

where F is the Faraday, A is the area of the electrolyte/electrode interface in cm^2, k^0 is the intrinsic rate constant in cm/s, C^* is the bulk concentration of species R and O in mol/cm^3, and α has the same definition as above. R and O denote the reduced and oxidized species respectively. From unpublished results generated in our laboratory, the anodic process was limiting the performance of the molten oxide electrolysis cell. This was concluded from the very sharp

increase of cathodic current when a very small negative overpotential was applied vs. the large overpotential required to obtain a small increase in anodic current. Considering the nature of depositing a metal ion from a liquid silicate into a pool of liquid metal vs. the nature of nucleating a new gaseous phase at the electrolyte/anode interface, this claim made intuitive sense.

There are several approaches to increase the rate of a heterogeneous reaction. Raising the temperature promotes faster diffusion and populates higher energy levels. Increasing the surface area, increasing the concentration of reactants (as long as adsorption and desorption are not rate limiting), and introducing a more effective catalyst are possibilities. Presented with the above equations for electrode kinetics, what parameters can be altered to enhance *i*, the current? Altering *T* would influence the magnitude of the exponential function, but this would be trivial because the cell temperature is proposed to be beyond the melting point of iron (m.p. 1538°C). Increasing the overpotential increases the reaction rate as long as charge transfer is rate limiting, but doing so is undesirable because then power consumption is increased. **Increasing the concentration of the anionic species, which is believed to be the free oxide ion, is the next obvious choice. Despite such an elementary proposal, it has never been considered in the literature!** Furthermore, different electrode materials have different intrinsic rate constants. In addition to comparing the currents generated in different electrolytes, the currents generated on different electrodes would also be investigated.

The validity of these arguments rests on the following assumptions:

- The overpotential is dominated by an activation process, i.e, the concentration overpotential is negligible
- The concentration of the free oxide ion at the outer Helmholtz plane is equal to the bulk concentration of the free oxide ion
- Mass transport of the free oxide ion is not rate limiting at 1575°C because diffusion is rapid, and the convection occurring as result of bubbling gaseous oxygen leads to a very thin double layer

- There is an abundance of reaction sites available on the anode, e.g., the electrode does not become blocked by O_2 gas.

If the hypothesis that increasing the concentration of the free oxide ion to increase the current is correct, there are important implications for power efficiency and throughput. But first, the free oxide concentration must be quantified and a scale must be chosen for comparing different electrolytes.

1.5 Basicity of Silicates[†]

1.5.1 Basicity and the Free Oxide Ion

Various indices have been used to express the basicity of molten oxides[57]. Basicity is a term carried over from the way metal oxides reacted with water. Network modifiers such as CaO and Na_2O formed alkaline solutions, network formers such as SiO_2 and B_2O_3 formed acids, and intermediates were amphoteric. Early workers drew analogies to these behaviors while trying to explain the dissociation of network anions to yield O^{2-} ions[58]. Higher values for basicity were interpreted to correspond with higher concentrations of O^{2-} ions.

The indices for basicity for steelmaking have been loosely tied to empirical observations and qualitatively indicate the presence of free oxide ions. Relating the free oxide concentration to thermodynamic parameters has been difficult because defining the activity of the O^{2-} ion in oxide melts cannot be measured directly. Relationships have been drawn from the solubility of CO_2 or emf values of Na_2O in a Na_2O-SiO_2 melt with respect to pure liquid Na_2O. However, the carbonate capacity may have varied when transition metal oxides were present, and Na_2O was not at dilute concentration. Thus the validity of these techniques is questionable[59].

One of the first theoretical models for molten systems was proposed by Temkin. When an oxide compound dissolves in a molten salt, it often completely dissociates with ideal mixing of the cationic and anionic lattices preserved. However, unlike molten halides, silicates are structurally

[†] For those unfamiliar with the structure of silicates, books by Richardson, Turkdogan, Mysen, Mysen & Richet, and Waseda & Toguri are recommended.

complex, and ideal mixing is rarely encountered in multi-component, network-forming systems. Extending Temkin's model to silicates is expected to be valid only at dilute concentrations in very highly modified melts, and is therefore not a suitable model for the majority of silicate systems[60].

Toop and Samis considered the distribution of oxygen as bridging (O^0), non-bridging (O^-), and free ions (O^{2-}), and considered the following equilibrium condition:

$O^0 + O^{2-} \Leftrightarrow 2O^-$.

The equilibrium constant was defined as[60]

$$K_{TS} = \frac{(a_{O^-})^2}{(a_{O^0})(a_{O^{2-}})}.$$

In the scenario in which the silicate network was fairly basic, i.e., the bridging oxygen activity was approximately constant, and the mixing was ideal so that mole fractions could replace the activities, the free oxide ion concentration would have a parabolic dependence on the non-bridging oxygen concentration. However, this case would not be applicable to acidic melts, and ideal mixing may not be a reasonable assumption. Kapoor and Frohberg improved the model by Toop and Samis but a discrepancy was still apparent[59].

Modern technology has enabled computation as another source for estimating the free oxide concentration. Using statistical mechanical considerations, the IRSID model gave the same trend as the model of Toop and Samis[61].

Spectroscopy has also been utilized to determine the concentration of free oxide ions. X-ray Photoelectron Spectroscopy a.k.a. Electron Spectroscopy of Chemical Analysis (XPS or ESCA) relies on differences in the binding energies of the different forms of oxygen. In the PbO-SiO_2 system, the proportion of the free oxide ion was roughly parabolic with increasing the PbO mole fraction[59]. In CaO-SiO_2 and CaO-Al_2O_3 melts which are relevant to the behavior in steel-making slags, Park and Rhee[62] monitored the free oxide proportion, and it too was roughly parabolic with increasing the mole fraction of CaO. In binary systems, the free oxide proportion has been proven to vary parabolically with increasing the concentration of network modifiers. But does the free oxide concentration depend on the particular network modifier present? How

would the free oxide ion concentration vary in ternary and higher order systems? And, does a scale or basicity indicator exist that gives the proportionality of the free oxide ion across multiple electrolyte compositions?

1.5.2 Optical Basicity

Of all the scales considered, the optical basicity offered the best one with regard to these questions. The model provided an estimate for the extent of negative charge borne by oxygen atoms, thus giving a global measure of the concentrations of bridging, non-bridging, and free oxide ions[57,58]. The optical basicity has been correlated with the refractive index, viscosity, and redox equilibria of transition metal oxides in glasses[63].

In steelmaking, the exchange of sulfur from the metal to the slag is often written as

$$\tfrac{1}{2}S_2(metal) + O^{2-}(melt) \Leftrightarrow \tfrac{1}{2}O_2(gas) + S^{2-}(melt),$$

with the equilibrium constant

$$K = \sqrt{\frac{f_{O_2}}{f_{S_2}}}\left(\frac{a_{S^{2-}}}{a_{O^{2-}}}\right).$$

As previously mentioned, there is not a thermodynamic definition for the activity of single ions. To circumvent this problem, the optical basicity scale was used and the sulfide capacity was shown to be correlated in 130 different compositions of binary, ternary, and quaternary mixtures containing CaO, MgO, Al_2O_3, and SiO_2[64].

The optical basicity of individual metal oxides was determined by monitoring the ultraviolet frequency shift that occurred when a tracer ion such as Tl^+, Pb^{2+}, or Bi^{3+} was introduced. The probe ion became coordinated by O^{2-} ions, and the extent of negative charge they received was dependent on the polarization of the oxygen ions. The frequency shift in the $^1S_0 \rightarrow {}^3P_1$ transition of the $d^{10}s^2$ probe ion corresponded to the electron donating ability of different oxides; hence a scale was created with acidic oxides having low electron donating ability and basic oxides having high electron donating ability. CaO was defined as 1.00[63].

Table 1.2. Optical Basicity Measured from Frequency Shifts[63]

Oxide	Optical Basicity	Oxide	Optical Basicity
Cs_2O	1.7	MnO	1.0
K_2O	1.4	ZnO	0.95
BaO	1.15	MgO	0.78
Na_2O	1.15	Al_2O_3	0.60
SrO	1.1	SiO_2	0.48
CaO	1.00	B_2O_3	0.42
FeO	1.0	P_2O_5	0.33
Li_2O	1.0		

An attribute of this scale is that the optical basicity values of individual metal oxides can be used to calculate the optical basicity of a mixture by simple addition. In the following equation, x_i is the mole fraction, n_i represents the number of oxygen atoms in the constituent oxide (2 for SiO_2, 3 for Al_2O_3), and Λ_i is the optical basicity of the constituent oxide[57].

$$\Lambda_{melt} = \frac{\sum_i x_i n_i \Lambda_i}{\sum_i x_i n_i}$$

Except for several alkali borates where Tl^+ generated two maxima in the frequency shift, this equation worked very well[58]. Predicted and measured values matched closely, an excellent measure of the robustness of this scale.

There has been some debate as to the values of Λ for individual oxides. Duffy and Ingram have been able to show the strong relationship of optical basicity and Pauling's electronegativity for glass forming oxides[58]. However, this treatment fell short when dealing with transition metal oxides, particularly when considering sulfide or phosphorous capacities of slags[57]. Nakamura has used Sanderson's equation for average electron density, $D = \alpha z / d^3$, where α is a parameter specific to a respective anion, z is the charge of the cation, and d is the cation-anion distance. This approach was extended to fluorides and chlorides[59]. As seen in Table 1.3, Nakamura's values are consistent with those listed above, but they are more compactly distributed.

Table 1.3. Nakamura's Optical Basicity Scale[59]

Oxide	Optical Basicity	Oxide	Optical Basicity
Cs_2O	1.18	ZnO	0.91
Rb_2O	1.17	CuO	0.89
K_2O	1.16	Sb_2O_3	0.84
Na_2O	1.11	Cr_2O_3	0.77
BaO	1.08	As_2O_3	0.72
Li_2O	1.06	Fe_2O_3	0.72
SrO	1.04	Al_2O_3	0.66
CaO	1.00	TiO_2	0.65
MnO	0.95	GeO_2	0.58
FeO	0.94	SiO_2	0.47
CoO	0.93	B_2O_3	0.42
Bi_2O_3	0.92	CO_2	0.40
MgO	0.92	P_2O_5	0.38
NiO	0.92	SO_3	0.29

Lastly, Mills has pointed out that when aluminum oxide is incorporated into the melt, cations are required to provide charge balance. He proposed that the metal oxide with the highest optical basicity would provide the charge balance, and the mole fraction used for this purpose should be subtracted from the calculation of Λ_{melt}[57].

Despite some of these issues, the optical basicity scale offered the best scale for this research. Unless otherwise noted, the values listed in Table 1.2 were those used to calculate Λ_{melt}, the optical basicity of the electrolyte.

1.6 SUMMARY

In this chapter, molten oxide electrolysis has been proposed as a breakthrough technology that may dramatically reduce greenhouse emissions from steelmaking. One of the challenges rests in the development of an inert anode suitable for the extremely harsh operating conditions. In trying to understand the underlying mechanism of oxygen evolution, it was revealed that what little literature existed showed no clear consensus on even the basics of the reaction mechanisms. By analyzing some of the parameters in the Butler-Volmer equation, a hypothesis was proposed in which increasing the basicity, i.e. the concentration of O^{2-}, of the electrolyte should enhance

the oxygen evolution rate at the anode. The primary outcome of this thesis is centered on this hypothesis. Lastly, the optical basicity scale was chosen because of its ability to take a mixture of constituent oxides and give the proportion of free oxide ions in a melt.

It was also the aim of this introductory chapter to provide the silicate specialist with some background on electrochemical techniques and the electrochemist with information regarding the nature of molten silicates. Both fields are vital for overcoming the challenges posed by developing the molten oxide electrolysis cell, but they are highly specialized and divergent. Thus, it may be possible that the small amount of literature on the topic of anodic polarization in molten silicates suffers from inaccuracies in interpretation and experimentation because the requisite knowledge base was not present. Conversely, electrochemists have identified reaction schemes that do not make intuitive sense to the silicate scientist.

Additionally, molten silicate science is compartmentalized into steelmaking, glassmaking, geochemistry, and even welding. These areas within the broader scope of molten silicates have different concerns and often disparate points of view because of the completely different natures of their end-products. This further complicates the matter of identifying suitable information because there are so many fields in which to search for references. A principal review for anodic polarization has not been composed until now, and never before has anyone proposed the free oxide ion concentration as a key parameter governing the value of the maximum sustainable current density at the anode.

CHAPTER 2 will discuss the design of the experiments, highlighting compensation resistance, furnace tube construction, materials selection, electrolyte selection, and current density measurements.

CHAPTER 3 describes the details of running the experiments, particularly the powder preparation, electrode construction, and electrochemical techniques.

CHAPTER 4 provides the results and discussion of cyclic voltammetry of different candidate anode materials and attempts to identify phases formed under anodic polarization.

CHAPTER 5 lies at the heart of the hypothesis, relating current density and optical basicity into a convenient engineering scale. Kinetic parameters, mainly the transfer coefficients, α_f and α_b, are proposed to be 0.5, and iridium is proposed as the candidate anode for future studies. The current density and overpotential relationships are discussed in context to power efficiency of the molten oxide electrolysis cell.

CHAPTER 6 lists a number of questions that should be considered if and when others research the feasibility of steelmaking from molten oxide electrolysis.

CHAPTER 7 is the conclusion of this thesis.

APPENDIX A lists the products and suppliers used to construct the furnace cap.

APPENDIX B provides a spreadsheet of roughly 40 additional compositions considered as electrolytes for this study and lists the phase diagram, liquidus temperature, mole percents of constituent oxides, and optical basicity of an array of eutectic liquids relevant to molten oxide electrolysis.

CHAPTER 2: EXPERIMENTAL DESIGN

2.1 PRUDENT ELECTROCHEMICAL PRACTICES IN MOLTEN OXIDES

As highlighted in 1.3.2 REDOX REACTIONS, square wave voltammetry is a superior technique because of its speed and sensitivity. Attempts to use SWV were unsuccessful; however, cyclic voltammetry was suitable and still provided many details in a reasonable experimental duration.

CV operates in a three electrode configuration by applying a potential on the working electrode vs. a reference electrode as a triangular waveform and monitoring the current response. The scan rate can be adjusted, and depending on the nature of the electrochemical reactions, it can indicate the reversibility of a reaction and/or give an approximation for the charging current. The current measured is comprised of two parts,

$$i_{net} = i_F + i_c$$

where the Faradaic current, i_F, is generated by charge transfer during an electrochemical reaction, and the charging current, i_c, is caused by the capacitance of the double layer, C_{dl} in Farads/cm^2. The absolute magnitude of the charging current is given as

$$|i_c| = AC_{dl}\nu .$$

A represents the surface area of the electrode, and v is the scan rate in V/s. At least some charging current is always present in CV because the potential is being continuously changed. Furthermore, the ratio of the peak current to the charging current can be shown to be directly proportional to C_{dl} and $\nu^{1/2}$, inversely proportional the concentration of the reactant, and a complex function of T because of the dependence on $\left(T/e^{-1/T}\right)^{1/2}$. These parameters must be considered when identifying peak heights in silicates, systems in which C_{dl} and T are inherently high. But more importantly, the scan rate must be slow enough and concentration of electroactive species high enough so that the current measured, i_{net}, is almost entirely due to the Faradaic current[15].

Another consideration is the uncompensated resistance, R_u, which is the resistance between the working and reference electrodes. This is a function of the resistivity of the electrolyte and

separation distance of the working and reference electrodes. R_u is important because the real applied potential at the working electrode is

$E_{WE} = E - i_{net}R_u$.

E_{WE} is the potential actually applied at the working electrode, and E is the potential applied assuming no solution resistance or contact resistance[15]. When i_{net} and R_u are very small, the latter term becomes trivial; however, in molten oxide systems, the resistance of the electrolyte can be very large. Despite the importance of *iR* compensation, almost none of the articles listed in 1.3 SURVEY OF ELECTROCHEMICAL MEASUREMENTS IN MOLTEN SILICATES mention if data was acquired utilizing it. Even a small current of 10mA passed through a cell in which R_u was 10Ω, would shift the peak potential by 0.1V. Many papers have hundreds of mA of current which can shift peak potentials by tenths of volts and change peak shapes.

Using the work of Semkow and Haskin[65] as a case study, the importance of v and R_u become clear. They were attempting to extract information about the amount of dissolved oxygen and free oxide ions in diopsidic melts at 1450°C. They stated their uncompensated resistance was $>10^{11}\Omega$, a value so large, it was uncertain that a device was capable of measuring it. (For example, a modern Fluke model 1550B ohmmeter requires 5000VDC to measure $10^{12}\Omega$[66].) They also speculated that the concentrations of oxygen and free oxide ions were very low. Conservatively assigning a value for C_{dl} at 150μF/cm^2 [46] and using a scan rate of 20V/s, i_c/A became 3mA/cm^2, which was roughly 10% of the peak height. More importantly, their very high scan rates were coupled with no *iR* compensation. At higher scan rates, large values of R_u tend to flatten out the wave and shift the reduction peak to more negative values, trends witnessed in the article written by Semkow and Haskin. Quoting Bard and Faulkner[15], "Uncompensated resistance can thus have the insidious effect of mimicking the response found with heterogeneous kinetic limitations." Despite their very rigorous and thoughtful analysis of the results obtained, the conclusions of the article by Semkow and Haskin[65] were unconvincing because their experiment did not measure what it set out to.

Electrochemical reversibility was another concept that was applied to systems in which it was not truly applicable[44]. In electrochemically reversible or Nernstian systems, a subtle change of electrode potential shifts the equilibrium at the surface of the electrode instantaneously. Also,

the charge transfer resistance is exceedingly small. For the condition of semi-infinite linear diffusion in a Nernstian system, the Randles-Sevčik equation is valid[15],

$$i_p = 0.4463\left(\frac{F^3}{RT}\right)^{1/2} n^{3/2} A D^{1/2} C^* \nu^{1/2}.$$

Maric, Brungs, and Skyllas-Kazacos used this equation to obtain the product of $C^* D^{1/2}$; however an overpotential needed to be applied, thus violating the Nernstian condition. Furthermore, electrochemical reversibility requires that the position of i_p be independent of scan rate, a condition not met in their work.

For irreversible systems, the mathematical treatments become arduous. Bard and Faulkner[15] give a case for total irreversibility, which may not be a bad approximation with oxygen evolution as the gaseous product is fugitive. It can be shown that the peak current in this situation is

$$i_p = 0.4958\left(\frac{\alpha F^3}{RT}\right)^{1/2} A D^{1/2} C^* \nu^{1/2}.$$

This equation must be modified for the number of electrons transferred. i_p has an additional dependence on the transfer coefficient and a different proportionality constant. Furthermore, i_p is also a function of $\nu^{1/2}$ in this scenario, so **simply plotting i_p vs. $\nu^{1/2}$ is not a diagnostic for "electrochemical" reversibility.**

It is important to use electrochemical techniques and equations that are applicable to the system under study and take into consideration the effects of high temperature, solution resistance, and double layer charging. The work conducted in this thesis rarely used scan rates greater than 0.250V/s and always utilized *iR* compensation techniques.

Researchers performing high temperature measurements must also be cognizant of temperature gradients and the usage of dissimilar lead wires contacting their electrodes. For example, if a digital multimeter was connected between two electrodes, the voltage measured may be a consequence of the electric field established by the temperature gradient from the hot zone to the cool end of the furnace. When dissimilar metals are used, thermoelectric voltages are set up and they can be substantial. To be accurate, one should measure the voltage of the short circuited electrode couple as a function of temperature over the temperature range of the experiment.

2.2 Temperature Profile within the Furnace

Regardless of the quality of the insulation surrounding the furnace and the positioning of the electrodes, a temperature profile should always be mapped. The hot zone of the furnace should be uniform in temperature to diminish convection. The electrolyte should be quiescent such that mass transport is due to diffusion down a chemical potential gradient, or else many of the electrochemical techniques and equations must be reconsidered. Convection is unavoidable in experiments that evolve gases, and while the vertical temperature profile may be uniform, convection due to external heating may be possible. These latter effects were not expected to profoundly influence the results.

At elevated temperatures, the dominant heat loss mechanism is radiative. This can be witnessed by the glow of the furnace tube and warmth sensed without physically contacting the furnace. To combat this type of loss, it is often desirable to construct a baffle to suspend within the furnace tube and reflect the radiation back toward the hot zone. However, including a baffle inside a furnace tube that would have an assortment of electrodes inserted and removed would have incorporated additional engineering challenges and was not pursued in these experiments.

The temperature profile also provides the difference between the actual temperature inside the furnace tube and the setpoint thermocouple outside the furnace tube. In molten silicates, it is difficult to place a thermocouple directly into the melt because the encapsulation material will degrade in the electrolyte. A refractory ceramic will be soluble in the electrolyte or suffer from interdiffusivity issues that arise from an abundance of iron oxide in the melt. Thus, rather than measure the temperature of the molten silicate directly, a correction must be made with the setpoint thermocouple. In this work, temperature profiles made using a custom built 36" Type B thermocouple revealed a uniform zone (±5°C) of roughly 3 inches; the setpoint was 1675°C to achieve a temperature of 1575°C within the hot zone.

For the specific consideration of electrochemistry in molten silicates, the difference between the setpoint and actual temperatures is of prime importance because the experiments are performed blindly and one cannot directly observe the molten silicate. One must be certain the contents of

the crucible have become a homogenous melt; 50°C could mean the difference between a two phase region and a homogenous liquid. Since temperature is a key parameter in many equations including i_p, Tafel slopes, diffusivity, etc., accurate and consistent control of the furnace conditions are paramount.

2.3 Furnace Tube and Cap Construction[†]

It was necessary to maintain a stable atmosphere, and it was desirable that the depths of the electrodes were adjustable. Unlike a system that was going to operate at 1000°C in which steel or nickel alloys such as Inconel could be used, a ceramic furnace tube was necessary for temperatures approaching 1600°C in oxidizing atmospheres. Only three materials are commonly distributed, namely mullite, alumina, and zirconia. Mullite is not recommended above 1600°C, and zirconia is cost prohibitive, leaving alumina. Unlike metals, ceramics have wide manufacturing tolerances when the diameter of the tube approaches 3 inches because slip-casting techniques have to be employed. McDanel Ceramics lists their tolerance at ±5%, which on 5" is ¼"! And, unless expensive finishing techniques such as centerless grinding are employed on the fired body, it is rare for a tube to be perfectly cylindrical.

These inconsistencies posed a problem for creating a seal. At the time of seal and cap construction, the lifetime of the furnace tube was unknown, and based on the results from a fellow group member who ran his furnace at 1725°C, it was not expected to last more than 5 or 6 runs. Rather than machine a complex cap that may not have been able to be used with different alumina tubes, off-the-shelf components were used from MDC Vacuum Products. A -425 silicone O-ring was used as a filler between the 4.5"OD tube and a 5"ID vacuum flange. (The author concedes this was not the best engineering practice, but the tube did not exhibit significant leaks as a very slow bubbling rate of argon through the inlet bubbler was matched by the outlet bubbler at room temperature and 1575°C.) Even with a water-cooled cap, a silicone O-ring was used because of its high temperature stability and ease of availability. While silicone does have higher oxygen permeability than most O-ring materials, molybdenum revealed hardly any oxidation after exposure above 1000°C for nearly 24 hours. Perhaps PTFE or Viton® could be

[†] For a list of products used, manufacturers, and materials, consult Appendix A.

used in place of silicone if oxygen permeability is a concern. Or, in a more elaborate design, it may be possible to use a double O-ring seal.

On top of the furnace tube, a copper gasket was inserted between knife-edge seats between the flange and the cap, also from MDC Vacuum Products. The cap was a blank flange of stainless steel that was machined on the inside to mate to the copper gasket. Through holes were milled around the outside to fasten the flanges on the tube with 5/16" – 24 hex head bolts.

The height of the electrodes had to be adjustable, and it was desirable for the cap to be useful for an array of electrode configurations. Furthermore, the crucible containing the molten silicate limited the spacing of the electrodes. Thus, any fittings used to hold the electrodes would need to have small clearances. A very nice solution was found by using Swagelok Ultra-Torr fittings that were bored-through. One side could be tightened, locking a Viton® O-ring onto the ceramic tube used to shroud the electrodes. The other side was threaded NPT-¼". Once the cap was tapped to accommodate NPT-¼" threads, the fittings were used with various electrodes, and residual holes were plugged with hollow hex plugs. The Ultra-Torr fittings could accommodate ¼" or ⅜" ceramic tubes. A schematic for the furnace cap is illustrated in Fig. 2.1.

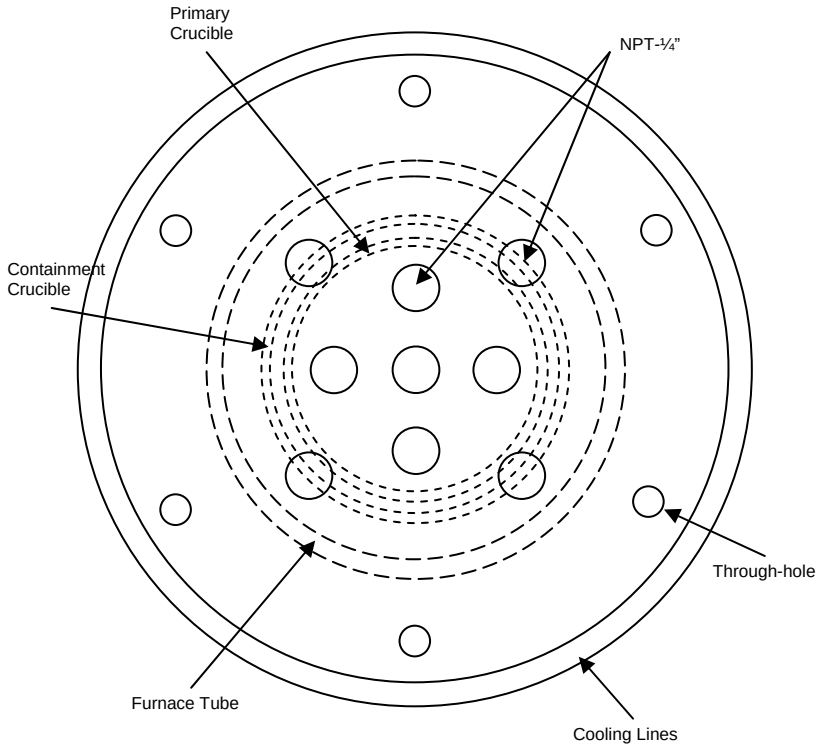

Figure 2.1 Top view of the cap. The center NPT – ¼" holes were used for inserting electrodes and the outer NPT – ¼" holes were used for the gas inlet and outlet.

At the bottom of the alumina furnace tube, alumina bubbles were used to provide a level surface for the crucibles. An outer "containment" crucible was placed dead center and filled with ¾" to 1" of alumina bubbles. The containment crucible was used in case of leakage of the electrolyte from the primary crucible. The "primary" crucible containing the molten silicate was placed within the containment crucible, also dead center and level. More about the crucible materials is described in 2.4 MATERIALS SELECTION. Figure 2.2 is a schematic of the assembled configuration. Maintaining level and centered positions for the whole assembly was essential because any natural convection occurring within the melt would be radially symmetric, the electrode positions would be radially symmetric and the working electrodes would be equidistant from the reference electrode, and the electrodes would not contact the crucible wall upon insertion.

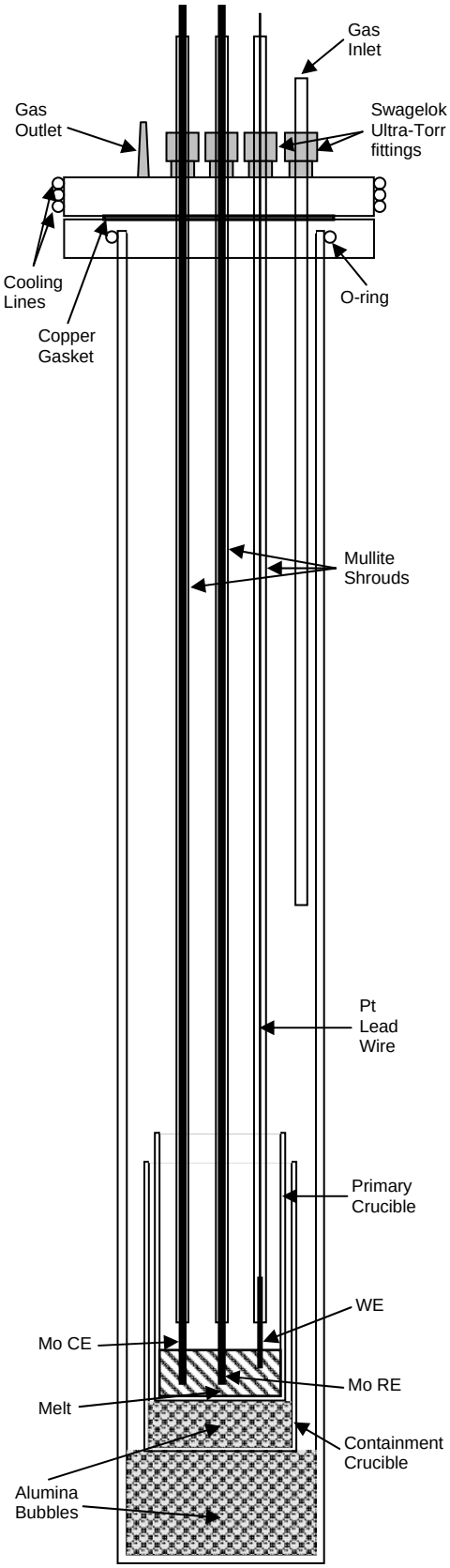

Figure 2.2 Profile of the furnace tube assembly (approximately to scale).

2.4 Materials Selection

2.4.1 Working Electrode/Anode

The exceedingly high operating temperatures for the molten oxide electrolysis cell constrain the choices for an inert anode material. Any host for alloying would have to be a platinum group or a refractory metal. Ceramics may also be considered for their high temperature stability, and since they possess electronic and/or ionic conduction mechanisms which are activated processes, their conductivities may be sufficient. However, even the most refractory ceramics would be soluble to a certain extent in a molten silicate.

2.4.1.1 Metals

The advantages of metal inert anodes as opposed to ones developed from ceramics or cermets guided the author to consider them for study. Advantages include typically higher electrical conductivities, improved fracture toughness and thermal shock resistance, elimination of porosity issues, and relative ease of fabrication into complex shapes either through casting or powder metallurgy[67]. It is known from the glass industry that platinum group metals have exceptional corrosion resistance in silicate melts; however, this does not preclude the possibility that under anodic polarization and oxygen evolution, corrosion, solubility, and volatility may become issues[68,69].

The platinum group metals are ruthenium, rhodium, palladium, osmium, iridium, and platinum. Osmium and ruthenium have high volatilities at the operating temperatures under oxidizing conditions[70]. Palladium has a melting point only several degrees higher than iron. Thus, the only platinum group metals to test are rhodium, platinum, and iridium. Only if the corrosion rates were extremely low would these be suitable as pure metal anodes. Perhaps their cost could be lowered by alloying, yet enough of the bulk property of the platinum group metal could be retained for good corrosion resistance and electrode activity.

The refractory metals are niobium, tantalum, molybdenum, tungsten, and rhenium. They have the highest melting points and lowest metal volatility. However, they are readily degraded by

oxygen at moderately high temperatures; as examples, molybdenum would catastrophically fail by MoO_3 vaporization, and rhenium would form Re_2O_7 which boils at 393°C[71]. Despite good high temperature mechanical properties and much lower costs than the platinum group metals, the refractory metals would not be suitable for anodes in molten oxide electrolysis. Under inert gases, refractory metals would be useful as electrodes in the experimental cell.

2.4.1.2 CERAMICS

Ceramics are not typically recognized for their ability to conduct electricity, and with few exceptions, they are vulnerable to thermal shock and creep at elevated temperatures. Upon first glance, ceramic materials may not be of much interest; however, their refractory properties to withstand corrosive environments stand out. If a refractory material possessed a low electrical resistivity, it may be a suitable candidate for the anode. Furthermore, ceramics are predominantly metal oxides and the anode environment will oxidize the majority of metals, carbides, and borides[72]. It would be desirable for a material to not be oxidized to higher metal valences, not dissolve into the electrolyte, and not form an electronically insulating film.

The majority of refractory materials utilized in the basic oxygen furnace and electric arc furnace are based on magnesia bonded with pitch or blended with chromia[73]. These withstand basic slags and iron, but have minimal electrical conductivity. From the glass industry, the refractory materials that are the most resistant to corrosion include Cr_2O_3, SnO_2, and ZrO_2[74]. Each of these materials possesses a different conduction mechanism: p-type semiconduction, n-type semiconduction, and ionic conduction, respectively. Interestingly, Arrhenius behavior is often associated with these mechanisms; therefore the extremely high temperatures should enhance the conductivity. It should be noted that the partial pressure of oxygen, traces of impurities, and/or dopants of different valence alter the mode of semiconduction in oxides[75]. Smyth[75] gives a fairly extensive description of various defect chemistries. Conductivity is also influenced by grain size, secondary phases residing on the grain boundaries, and formation of liquid phases[76,77].

Cr_2O_3 is highly corrosion resistant, serving in fiberglass making, one of the most severe glass melting operations[73,74,78]. Like most ceramics, it suffers from poor thermal shock resistance[78]. Despite its corrosion resistance, it is undesirable for many glassmaking applications as dissolved chromium ions impart deep color[72,74,78]. However, this is irrelevant to molten oxide electrolysis, and chromium may impart enhanced qualities to the cathode product for stainless steel. Cr_2O_3 does have some tendency for volatilization above the melt line, but compared with all other glass furnace refractories, dense Cr_2O_3 has the best conductivity aside from SnO_2[78]. Additionally, Cr_2O_3 exhibits p-type semiconduction, which is favored by oxidizable cations in atmospheres with high partial pressures of oxygen at high temperatures[75].

SnO_2 possesses very high corrosion resistance and has the lowest resistivity of all glass furnace refractories[78]. From 1000°C to 1400°C, the resistivity is only between 0.0025 and 0.0045Ωcm[79]. However it is limited by its expense, poor thermal shock resistance, and volatility and reduction above 1500°C, and it is never used outside glass contact[78]. The current density is also performance limiting so that a large cross sectional area is necessary in glass melting applications[74,78]. SnO_2 may seem like a good choice for a candidate anode because of its good electrical conductivity; however, dissolution of tin and deposition in the cathode product may prove to be highly detrimental to the iron or steel. Tin cannot be tolerated above 0.05%[80]. In fact, tramp elements including tin and copper accrue over time and cannot be removed from steel. They are merely diluted by addition of virgin iron into charges of scrap high in residual elements[80].

ZrO_2 suffers from poor thermal shock resistance unless stabilized by CaO, MgO, or Y_2O_3[72]. Refractories containing zirconium oxides are not resistant to slags containing iron or manganese oxides. Also, while ZrO_2 performs well in acidic slags, basic slags react strongly with it[77]. Despite being an oxygen ion conductor, the high concentration of iron oxide and the basic nature of the slag in the molten oxide electrolysis cell would degrade a ZrO_2 anode quickly.

Ceramics offer refractoriness and possibly sufficient conductivity at elevated temperatures, but the difficulty of manufacturing ceramic electrodes and lack of a supplier on the lab scale

excluded them from this study. The author merely wanted to highlight some of their properties which may be helpful for future development of ceramic inert anodes. This study was restricted to platinum group metals; owing to its high melting point, rhenium was also included for initial comparisons.

2.4.2 Counter Electrode/Cathode

The counter electrode (which operated primarily as a cathode) utilized in these studies was molybdenum. Mo offered good stability in the silicate when no transition metal oxides were present, but it was necessary to run the experiments under flowing argon to prevent oxidation of the metal above the surface of the melt. Other refractory metals may have been suitable for contact with the molten silicate, also necessitating an inert atmosphere. Platinum group metals are costly, and their alloys and intermetallics with iron and silicon would have had melting temperatures below 1575°C.

2.4.3 Reference Electrode

The reference electrode is critical for controlled potential techniques because it establishes a benchmark value of potential against which all measurements of potential difference are based. A reference electrode should possess a known potential that approaches ideal nonpolarizability, meaning the passage of current through the cell should not affect the potential of the reference electrode[15]. Also, the contents of the reference electrode must not contaminate or be contaminated by the contents of the bulk electrolyte. Typically a reference electrode is isolated from the bulk electrolyte either through an ionically conducting membrane or a sintered frit.

Outside of room temperature aqueous (and some organic) systems, a true reference electrode is difficult to construct or implement. In these situations, a quasi-reference or pseudo-reference electrode is utilized. A quasi-reference electrode is typically a metal wire that is immersed into the electrolyte under the assumption that the bulk solution remains constant. Although the potential is unknown unless standardized by comparison to a true reference electrode, the potential remains fixed[15].

In molten silicates, depending on the contents of the melt, a true reference electrode is very difficult to implement. The glass industry has used yttria stabilized zirconia as an oxygen ion conductor between a platinum electrode in a reference gas with defined oxygen partial pressure and the molten glass. These electrodes were found to suffer from short lifetimes because of the thin zirconia membrane[58]. Additionally, in slags rich in iron oxide, zirconia would likely be degraded[77].

Alternative reference electrodes have been pursued to overcome the disadvantages of zirconia reference electrodes. It was observed that molybdenum used as heating electrodes in electric glass melters provided extremely constant potentials caused by the equilibrium of the metal with one of its metal oxides. Suitable metals and metal oxides would require high melting points, low solubilities into the electrolyte, and formation of dense, thin, coherent layers of metal oxide. Examples included $Mo|MoO_2$, $W|WO_2$, and $Ta|Ta_2O_5$[58]. A German patent highlighted some of the theory behind the $Mo|MoO_2$ reference electrode[81].

For simplicity of construction and because it was already being used as the counter electrode, molybdenum was chosen as a reference electrode. This was not before a failed attempt to construct a true reference based on aluminum metal in contact with aluminum oxide in solution was made. If the system could have been successfully constructed, it would have been made with the following guidelines. Liquid aluminum metal at 1575°C would have had a density less than $2.7 g/cm^3$ and possessed a low vapor pressure. It would have floated atop a ternary eutectic mixture of $SrO\text{-}CaO\text{-}Al_2O_3$ with the SrO and CaO not being reduced aluminothermically. The aluminum would have contacted either carbon or tungsten which would have served as the current lead. The assembly would have been contained within a high purity boron nitride sheath. A small hole would have been drilled and packed with boron nitride frit to connect the reference electrolyte with the bulk electrolyte. It may have been a good concept, but implementation was almost impossible due to differential thermal expansions of the reference electrolyte and boron nitride. Additionally, the boron nitride was not easily wetted by the bulk electrolyte, and it would have only been useful at low partial pressures of oxygen due to oxidation of BN.

Oxygen reference electrodes have been theoretically conceptualized for possible usage with steelmaking slags. In previous investigations, the oxygen reference electrode utilized a metal/metal oxide mixture contained within a zirconia tube. The metal/metal oxide would equilibrate, defining p_{O_2} of the reference; however, it was argued that the equilibrium was ill-defined because oxygen transfer through the zirconia and the exchange of the redox reaction of ferrous and ferric ions may not be equilibrated in the duration of monitoring the slag. To combat this, it was suggested that a Ta|Ta_2O_5 or a Ti-Mo|TiO_2 reference be in direct contact with the slag[82]. Thus, from theoretical considerations coupled with the ease of construction, availability, and cost of molybdenum rods, Mo|MoO_2 provided the best choice for the reference electrode.

A Mo|MoO_2 electrode was also ideally suited for studying the oxygen evolution reaction in melts of varying basicity. The potential difference between the reference electrode and an anodically polarized working electrode would be constant. Two equilibria can be expressed as follows:

RE: $Mo + 2O^{2-} \Leftrightarrow MoO_2 + 4e^-$

WE: $2O^{2-} \Leftrightarrow O_2(g) + 4e^-$

The Nernst equation for each of these reactions is then

RE: $E = E_0' - \frac{RT}{4F} \ln \frac{a_{Mo} a_{O^{2-}}^2}{a_{MoO_2}}$

WE: $E = E_0' - \frac{RT}{4F} \ln \frac{a_{O^{2-}}^2}{f_{O_2}}$

The activity of a condensed phase is 1, and since pure gaseous oxygen bubbles are being produced locally on the anode, f_{O_2} can be approximated as 1. This behavior is analogous to the reversible hydrogen electrode in aqueous solutions of varying pH[83].

2.4.4 CRUCIBLE

Selection of a proper crucible material was important so that the molten silicate would be contained for the duration of experiment. The melt should not be contaminated by the degradation of the crucible or else electroactive species would interact or the basicity of the

electrolyte would be altered. In an oxidizing environment and at temperatures approaching 1600°C, only a handful of crucible materials can be considered.

Platinum group metals were out of question because the vertical crucible furnace would not allow for the silicate to be easily poured out while molten. Additionally, iron oxide in the slag or liquid metals functioning as the cathode would have attacked these crucibles.

Molybdenum and tungsten were not as costly as platinum group metals, but they were still expensive. Their usage would have required deposition of silicides to prevent oxidation during oxygen evolution. Mo would also have exchanged with iron ions in melts applicable for electrolysis.

Graphite posed difficulties because oxygen evolution would have resulted in carbon dioxide formation. Contamination of the electrolyte with carbonate ions was a possibility, and it may have carbothermically reduced iron, thus casting doubt on the efficacy of the electrolysis process.

Ceramics certainly avoided problems of oxidation; however, dissolution into the slag was possible. Zirconia would have been degraded by iron oxide slags[77]. Magnesia was not widely available, and a conversation with Ozark Technical Ceramics revealed that MgO crucibles may be liquid phase sintered, limiting their useful temperature range to only 1150°C. Alumina in the presence of molten silicates containing MgO and CaO could produce intermediate layers of hercynitic spinel or $CaAl_{12}O_{19}$[84]. Furthermore, with an electrolyte containing roughly 15 to 20wt% Al_2O_3, alumina crucible dissolution would be reduced[85]. Thus, alumina, a widely available crucible material that is relatively economical when compared with the other single-use candidates, was chosen for this study.

2.5 Electrolyte Selection

Aiken[12] astutely pointed out that the metal oxides in the electrolyte must be more electropositive than iron. The standard free energy of formation is directly related to the

standard potential of an electrochemical reaction via the Nernst equation. Assuming activities will not contribute too greatly to the applied potential at which metal oxide will be separated to metal and oxygen gas, any metal oxides lying below iron oxide will reside in the melt so long as sufficient iron ions are available for reduction. Any metals less electropositive than iron will deposit at the cathode. The Ellingham diagram (Fig. 2.3) illustrates this concept. While potassium oxide and sodium oxide would have aided in lowering the melting temperature of the electrolyte and enhancing the ionic conductivity, they could not serve as fluxing agents in this system.

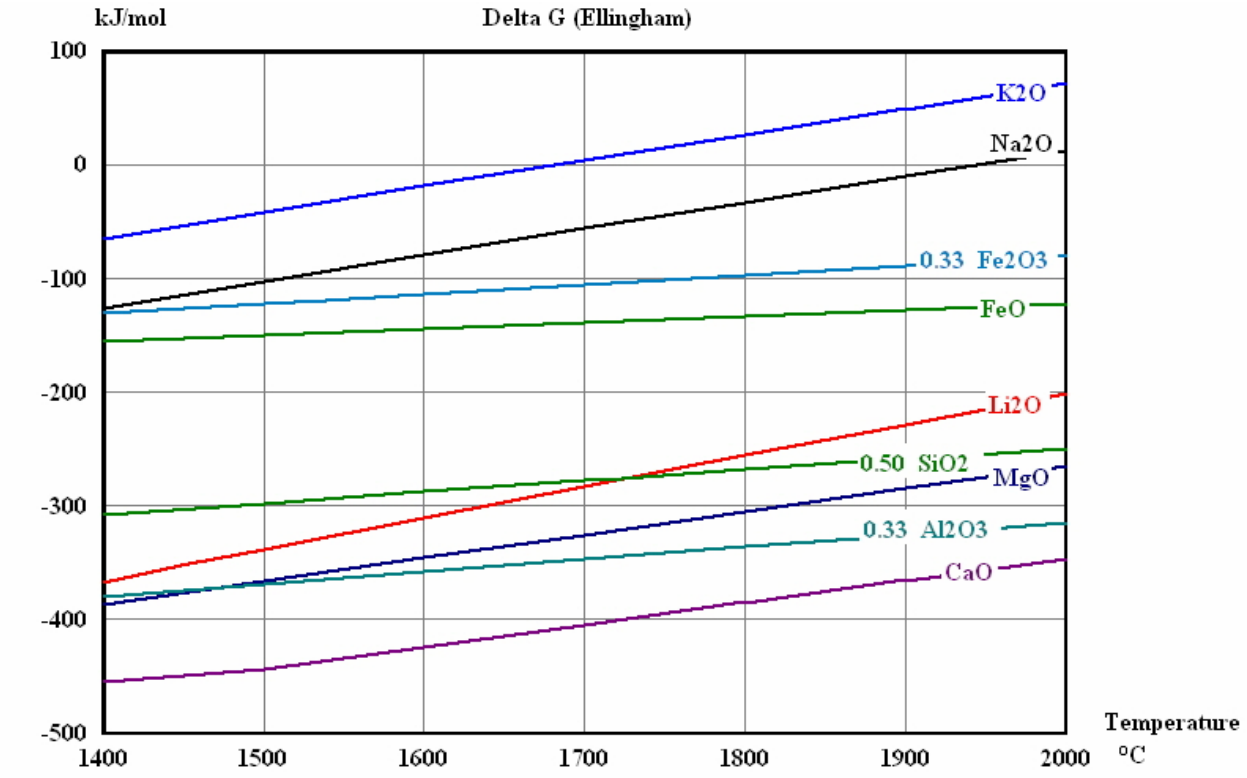

Figure 2.3 Ellingham diagram (calculated using HSC Chemistry[86]) at 1atm p_{O_2} illustrating metal oxides suitable for the electrolyte in a molten oxide electrolysis cell.

Compositions for the electrolyte were based on several criteria. From an array of phase diagrams[87], eutectic compositions for FeO-CaO-MgO-Al_2O_3-SiO_2 (as well as Li_2O) were identified. Since alumina crucible dissolution was of concern in our experimental setup, the electrolyte was required to possess a high enough alumina concentration (15 to 20wt%). The liquidus point of the electrolyte was desired to be below 1450°C so that the system was fully

molten at 1575°C after ramping at 85°C/h and a 1h soak. Also, it was desirable for the electrolyte to be molten without the presence of iron oxide so that if the operating electrolysis cell was exhausted of iron oxide, the electrolyte would still be molten. The optical basicity values were chosen to range from highly acidic (0.55) to highly basic (0.70). Table 2.1 lists the composition of the five electrolytes chosen. The optical basicity values were calculated using the values in Table 1.2. Also note that no correction as suggested by Mills[57] has been made for the optical basicity values listed in Table 2.1.

Table 2.1. Optical Basicity of Candidate Electrolytes. (Compositions in mole percent.)

Name	Melting Point(°C)	CaO	MgO	Al_2O_3	SiO_2	Λ_{melt}
SCAMA1	1222	11.053	13.989	11.054	63.905	0.555
S1A	~1320	18.654	24.184	11.658	45.503	0.605
SCAMB2	1234	33.994	11.991	10.011	44.004	0.632
SCAMB3	~1400	38.870	14.629	10.894	35.607	0.661
SCAMB1	1420	43.690	17.235	11.768	27.307	0.693

The optical basicity values listed for the electrolytes were calculated based on powder composition pre-firing. It was assumed that volatilization of the powders had a trivial effect on the post-fired composition as there was almost no condensed phases observed on the walls of the furnace tube or cap. Alumina crucible dissolution was not apparent with these electrolytes. SCAMA1, SCAMB1, and SCAMB2 were eutectics from quaternary phase diagrams. S1A was related to a ternary eutectic for CaO-MgO-SiO_2. SCAMB3 roughly bisected SCAMB1 and SCAMB2. For a complete listing of melts considered for this study, consult APPENDIX B.

2.6 DETERMINING CURRENT DENSITY

The current density is a crucial performance indicator of the candidate anodes. Determination of surface area could not be done by identifying the melt line or shrouding the electrode. In the severe environment of the molten silicate, ceramic cements dissolved into the electrolyte. A microdisk design failed because the boron nitride sheath used was not easily wettable by the molten silicate, and the ceramic binder leached out leaving volume into which the molten silicate could wick. Thus, the best method for determining the current density accurately and reliably for the anode candidates relied on bare electrodes and the relationship between current and area.

The current is directly proportional to the interfacial contact area of the electrode and the electrolyte. In the proposed cap design illustrated in Figs. 2.1 & 2.2, the depth of the electrode could be adjusted consistently with the Ultra-Torr fittings and a micrometer. By monitoring the current as a function of electrode depth, a plot of the current vs. the change in surface area was made. Since $i \propto A^1$, $\frac{di}{dA} = slope = j$, where j is the current density. The areas utilized were the geometric surface areas. Figure 2.4 illustrates this concept for an Ir working electrode in SCAMB2. The scan rate was 20mV/s, the temperature was 1575°C, and the potential was 2.0V vs. Mo|MoO_2. Additionally, from the x-intercept, the initial depth of immersion can be calculated and used to estimate the immersion depth at any point. While making these measurements, it was assumed that wetting of the electrolyte was constant and that the edge effects on the working electrode were inconsequential.

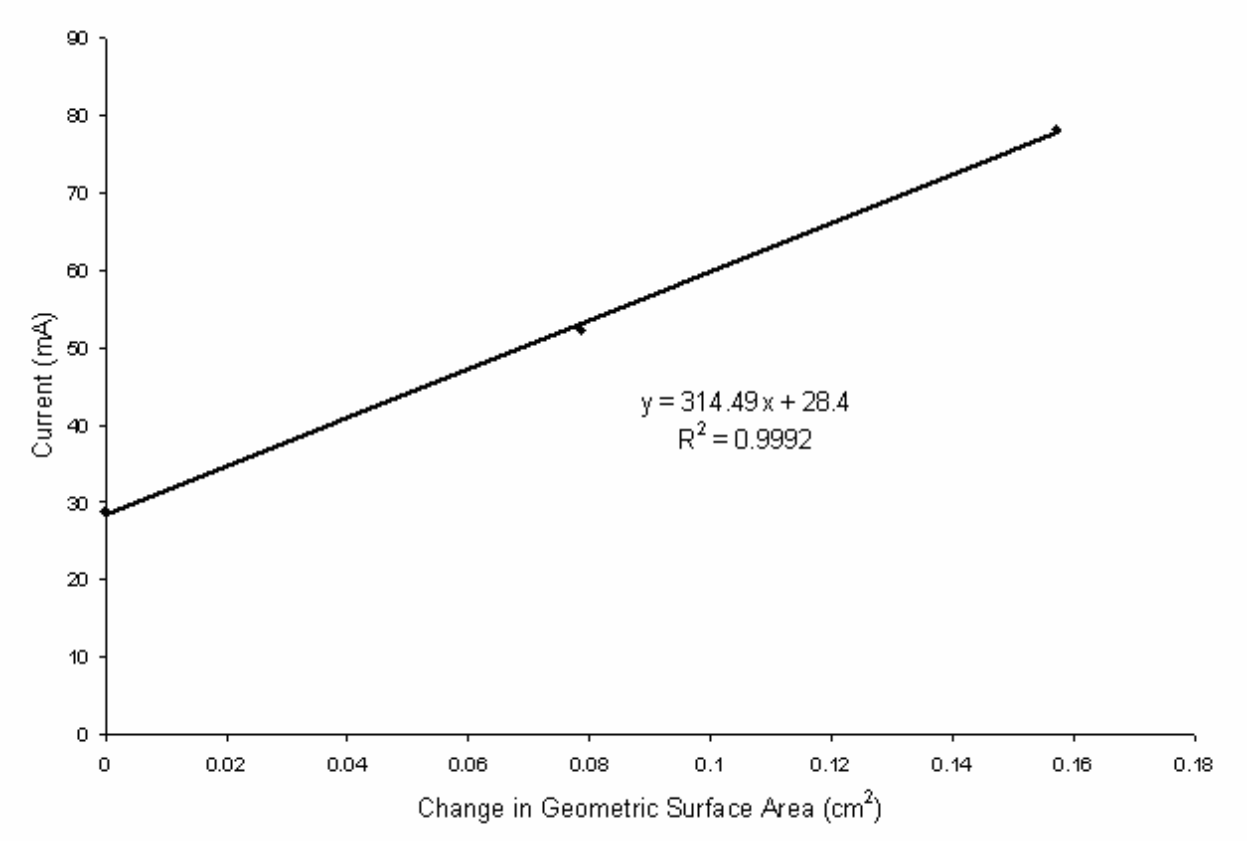

Figure 2.4 The relationship of current and geometric surface area and how it can be used to determine the current density. In this figure, the slope has units of mA/cm^2. The initial depth of immersion was calculated to be 5.6mm.

2.7 SUMMARY

Issues of containment, electrode placement, reference electrode composition, and electrode area determination, all trivial in a room temperature setup, become challenging design considerations when faced with determining accurate electrochemical measurements at 1575°C in molten silicates. From an electrochemistry standpoint, the effects of temperature and potentially high uncompensated resistance values must be understood and corrected. Materials selection is essential for duplicable results and equipment not failing prematurely. Key parameters for the properties of the electrolyte were identified with particular attention paid to the alumina content, melting point, and basicity. Lastly, a methodology for monitoring the current density was provided.

CHAPTER 3: EXPERIMENTAL DETAILS

3.1 POWDER PREPARATION

As-received powders of silicon (IV) oxide, calcium oxide, magnesium oxide, and aluminum oxide were stored in glass jars in a drying oven at 100°C. It was assumed that powders were shipped dry from the distributor and that by storing in the drying oven, additional adsorption of water or carbon dioxide would be minimized. Thus, no compensation for losses on ignition was made for the composition of the electrolyte. Metal oxides were of >99% purity, had low losses on ignition, and were below -325 mesh.

Powders were measured in 200g batches in ratios specified by the particular electrolyte composition. The batches were dry milled with no milling media in 500mL Nalgene bottles at low RPM for roughly 24h. Prior to being positioned on the mill, electrical tape was wound around the cap to seal out moisture.

3.2 ELECTRODE CONSTRUCTION

Molybdenum served as the counter electrode and quasi-reference electrode. Molybdenum rods (Buffalo Tungsten) 0.125”D x 36”L were degreased with a citrus based solvent (PF Solvent from PT Technologies). Mullite tubes (McDanel) 0.25”OD x 0.1875”ID were cut to 33”. Compared with alumina, mullite offered tighter tolerances for the Swagelok Ultra-Torr fittings. The molybdenum rod was positioned within the mullite tube such that 1” remained exposed at the top to interface with the potentiostat. Since the molten electrolyte was only on the order of 1”, wicking of the electrolyte up the mullite shroud was guaranteed to be avoided. In order to seal the molybdenum and mullite, PTFE tape was wound tightly around the molybdenum rod 1” from the top. This was then twisted into the mullite tube. PTFE tape was also wrapped around the outside of the mullite to seal the molybdenum/mullite joint. Attempts were made using PTFE/FEP Dual-Shrink^{TM} tubing (Zeus) to seal the molybdenum/mullite joint, but it was not able to be used because the collapse ratio of the heat shrink tubing was not sufficient to tightly seal down to 0.125”.

The working electrode was constructed using a 0.25”OD x 0.125”ID x 30”L mullite tube (McDanel). A Pt wire (Alfa Aesar) of 0.368mm diameter (Alfa Aesar) served as the current lead. 0.5mm diameter wire was used as the working electrode. Pt, Ir, and Re were supplied by Alfa Aesar, and Rh was purchased from Goodfellow. A mechanically rigid junction was made simply by wrapping the 0.368mm Pt wire several times around a 5cm length of the stiffer 0.5mm material. The 0.368mm Pt wire was crimped onto the working electrode using clean pliers. At elevated temperatures, slight interdiffusion of the platinum group metals ensured electrical conduction and withdrawal of the working electrode from the silicate. Roughly 1” was left exposed beyond the end of the mullite tube. At the top of the working electrode assembly, the 0.368mm Pt wire was threaded through a rubber boot using a syringe as a guide. The remaining length of the Pt was wound on the rubber boot to fix the exposed length of the working electrode.

3.3 Furnace Assembly

The vertical crucible furnace (Mellen) used for these experiments was capable of achieving 1800°C with molybdenum disilicide elements. A 5.5”OD x 5”ID x 24”L 99.8 alumina round bottom, closed-one-end furnace tube (McDanel) sat within a ceramic disk machined in-house to permit the tube to stand vertically. At the throat of the furnace, alumina wool (Cotronics) was packed around the 5.5”OD furnace tube. Hollow alumina bubbles (Zircar) were used to provide a surface on which a 4.5”OD x 4.125”ID x 30”L 99.8 alumina round bottom, closed-one-end furnace tube (McDanel) could rest. The 0.25” gap between the two furnace tubes was insulated with a lower grade of aluminosilicate wool (Cotronics).

After leveling, the 4.5”OD x 4.125”ID x 30”L furnace tube was filled with roughly 300mL of alumina bubbles to provide a level surface on which to place the 750mL cylindrical alumina “containment” crucible (McDanel). Prior to being placed dead center within the furnace tube, the containment crucible was filled with approximately 1” of alumina bubbles. These would prevent the 500mL cylindrical alumina “primary” crucible (McDanel) and containment crucible from joining. Additionally, the abundance of alumina would crystallize the bulk of the electrolyte in the event of leakage.

The primary crucible was filled with 200g of electrolyte and centered within the containment crucible, and the furnace tube was again checked for level. A square scaffold was positioned around the top of the 4.5"OD x 4.125"ID x 30"L furnace tube and rested on the cover of the furnace. The height of the top plate could be adjusted with nuts on studs to lock the cap in place. First, this prevented lateral movement of the furnace tube when adjusting the electrodes. Second, in the unlikely event of the furnace tube rupturing, the scaffold would prevent the cap from crashing into the furnace.

Krytox® RFE O-ring grease (Dupont/Loctite) specifically formulated not to degrade silicone O-ring materials and withstand continuous operating temperatures at 260°C was applied to the top of the 4.5"OD x 4.125"ID x 30"L furnace tube. A -425 silicone O-ring was inserted over the furnace tube. As described previously in 2.3 FURNACE TUBE AND CAP CONSTRUCTION, a flange was fitted over the O-ring, a copper gasket was inserted in the knife-edge seal, and the cap was placed on the flange. Since the electrode shrouds were 0.25", the cap was fitted with the Ultra-Torr couplings, plugs, and barbed gas outlet before being placed on the furnace tube. All NPT-¼" fittings were wrapped with PTFE tape. Six 5/16" – 24 snugly tightened hex cap bolts fixed the cap to the flange. Next, the flange and cap were pushed down until the cap contacted the furnace tube, and the scaffold was raised to lock the cap in place. For the duration of the experiment, the cap was cooled via a recirculating chiller (VWR) set for 15.5°C at a flow rate of 1.4 gallons per minute.

The electrodes were inserted starting at the center with the reference electrode. The knurled end and the ferrule from the Ultra-Torr fitting were slid up the electrode, and a Viton® O-ring was lubricated with silicone grease. The counter electrode and up to three working electrodes were inserted in the remaining spaces (see Fig. 2.1). The height of the electrodes during heating of the furnace was roughly 16" below the top of the furnace tube. The inlet gas tube was mullite (McDanel) 0.25"OD x 0.1875"ID x 20"L. It was inserted opposite the gas outlet.

The gas inlet was connected in series with a bubbler filled with silicone oil. Pre-purified 99.998% argon (Airgas) was bubbled through at roughly 165cc/min into the furnace for the duration of heating, running experiments, and cooling the furnace. This was necessary to

prevent oxidation of the molybdenum electrodes. The outlet gas was also routed through a bubbler containing silicone oil and vented. The quality of the seal was determined by visual inspection of the bubbling rates of both the inlet and outlet bubblers, especially when no power was applied to the furnace elements.

3.4 Temperature History

The furnace was heated from room temperature to 1675°C at a ramp rate of 85°C/h. The setpoint temperature was approximately 100°C higher than the measured temperature of the hot zone. Before lowering the electrodes, the electrolyte soaked for one hour to equilibrate the hot zone and to ensure a fully molten electrolyte. The duration of the electrochemistry experiments was on the order of 8h. After withdrawing the electrodes from the melt, the furnace was cooled at a ramp rate of 85°C/h back to room temperature.

3.5 Electrode Immersion

The reference electrode was the first electrode to be immersed into the electrolyte. Since it was positioned in the center of the furnace, it could lock the primary crucible in place while the other electrodes were adjusted. The counter electrode was the second electrode immersed. The working electrodes were lowered individually; when not engaged in electrochemical measurements, they remained out of contact with the electrolyte. The leads for the reference, counter, working, and sense electrodes from the potentiostat were connected to the corresponding electrode in the furnace. The working electrode was lowered in very small increments while monitoring the open circuit potential (OCP). Once a reading for the open circuit potential was witnessed, the height of the working electrode was fixed by tightening the Ultra-Torr fitting. The reference and counter electrodes were then raised slightly to avoid contacting the crucible.

The height of the working electrode was adjusted using a set of digital calipers capable of measuring 0.01mm (Mitutoyo). The author concedes that a better device would have been a depth micrometer; however, the complications of construction and the linearity of the data

obtained using the digital calipers justified the technique used in this thesis. The working electrode was lowered in 5.0mm increments.

3.6 Cyclic Voltammetry

The potentiostat used in these experiments was a PARSTAT® 2273 (Princeton Applied Research/AMETEK). Software included PowerCORR® Rev. 2.47 to monitor OCP and PowerCV® Rev. 2.46 to measure the compensation resistance and perform cyclic voltammetry (Princeton Applied Research/AMETEK). When the working electrode was inserted into the electrolyte, the OCP was monitored until it became stable. Typical OCP values for the platinum group metals were 300±30mV vs. $Mo|MoO_2$. Next, the working electrode was cycled at 100mV/s between -0.1 and 1.2V until the *i* vs. *E* curves were indistinguishable. This usually required 5 or 6 cycles. The least electroactive region was recorded and later used as the baseline voltage in *iR* compensation measurements. The PFIR application of PowerCV® determined R_c which was 70% of R_u. Any greater value for R_c resulted in instability during CV. These steps were performed any time the working electrode height was changed. This is important to consider as R_u was found to depend on immersion depth.

Once the value for R_c was determined, cyclic voltammograms were recorded at 250, 100, 50, and 20mV/s (and occasionally 500 and 10 as well). In the majority of cases, the scans were performed applying positive potentials starting at 0V vs. $Mo|MoO_2$. Typical upper vertices included 1.2V and 2.0V. Comparisons of current density measurements were made at 2.0V vs. $Mo|MoO_2$.

CHAPTER 4: BEHAVIOR OF CANDIDATE ANODES

4.1 RESULTS

The first investigations of working electrode materials were performed in S1A. This composition was a modified form of an electrolyte used previously in our lab, and it also had an intermediate optical basicity value. It was thought that if an electrode failed in S1A, it would also fail in more acidic or basic melts.

Electrodes were typically subjected to potentials ranging from -0.1 to 2.0V vs. Mo|MoO_2 at scan rates of 250, 100, 50, and 20mV/s. Fig. 4.1 depicts the behavior usually witnessed on the platinum group elements. Starting at 0V vs. Mo|MoO_2 and moving toward more positive potentials, the only current was due to the capacitance of the double layer. At roughly 1V, a peak was witnessed on iridium and rhodium, whose identity will be discussed later. Beyond 1.1V, the measured current appeared jittery, suggesting the coalescence and evolution of oxygen gas bubbles. At roughly 0.75V, the current changed to cathodic, owing possibly to reduction of oxygen molecules to free oxide ions. Scans were restricted from going less negative than -0.1V to prevent silicide formation on the working electrode.

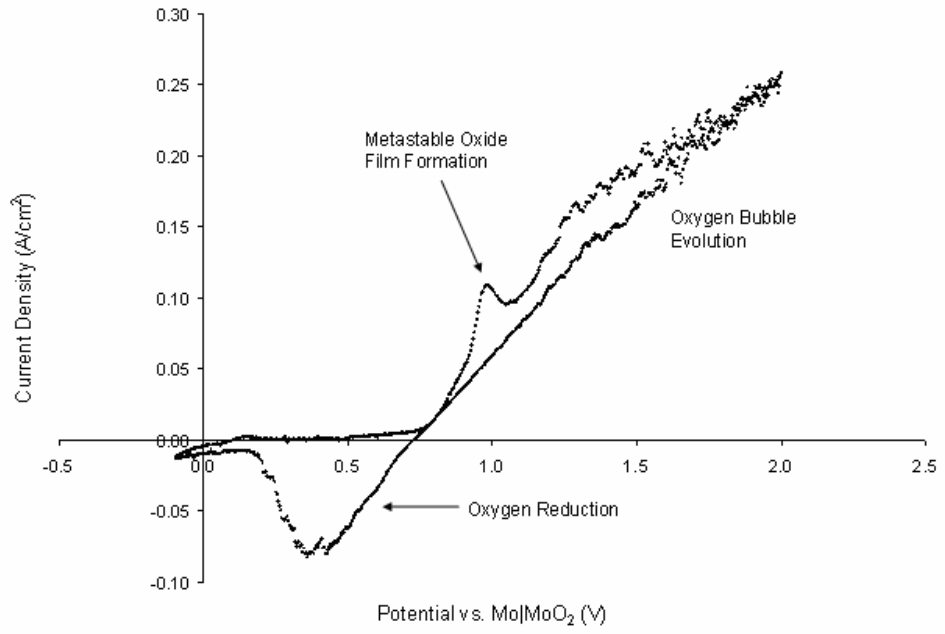

Figure 4.1 Typical features of cyclic voltammograms in molten aluminosilicates at 1575°C. WE: 0.5mm Ir CE: Mo RE: Mo|MoO_2 Scan Rate: 100mV/s Melt: S1A

4.1.1 Working Electrode/Anode Trials

The four candidates chosen for the working electrode were iridium, rhodium, platinum, and rhenium. Rhenium was included to explore the behavior of the refractory metals. Each electrode was subjected to the same range of potentials and spent roughly the same period of time (2-3h) in the electrolyte. Figs. 4.2 through 4.5 show the scans of Ir, Rh, Pt, and Re respectively in S1A. More will be discussed in 4.2 Discussion, but it is worth mentioning briefly that rhodium sporadically exhibited two peaks in the passivation region, and rhenium possessed properties altogether different from the platinum group elements. The peaks associated with metastable film formation and oxygen reduction were scan rate dependent, while the oxygen bubble evolution current appeared scan rate independent.

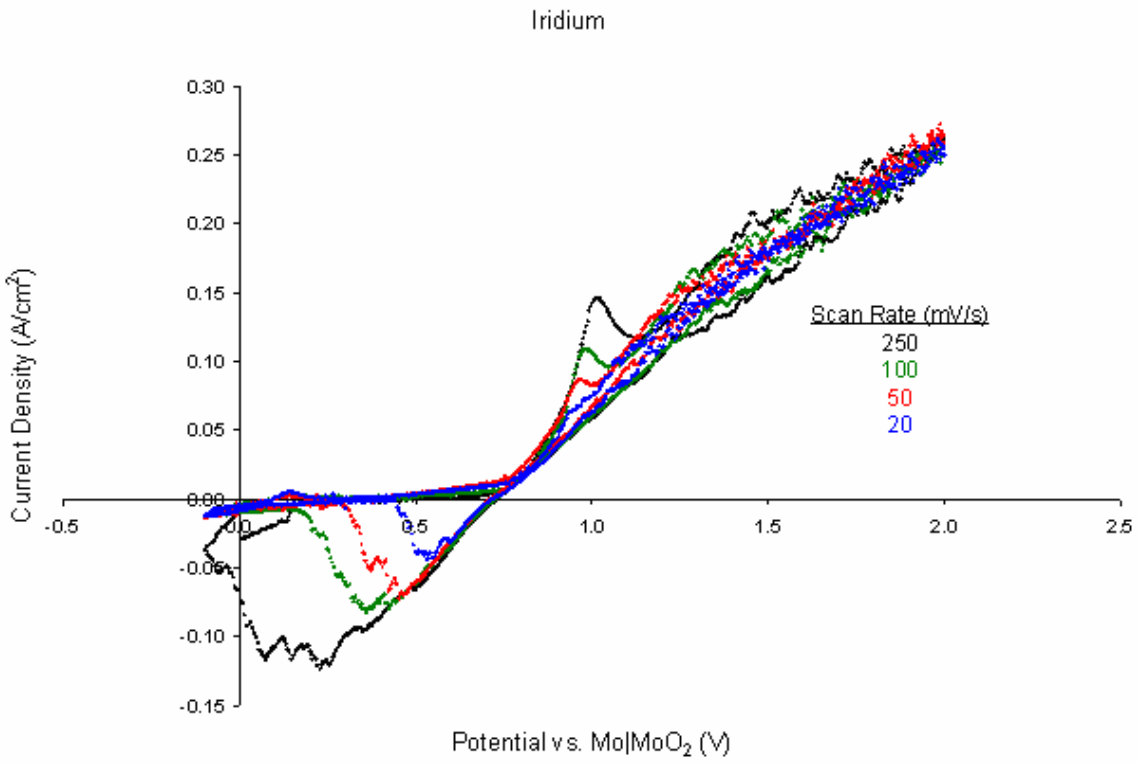

Figure 4.2 Cyclic voltammograms on Ir. WE: 0.5mm Ir CE: Mo RE: Mo|MoO_2
Scan Rates: 250, 100, 50, 20mV/s Melt: S1A

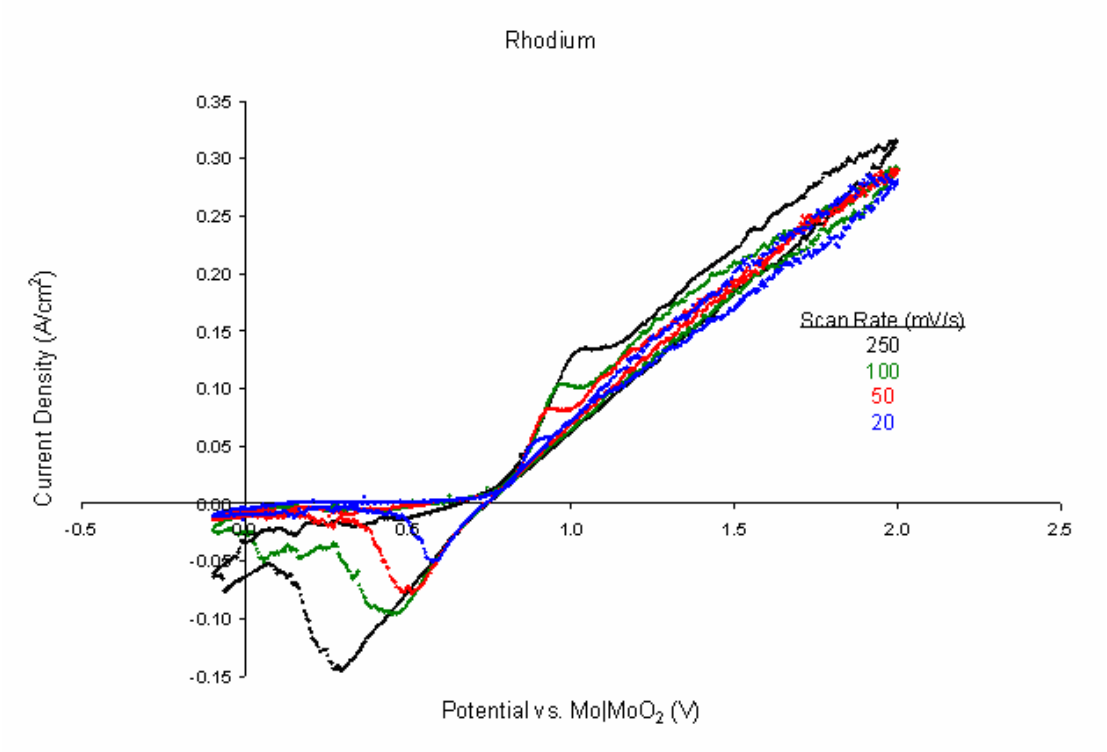

Figure 4.3 Cyclic voltammograms on Rh. WE: 0.5mm Rh CE: Mo RE: Mo|MoO_2 Scan Rates: 250, 100, 50, 20mV/s Melt: S1A

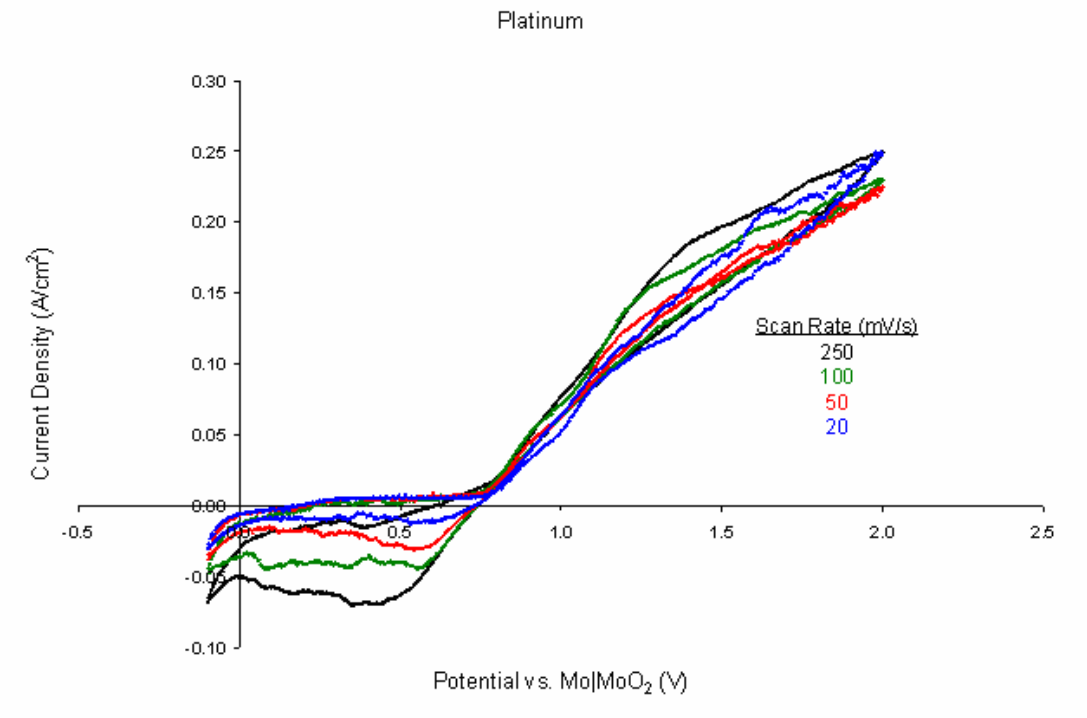

Figure 4.4 Cyclic voltammograms on Pt. WE: 0.5mm Pt CE: Mo RE: Mo|MoO_2 Scan Rates: 250, 100, 50, 20mV/s Melt: S1A

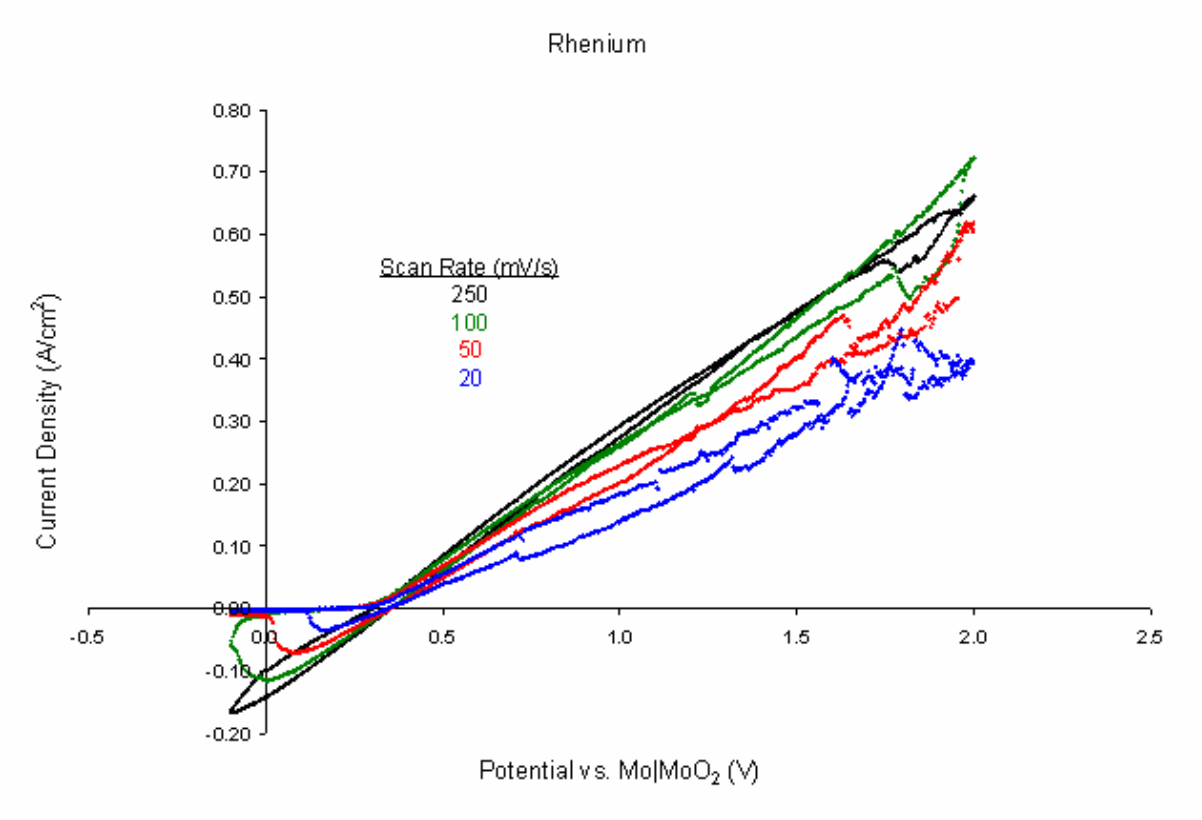

Figure 4.5 Cyclic voltammograms on Re. Note that while all other cyclic voltammograms were recorded at 70% *iR* compensation, only 5% was applied on Re. WE: 0.5mm Re CE: Mo RE: $Mo|MoO_2$ Scan Rates: 250, 100, 50, 20mV/s Melt: S1A

4.1.2 A Closer Look at Peak Behavior

Figs. 4.2 through 4.5 share similar features as highlighted in Fig. 4.1, but several notable differences can be seen. Iridium (Fig. 4.2) and rhodium (Fig. 4.3) had peaks positioned around 1.0V, but similar peaks were not encountered on platinum (Fig. 4.4). Instead, platinum appeared to have small anodic and cathodic waves around 0.25V. Rhenium (Fig. 4.5) had a dramatic rise in anodic current starting around 0.3V whereas the platinum group elements did not experience a significant anodic current until 0.8V and beyond. In order to better comprehend the peaks, particularly those witnessed on iridium and rhodium, scans were performed at 50mV/s and the upper and/or lower switching potentials were shifted incrementally.

Fig. 4.6 demonstrated that the anodic passivation peak on iridium remained at the same potential and was the same magnitude regardless of whether the scan is performed starting from 0V in the

forward direction or from 1.4V in the reverse direction. Rhodium intermittently possessed single peaks (Fig. 4.3) or double peaks (Fig. 4.7) in its passivation region. There was no correlation with the basicity of the melt. Platinum (Fig. 4.8) exhibited no peaks when applying positive potentials, but instead indicated redox reactions centered at 0.25V. No such tests were performed with the rhenium working electrode because rhenium was so badly degraded after its initial experiment in S1A that all future trials with it were abandoned.

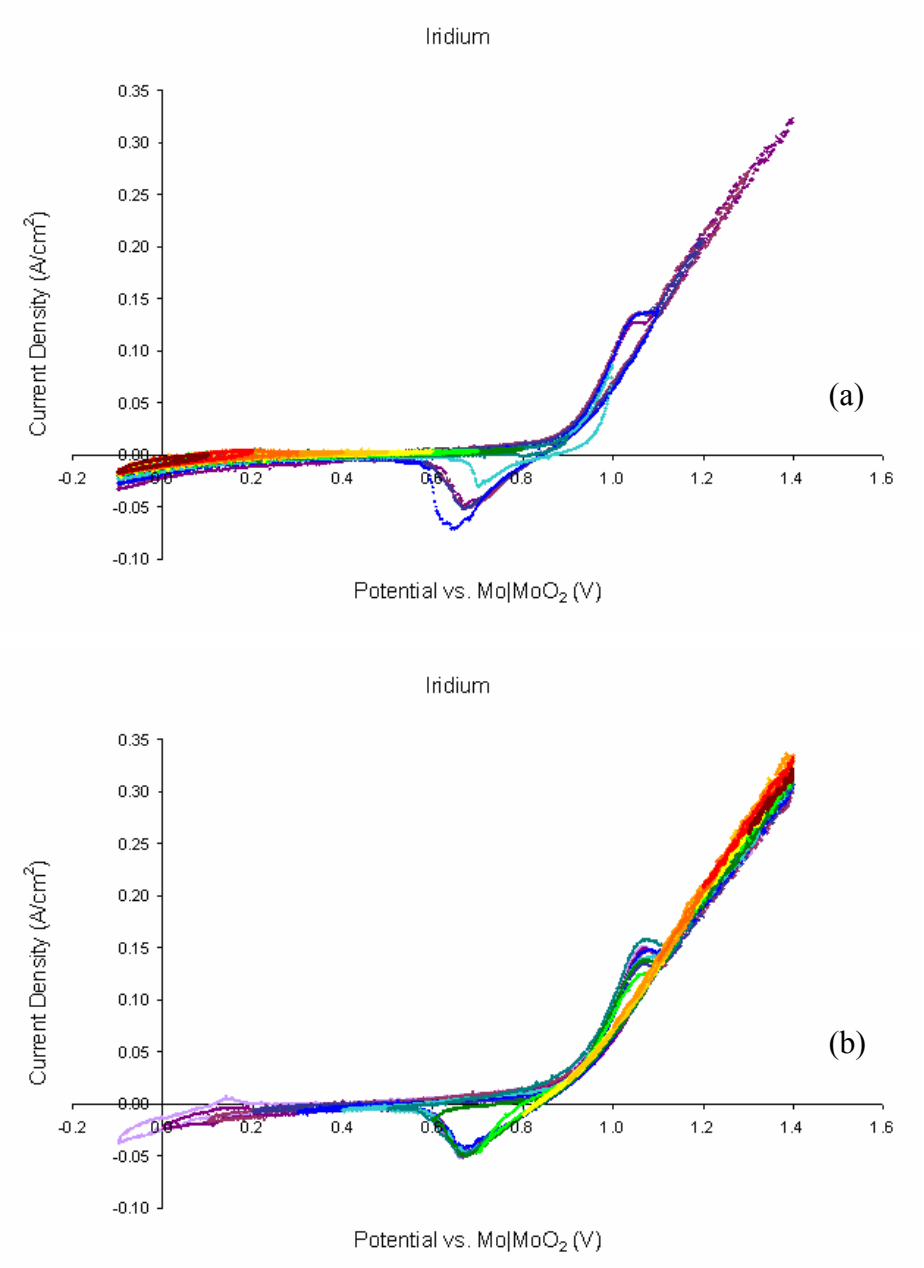

Figure 4.6 Shifting the upper (a) and lower (b) switching potential by increments of 0.1V. WE: 0.5mm Ir CE: Mo RE: Mo|MoO_2 Scan Rate: 50mV/s Melt: SCAMB1

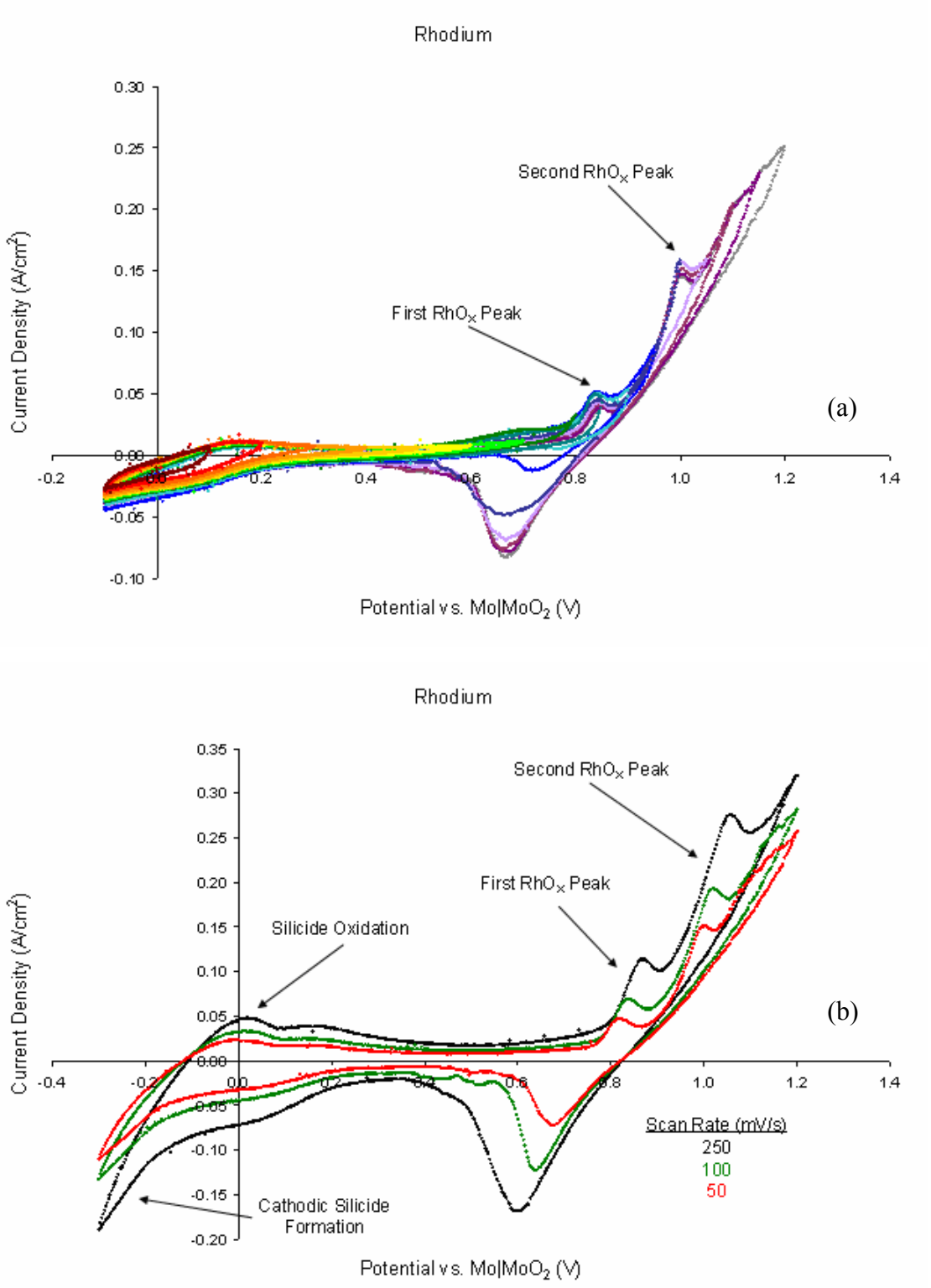

Figure 4.7 (a) Incrementally increasing the upper switching potential to investigate the anodic and cathodic relationships of passivation peaks on rhodium. Scan Rate: 50mV/s (b) Both peaks shift position and increase in magnitude with scan rate. Scan Rates: 250, 100, 50mV/s
WE: 0.5mm Rh CE: Mo RE: Mo|MoO_2 Melt: SCAMB1

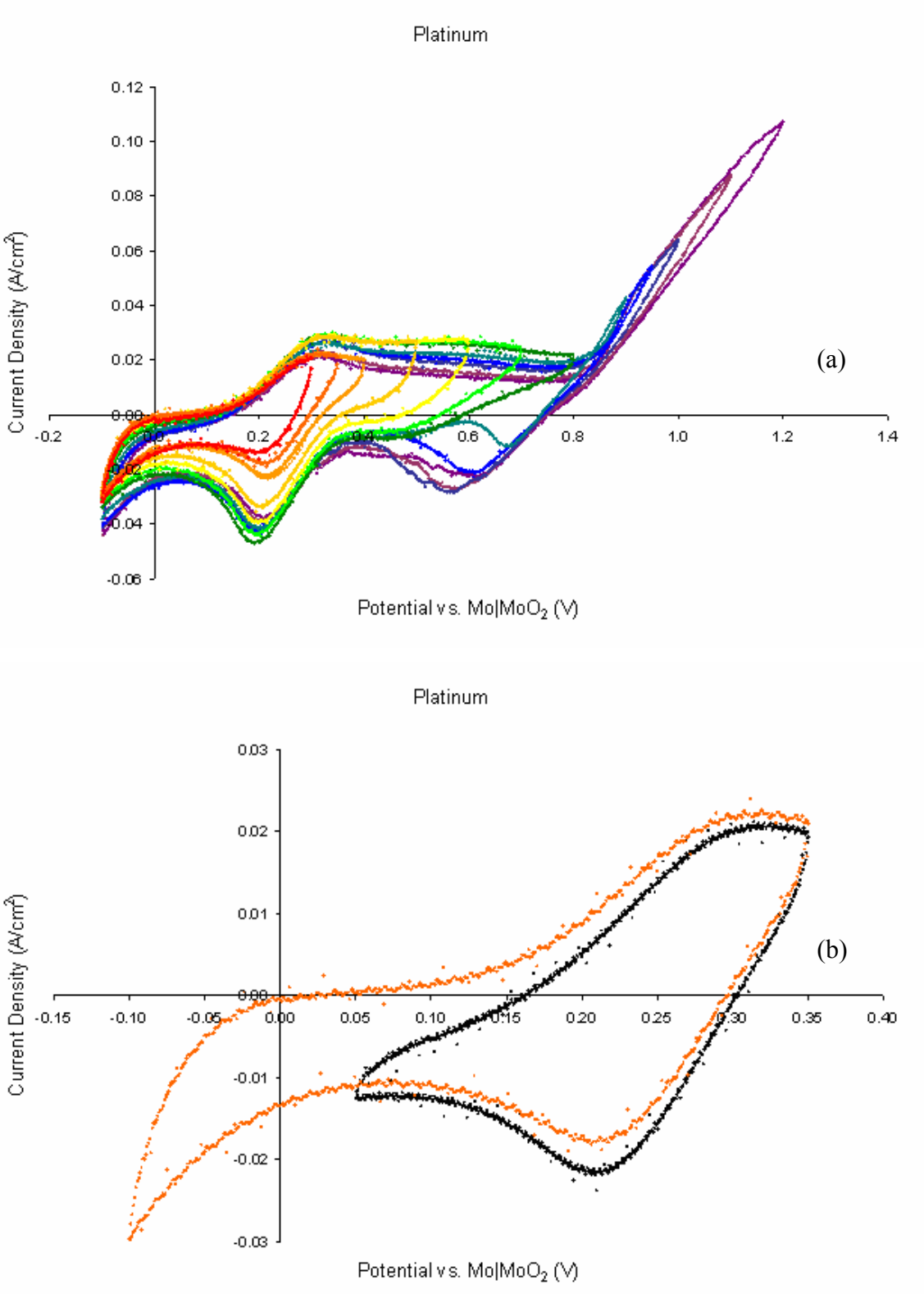

Figure 4.8 (a) Incrementally increasing the upper switching potential. (b) CV indicating the anodic peak at approximately 0.3V is independent of silicide formation. WE: 0.5mm Pt CE: Mo RE: Mo|MoO_2 Scan Rate: 50mV/s Melt: SCAMB2

4.2 Discussion

4.2.1 Oxygen Evolution and Reduction

Fig. 4.1 illustrates the typical behavior encountered on platinum group elements. If the breakdown voltage of MoO_2 is used to estimate where molecular oxygen formation is expected thermodynamically (0.686V vs. Mo|MoO_2), it is clear that a substantial overpotential must be applied to generate oxygen bubbles. Oxygen gas evolution is indicated by the "jitteriness" of the *j* vs. *E* plot. What is not easily identifiable is the potential at which free oxide ions are oxidized to form oxygen molecules. These molecules must then coalesce into a bubble of critical radius to detach from the electrode and float upwards through the viscous aluminosilicate medium. Not only does oxygen evolution have an activation overpotential associated with it, but iridium (Fig. 4.2) and rhodium (Fig. 4.3) possess additional signals around 1.0V, interfering with analysis of this reaction.

What can be stated with certainty is that oxygen gas evolution is not mass transfer limited. In a range of electrolytes with optical basicity values beyond 0.6, the scan rate had no impact on *j* vs. *E* behavior (Figs. 4.2 to 4.4). In fact, even up to 3.5V vs. Mo|MoO_2 at a scan rate of 500mV/s, there was no indication of a mass transfer, i.e. diffusion limited, peak (Fig. 4.9). Even at this exceedingly high potential, the iridium electrode remained intact, suggesting that free oxide ions can quickly diffuse to reach the anode surface or there is a high concentration of free oxide ions. Otherwise, electrons would have been ripped away from the iridium working electrode, forming Ir^{n+} species that would have dissolved into the molten aluminosilicate electrolyte.

Oxygen bubble reduction is suggested for the cathodic wave which starts around 0.75 to 0.80V. It is interesting to note that platinum does not seem to have any passivation peak(s) in this region as indicated with iridium and rhodium. Thus, the cathodic wave is assumed to be wholly attributed to the reduction of oxygen molecules to free oxide ions and not related to reduction of oxide phases formed on the electrode surface during anodic polarization. Fig. 4.4 shows the scan rate dependence of this cathodic wave on a platinum working electrode. At high scan rates, when returning from 2.0V to 0.7V, there is not sufficient time for the bubbles generated during the forward half-cycle to diffuse away from the working electrode. Any remaining oxygen

molecules are reduced back to free oxide ions. Even at the slowest scan rates (20mV/s), the amount of O_2 in the vicinity of the working electrode is substantial. Since the scan rate is lower, a smaller cathodic peak is observed. Scan rates of 100 and 50mV/s show intermediate behavior as also witnessed in Figs. 4.2 and 4.3 on iridium and rhodium.

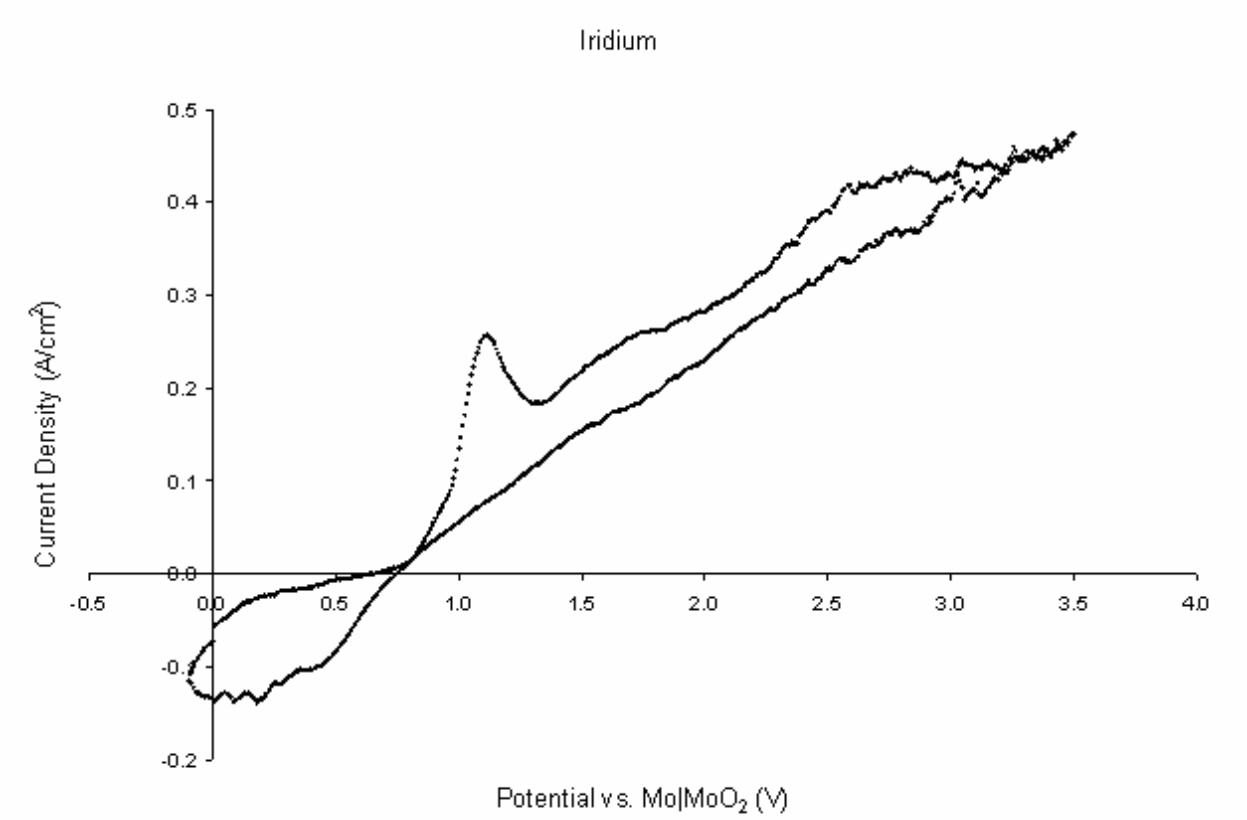

Figure 4.9 Oxygen evolution behavior up to 3.5V vs. Mo|MoO_2 illustrating that mass transport of the free oxide ion is not rate-limiting. WE: 0.5mm Ir CE: Mo RE: Mo|MoO_2
Scan Rate: 500mV/s Melt: S1A

Upon further inspection, for CVs with upper switching potentials of 2.0V on working electrodes of approximately 0.2cm^2 in S1A, the charge passed for the duration of the oxygen reduction peak was on the order of 0.045C. In other electrolytes, regardless of the working electrode material, the same value (0.045C) for charge passed was recorded. The electrolyte in the vicinity of the working electrode was likely saturated by O_2 molecules. It makes sense that the physically dissolved O_2 concentration is the same in all the electrolytes examined if one considers that the value is strongly dependent on temperature but not composition for melts free of transition metal oxides[58].

4.2.2 Identification of Phases Formed

As noted in Fig. 4.1 and witnessed in subsequent figures, peaks appeared on iridium and rhodium prior to oxygen evolution. These peaks were attributed to the formation of metastable oxide films. The behavior is not unlike the formation of passive films of chromium (III) oxide on stainless steel in aqueous solution in which a kinetically stable barrier layer exists until a high enough potential is reached to drive oxidative dissolution[88]. With any passive film, two processes are taking place: the passive film is forming (dL^+/dt) adding to the barrier layer thickness, and/or the passive film is being consumed (dL^-/dt). When the magnitude of dL^-/dt is greater than $(dL^+/dt)_{L=0}$, the passive film no longer exists and the system becomes transpassive. However, unlike chromium oxide on stainless steel, the dL^-/dt term at 1575°C is attributed to thermodynamic decomposition to metal and oxygen gas and not dissolution to ionic species. Table 4.1 lists the Gibbs free energy for a series of reactions involving the platinum group elements and oxygen. Dissolution of the platinum group elements was not witnessed as there was no coloration of the electrolyte near the working electrode. In additional experiments performed with Prof. Dihua Wang with pressed pellets of IrO_2 at 1575°C, whether left at open circuit or under anodic polarization, transformation to iridium was the result with no indication of iridium oxide or colloidal iridium metal in the electrolyte.

The notion of a transpassive state for iridium and rhodium is supported by observations of Higgins[54] in which a monolayer of PtO_2 was formed on platinum working electrodes and the oxygen evolution voltage increased with current density. He witnessed double layer charging, formation of an oxide film, and oxygen evolution. However, at higher current densities, Higgins noted that smaller coverage of the working electrode would occur before oxygen evolution. Application of higher current densities would be analogous to applying a higher potential. This higher potential was likely beyond the transpassive potential, beyond which metastable PtO_2 would not be formed at all. Higgins' observations can be used to support the passivation peaks witnessed on iridium and rhodium, but for reasons unknown, at 1575°C in this work, no strong indication of passivation was observed around 1.0V on platinum in any electrolyte except for the slight inflections at 250, 100, and 50mV/s in Fig. 4.4

The phase of the oxide species on iridium has been speculated to be IrO_2. Table 4.1 lists the decomposition voltages and potentials vs. Mo|MoO_2 for a variety of phases of each candidate working electrode. The calculated potential for IrO_2(s) formation is in very close agreement with the observed potential of 0.82V vs. Mo|MoO_2 (Figs. 4.1, 4.2, 4.6).

Rhodium sporadically exhibited either one passivation peak or two passivation peaks (Figs. 4.3, 4.7). Additionally, rhodium had many oxide phases with decomposition potentials in the range of 0.8 to 1.0V (Table 4.1). No two oxide species can be identified with certainty, although it is anticipated that the phase formed around 0.77V vs. Mo|MoO_2 contained a rhodium cation of lower ionic charge than the phase formed around 0.87V. This is not only supported by the calculated values in Table 4.1, but also a phase such as Rh_2O_3 may decompose to yield the following reaction:

$$2Rh_2O_3(s) \Rightarrow 2Rh(s) + 2RhO_2(s) + O_2(g).$$

This is highly speculative, but makes some intuitive sense if decomposition occurs by rhodium atoms being deposited at the bulk metal substrate/oxide film interface and oxygen molecules being ejected from the oxide film/electrolyte interface. RhO_2 would result, and because of enhanced electronic conductivity and/or a much thinner layer thickness, the current could increase once again to yield a second passivation peak. In cases where only one peak is observed, RhO_2 is likely the oxide phase present.

Table 4.1 Calculated decomposition potentials[89] and EMF series (1atm p_{O_2})

Reaction	n	ΔG (J)	E vs. O^{2-}/O_2 (V)	E vs. Mo|MoO_2 (V)
$MoO_2(s) \Rightarrow Mo(s) + O_2(g)$	4	264,826.5	-0.686	0.000
$IrO_2(s) \Rightarrow Ir(s) + O_2(g)$	4	-61,325.4	0.159	0.845
$2Rh_2O(s) \Rightarrow 4Rh(s) + O_2(g)$	4	33,206.4	-0.086	0.600
$2RhO(s) \Rightarrow 2Rh(s) + O_2(g)$	4	-76,310.2	0.198	0.884
$Rh_2O_3(s) \Rightarrow 2Rh(s) + \frac{3}{2}O_2(g)$	6	-97,556.7	0.169	0.855
$RhO_2(s) \Rightarrow Rh(s) + O_2(g)$	4	-89,970.7	0.233	0.919
$PtO_2(g) \Rightarrow Pt(s) + O_2(g)$	4	-166,084.0	0.430	1.117
$Re_2O_7(g) \Rightarrow 2Re(s) + \frac{7}{2}O_2(g)$	14	474,628.7	-0.351	0.335

From purely thermodynamic arguments, the formation of oxide phases of platinum group metals at 1575°C is dubious. Clearly, with such large negative values for ΔG, the formation of an oxide phase is counterintuitive. However, one must consider that the interfacial region between the electrode and electrolyte is driven far from equilibrium. The very fact that the oxide phase has a large negative free energy and the temperature is 1575°C should support the notion that thermal decomposition is rapid. This is shown qualitatively on iridium (Fig. 4.3) and rhodium (Fig. 4.4) working electrodes where for slow scan rates (20mV/s), almost no passivation peak appears because almost as soon as any oxide species are produced, the oxide decomposes to yield metal and O_2 molecules. Furthermore, as was described in 4.2.1 OXYGEN EVOLUTION AND REDUCTION, the same value for charge passed during the cathodic wave (0.045C) was witnessed on all platinum group element working electrodes in all electrolytes. Any contribution to the cathodic wave from oxide film decomposition has been dismissed with the conclusion that any oxide phases formed during the forward scan decomposed rapidly. Thus, in the window of oxide film metastability, some oxygen gas evolution is due to oxide decomposition. Since the dL^-/dt term should be independent of applied potential, and since IrO_2 and RhO_x are anticipated to be metastable for only a small potential range, beyond 1.1V, all the anodic current is due to the net reaction,

$$2O^{2-} \Rightarrow O_2(g) + 4e^- .$$

On neither iridium nor rhodium, no other oxide phases are expected aside from IrO_2 and RhO_x. First, the calculated values listed in Table 4.1 correspond nicely with the observed potentials for oxide film formation. Second, considerations drawn from the CaO-IrO_2 binary phase diagram as well as the nature of the electrochemical double layer tend to rule out iridate, and by similar chemistry, rhodonate phases. There are no thermodynamically stable binary compounds of CaO and IrO_2 above 1240°C, and there are none of CaO and Rh_2O_3 above 1320°C[87]. Since the existence of IrO_2 is thermodynamically not favorable, this argument bears little weight in the context of this chapter. However, to form a stable iridate phase, a divalent ion would have to diffuse to the surface of the electrode and be present to react with an Ir-O complex. In order to reach the electrode/electrolyte interface, the Ca^{2+} or Mg^{2+} ion would not only be repelled by the anodically (+) polarized iridium anode, but it would also have to diffuse through the inner plane of the double layer which would be comprised of densely packed anions. On the other hand, to

form IrO_2, adsorbed oxygen species could react on the iridium surface with essentially no mass transport limitations, and therefore react as rapidly as charge transfer can occur. For these reasons, IrO_2, and by analogy, RhO_x, are suggested as the only possible metastable oxide phases.

Attempts were made to calculate the thickness of the film based on the peak height (i_p) and position of peak potential (E_p)[55]. However, it was soon realized that the equations were not applicable because there was not an appreciable concentration of Ir^{n+} in the electrolyte[90]. This explained the nonphysical, negative film thicknesses obtained. Perhaps the Point Defect Model by MacDonald[88] and coworkers may be applicable. The PDM is interesting because it can account for potential dependent and independent processes, and the metal ions of the passivation layer do not have to be in solution. The model is complicated and would require refinement to deal with thermal decomposition of the passivation layer as opposed to dissolution. Adding to its appeal, the PDM has been shown to work well with PtO defect chemistries in aqueous environments[90].

Platinum did not exhibit a discernable passivation peak around 1.0V like iridium and rhodium. Excluding the oxygen evolution reaction and cathodic reduction of molecular oxygen to free oxide ions, the features of the platinum working electrode were puzzling. First, when considering passivation of the platinum surface, it may be possible for the decomposition rate of PtO_2 to be so rapid, that unless scan rates on the order of 1V/s were employed, no peak would exist. Of course, scanning at this rate might introduce artifacts due to the high C_{dl} and R_u values (See 2.1 PRUDENT ELECTROCHEMICAL PRACTICES IN MOLTEN OXIDES). Perhaps iridium and rhodium have the ability to grow a metastable oxide film of several nm but platinum can only grow a monolayer resulting in an imperceptible current. Second, it was peculiar that platinum exhibited anodic and cathodic waves around the potential of 0.25V (Fig. 4.8). The separation distance of $i_{p,a}$ and $i_{p,c}$ was 0.09V. For reversible systems, the separation of $E_{p,a}$ and $E_{p,c}$ is $2.3RT/nF$[15]. At 1575°C (1848K), the separation distance is $0.367\text{V}/n$; 0.09V for ΔE_p indicates that the number of electrons transferred was 4.

This pair of peaks (Fig. 4.8) appeared whether platinum was the first working electrode immersed in the electrolyte or the last. The most likely transition metal species would have been

molybdenum. Not only was the potential 0.25V away from the $Mo|MoO_2$ reference electrode, but the value of *n* equal to 4 did not correspond to a likely redox couple involving Mo^{n+}. Had *n* been 2, maybe a Mo^{4+}/Mo^{6+} redox couple was present, but the large shift from the reference electrode was still inexplicable. These peaks were not seen on the other candidate anode materials, so a transition metal impurity in the electrolyte was improbable. Perhaps platinum formed a stable phase on its surface that remained intact despite the application of high potentials and oxygen evolution. As shown in Fig. 4.8, the cathodic peak always appeared regardless of the upper switching potential. A calcium platinate phase would be highly unlikely, as even the highest decomposition temperature encountered on the $CaO\text{-}PtO_2$ phase diagram is 1035°C[87]. Although the *E* value for $PtO_2(g)$ was listed in Table 4.1, the value for $PtO_2(s)$ is not expected to be different by more than 0.04V if the formula Higgins[54] lists is extrapolated beyond 1550°C to 1575°C.

Rhenium degraded rapidly as oxygen was produced since the boiling point of Re_2O_7 is 393°C[71]. Other than a small, needlelike protrusion from its junction with the platinum lead wire, it had decomposed entirely. CVs of the rhenium working electrode showed a significant increase in anodic current at 0.31V, a value very close to the predicted formation potential of 0.335V. The fact that the free oxide ions reacted at potentials nearly 0.4V less than the anticipated value of 0.686V is analogous to the interaction of oxygen and carbon in Hall-Héroult cells for the electrolytic production of aluminum. Because the reaction of oxygen and carbon is so favorable, the usage of carbon anodes results in a theoretical reduction of 1.0V of the alumina decomposition potential[91]. Despite the significantly greater current densities of rhenium when compared with the platinum group metals in S1A, rhenium proved consumable. Unless the oxides of the refractory metals possessed sparingly low volatilities, as a group, they are not expected to be satisfactory anodes.

4.3 SUMMARY

CVs of the four candidate anodes were presented in this chapter. The platinum group elements exhibited similar behavior; however, platinum did not exhibit a passivation peak, and it possessed a peculiar pair of anodic and cathodic waves around 0.25V. Iridium and rhodium

likely possessed metastable oxide phases formed at approximately 1.0V vs. Mo|MoO_2. Thermodynamic calculations suggested the phase formed on iridium was IrO_2. Rhodium sporadically exhibited either one peak or two peaks, and a rationale was discussed suggesting decomposition of Rh_2O_3 to yield Rh, RhO_2, and O_2, with RhO_2 as the second passivation phase. Rhenium decomposed to yield Re_2O_7, a highly volatile gaseous oxide. This feature was analogous to carbon dioxide formation on graphite in Hall-Héroult cells.

At 1575°C in aluminosilicate melts, the onset potential for the free oxide ion to electrochemically react to yield oxygen molecules is anticipated to be around 0.75±0.05V vs. Mo|MoO_2. On iridium and rhodium, the reaction of oxygen and metal yields a metastable oxide phase that thermally decomposes to yield a small amount of oxygen gas. However, once the applied potential is beyond the transpassive potential, i.e. IrO_2 and RhO_x are no longer metastable and do not form, all oxygen evolution is attributed to the reaction of free oxide ions to gaseous oxygen.

CHAPTER 5: INFLUENCE OF ELECTROLYTE COMPOSITION ON PERFORMANCE

5.1 CURRENT DENSITY AS A FUNCTION OF OPTICAL BASICITY

The hypothesis stated in CHAPTER 1 regarded the concentration of the free oxide ion, $C^*_{O^{2-}}$, as a significant design parameter for governing the current density achieved on the anode at a defined overpotential. The optical basicity scale was chosen because of its ability to provide a global measure for the free oxide ion concentration[57]. This section will discuss the results of experiments performed in the five aluminosilicate electrolytes outlined in 2.5 ELECTROLYTE SELECTION, and will develop a functional relationship of current density and optical basicity on iridium, rhodium, and platinum anodes.

Fig. 5.1 displays the *j* vs. *E* response of an iridium working electrode in the five electrolytes. As described in 2.6 DETERMINING CURRENT DENSITY, *j* was determined for each electrode by calculating the slopes of current vs. area of immersion lines at fixed scan rates. Current densities determined from experiments performed in different trials but using electrolytes of the same composition were most consistent on iridium (within 5%), followed by platinum (within 6%) and rhodium (within 18%). When trend lines were plotted through the average values for current density (Fig. 5.2), the data was highly linearly correlated, with R^2 values above 0.9 (Table 5.2).

The most significant finding of these plots was that the oxygen evolution current increased with increasing optical basicity. It is also to be noted that the Mo|MoO_2 quasi-reference electrode was effective as the peak positions of IrO_2 passivation and oxygen reduction were consistent across all electrolytes. Rhodium and platinum exhibited the same trends as iridium, although the current density values obtained at $\Lambda_{melt} = 0.632$ were a bit lower than anticipated. Table 5.1 lists the average current density achieved for each working electrode at 2.0V vs. Mo|MoO_2 and 20mV/s. It was important to maintain identical experimental conditions and use slow scan rates to minimize temperature effects and the contribution of the charging current to the net current. Fig. 5.2 is a plot of current density as a function of optical basicity for each working electrode at 2.0V vs. Mo|MoO_2. The trend lines are drawn with respect to the data points listed in Table 5.1.

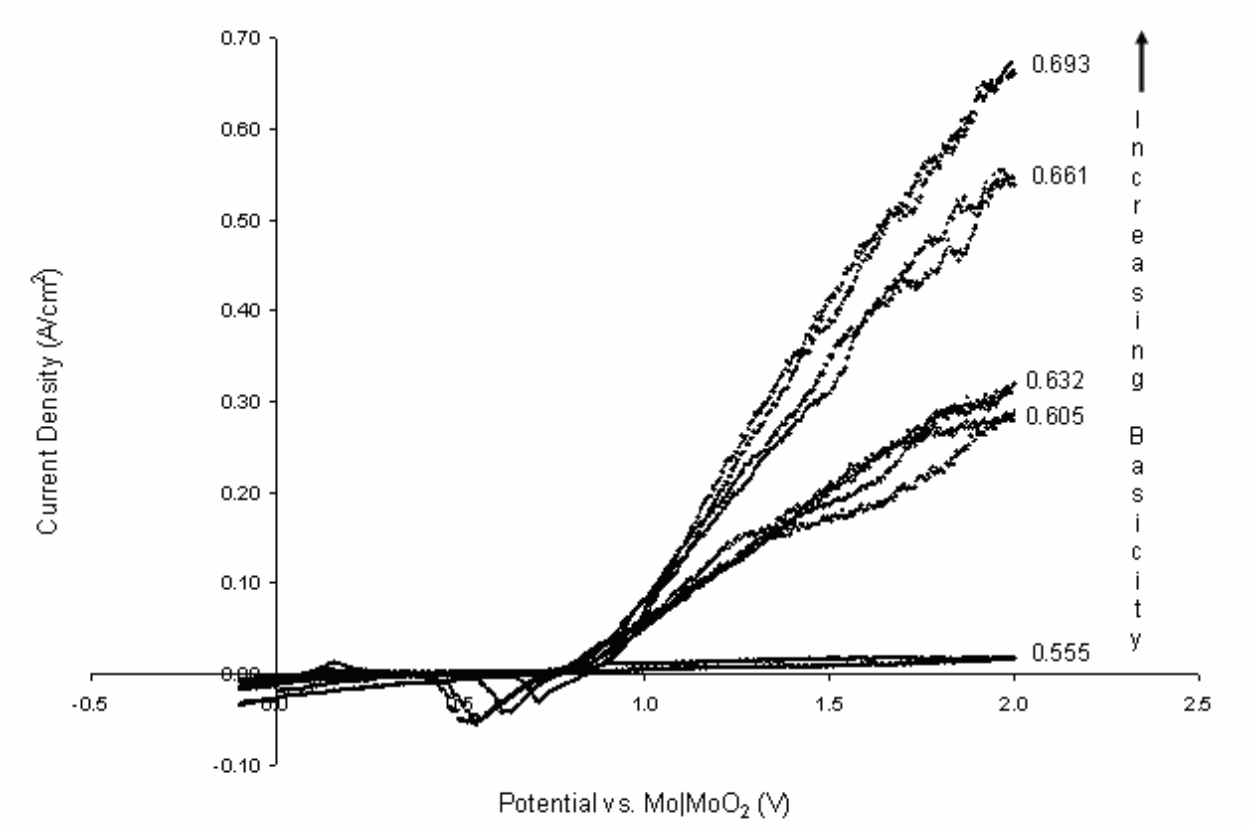

Figure 5.1 CVs with an iridium working electrode in each of the five electrolytes. Optical basicity values listed adjacent to each voltammogram. WE: 0.5mm Ir CE: Mo RE: Mo|MoO_2 Scan rate: 20mV/s

Table 5.1 Average Current Density of Working Electrode at 2.0V vs. Mo|MoO_2 and 20mV/s

		Current Density (A/cm^2)		
Melt	**Optical Basicity**	**Iridium**	**Rhodium**	**Platinum**
SCAMA1	0.555	0.018	0.030	0.025
S1A	0.605	0.276	0.278	0.245
SCAMB2	0.632	0.312	0.312	0.223
SCAMB3	0.661	0.535	0.387	0.336
SCAMB1	0.693	0.641	0.542	0.579

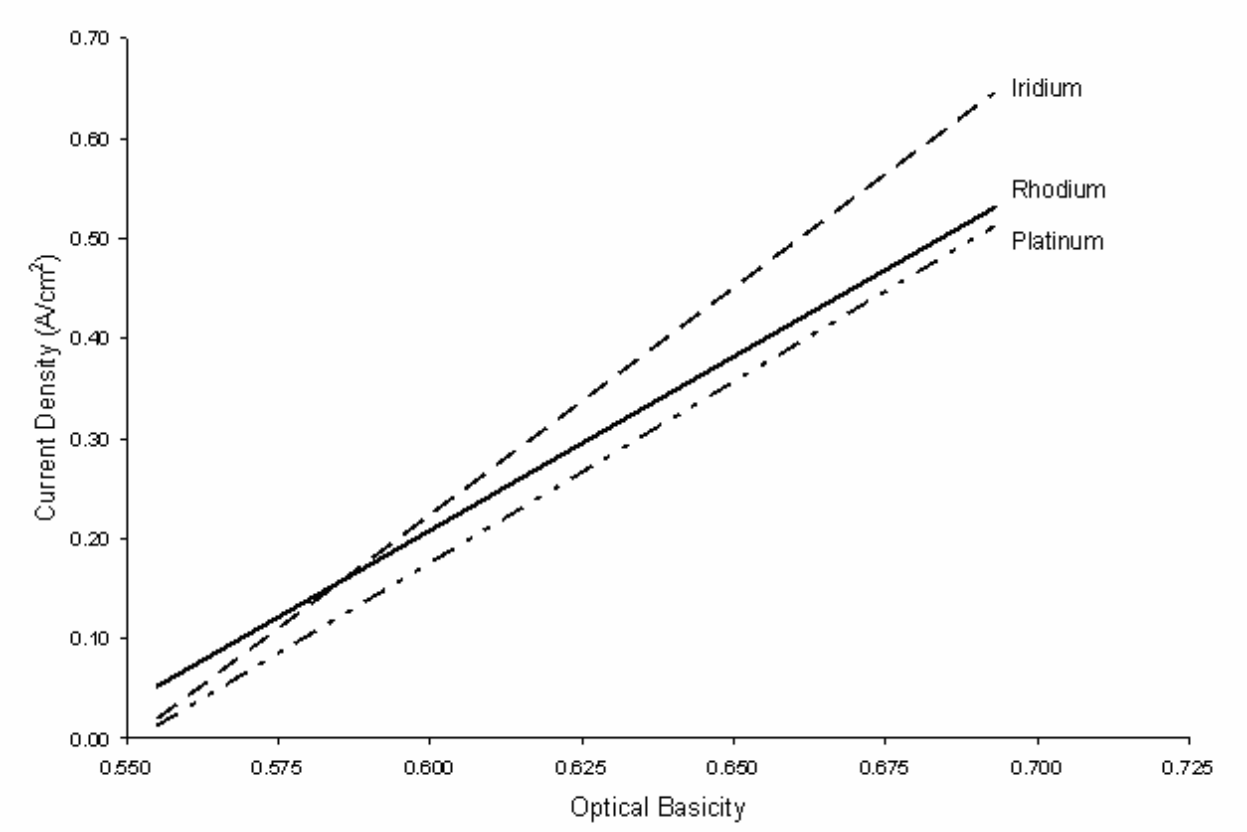

Figure 5.2 Current density as a function of optical basicity. Trend lines calculated from data points listed in Table 5.1.

Table 5.2 Equations Describing j vs. Λ_{melt} for Lines Plotted in Fig. 5.2

Working Electrode	**m**	**b**	**Correlation (R^2)**
Iridium	4.540	-2.500	0.9773
Rhodium	3.472	-1.875	0.9681
Platinum	3.621	-1.996	0.9037

The validity of the trend lines as accurately predicting current densities from other electrolyte compositions was supported by a potentiodynamic test on an iridium plate ($2.52cm^2$) in S1A + 10wt% FeO. Λ_{melt} equaled 0.626. Since the oxygen evolution current showed no dependence on the scan rate, the data from 20mV/s experiments were applicable to the near steady state conditions of the potentiodynamic trial. The estimated value for j for this composition was $0.342A/cm^2$ compared with the experimental value of $0.351A/cm^2$ at 2.0V vs. $Mo|MoO_2$. Considering the difficulties of making both accurate and precise measurements at 1575°C, agreement to within ±3% was astounding.

The notion that the current density was a linearly proportional function of optical basicity was also supported by voltammetric studies of Na_2O-SiO_2 on platinum at 1000°C[45]. This relationship was not explicitly stated in the authors' discussion. When the mole fractions were tabulated as optical basicity values (Table 5.3), and the peak current densities at 50mV/s around 0.45V vs. a Pt quasi-reference electrode were plotted (Fig. 5.3), a linear relationship was obtained. Unlike the aluminosilicate melts studied at 1575°C in this thesis, the molten sodium silicates exhibited a diffusion controlled peak and the temperature was only 1000°C. Nevertheless, a linear trend was witnessed.

Table 5.3 Optical Basicity and Peak Current Density for Na_2O-SiO_2 at 1000°C

X_{Na_2O}	X_{SiO_2}	Λ	$j(A/cm^2)$[45]
0.222	0.778	0.564	0.018
0.250	0.750	0.576	0.029
0.286	0.714	0.592	0.043
0.333	0.667	0.614	0.053
0.400	0.600	0.648	0.105

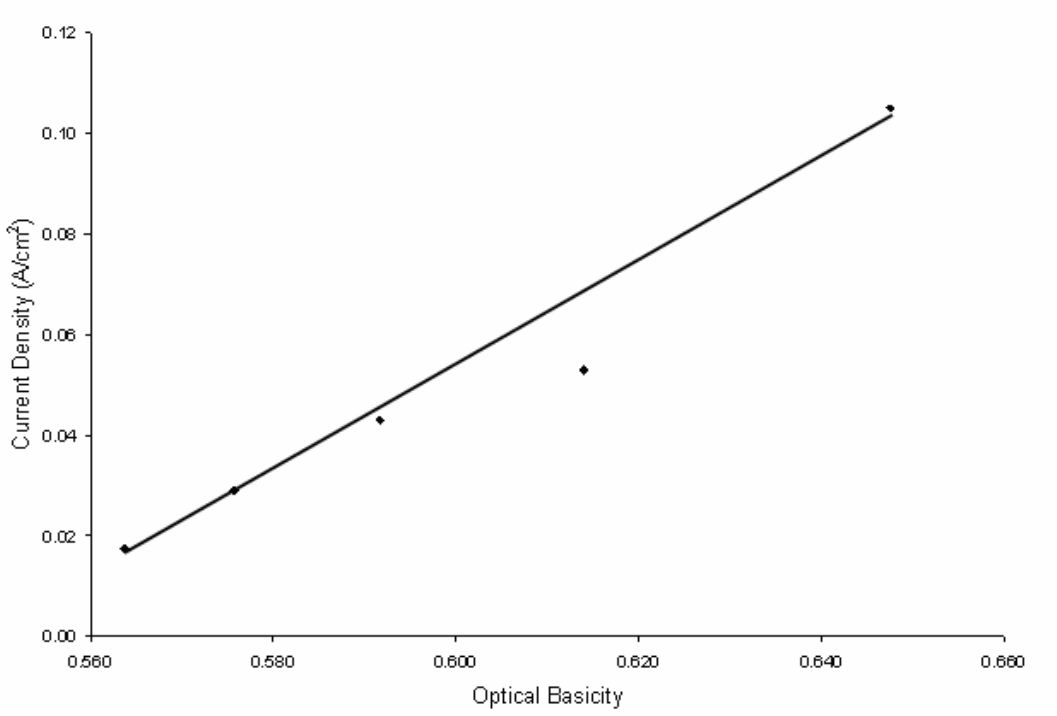

Figure 5.3 Trend obtained from reference[45] for *j* vs. Λ in molten sodium silicates at 1000°C. Note that the data point at Λ = 0.614 was omitted from the trend line. WE: 1.0mm Pt CE: Pt RE: Pt Scan Rate: 50mV/s

Since the oxygen molecules must coalesce into a critical size to form a bubble which subsequently detaches and floats away, it is worth considering the possibility that the viscosity of the electrolyte has an effect on the current density. Since the CVs (Figs. 4.2 through 4.4) revealed no dependence on scan rate, and thus no limiting current due to mass transfer of reactants or products, this seems to rule out any influence of the viscosity on the apparent electrode kinetics in these experiments. If the viscosity were high, the oxygen bubbles would have required a long time to diffuse away from the electrode surface. Any bubbles adhering to the anode would have been areas of electrochemical inactivity because the electrolyte would have been physically blocked from interacting at the anode surface. No anode effect as witnessed with CO_2 on carbon in molten salts was encountered, likely because the surface energies of O_2 on platinum group elements in molten silicates were drastically different; the bubbles need grow only to small diameters before detaching. It was likely that the viscosity was comparable in all the electrolytes studied, and therefore was not an experimental variable. This was supported by Fig. 9.87a-e, Table 9.26, and Fig. 9.96(I-VII) in the Slag Atlas[57]. From Fig.

9.87a-e, S1A, SCAMB2, and SCAMB3 were estimated to have viscosities between 7 and 9 Poise at 1500°C. A variety of synthetic blast furnace slags comprised of CaO-MgO-Al_2O_3-SiO_2 were listed and plotted in Table 9.26 and Fig. 9.96(I-VII), respectively. Remarkably, at 1575°C, all measured viscosity values fell between 3 and 4 Poise.

Even if the relationship of j with Λ_{melt} was in fact caused by a different mechanism unrelated to the free oxide concentration, there was no denying that the linear equations (Table 5.2), applicable to a wide range of molten aluminosilicate electrolyte compositions, could serve as a simple engineering scale to enhance productivity at the anode.

5.2 Relationships of j with $C^*_{O^{2-}}$ and p_{O_2}

In the previous section, it was established that the current density exhibited a linear trend with increasing optical basicity (Figs. 5.2, 5.3). It was presumed that the current density increased with optical basicity because the free oxide ion concentration increased. If there truly was a causal relationship of $C^*_{O^{2-}}$ on j, the hypothesis of increasing $C^*_{O^{2-}}$ to enhance the anodic current was correct. It was assumed there were no other variables affecting the values obtained for j. The underlying mechanism of this behavior is developed in this section.

As highlighted in 1.5.1 Basicity and the Free Oxide Ion, the proportion of free oxide ions has been found to increase with network modifier content in a roughly parabolic fashion[59-62]. Although Park and Rhee[62] studied the binary CaO-SiO_2 system while the electrolytes in this thesis were CaO-MgO-Al_2O_3-SiO_2 quaternary compositions, it was thought that by adjusting all data to the optical basicity scale, the free oxide ion concentrations would be consistent.

Park and Rhee[62] used XPS to obtain the proportion of free oxide ions in a series of glasses quenched from 1600°C. Table 5.4 adapts their data and manipulates it using molar volumes to calculate the free oxide concentration, $C^*_{O^{2-}}$, in units of mol/cm^3. Note that the notation of Park and Rhee was maintained for $X_{O^{2-}}$. This was not the mole fraction of free oxide ions in the glass but rather the proportion of the free oxide ion of the total amount of oxygen atoms. Also, values

for the molar volumes of CaO-SiO_2 mixtures were not able to be found for 1600°C, so values for 1700°C were assumed to be adequate. Figure 5.4 presents the data of Table 5.4 graphically.

Table 5.4 $C^*_{O^{2-}}$ Calculated from Proportion of Free Oxide Ions in CaO-SiO_2

X_{CaO}	X_{SiO_2}	Λ_{melt}	$X_{O^{2-}}$ [62]	V_{1700} ($10^{-6}m^3$)[59]	$C^*_{O^{2-}}$ (mole/cm^3)
0.574	0.426	0.689	0.0048	21.4	32.0 x 10^{-5}
0.520	0.480	0.663	0.0025	21.9	16.9 x 10^{-5}
0.492	0.508	0.650	0.0017	22.0	11.7 x 10^{-5}
0.448	0.552	0.630	0.0011	22.1	7.72 x 10^{-5}
0.400	0.600	0.610	0.0004	22.5	2.84 x 10^{-5}
0.352	0.648	0.591	0.0003	22.8	2.17 x 10^{-5}

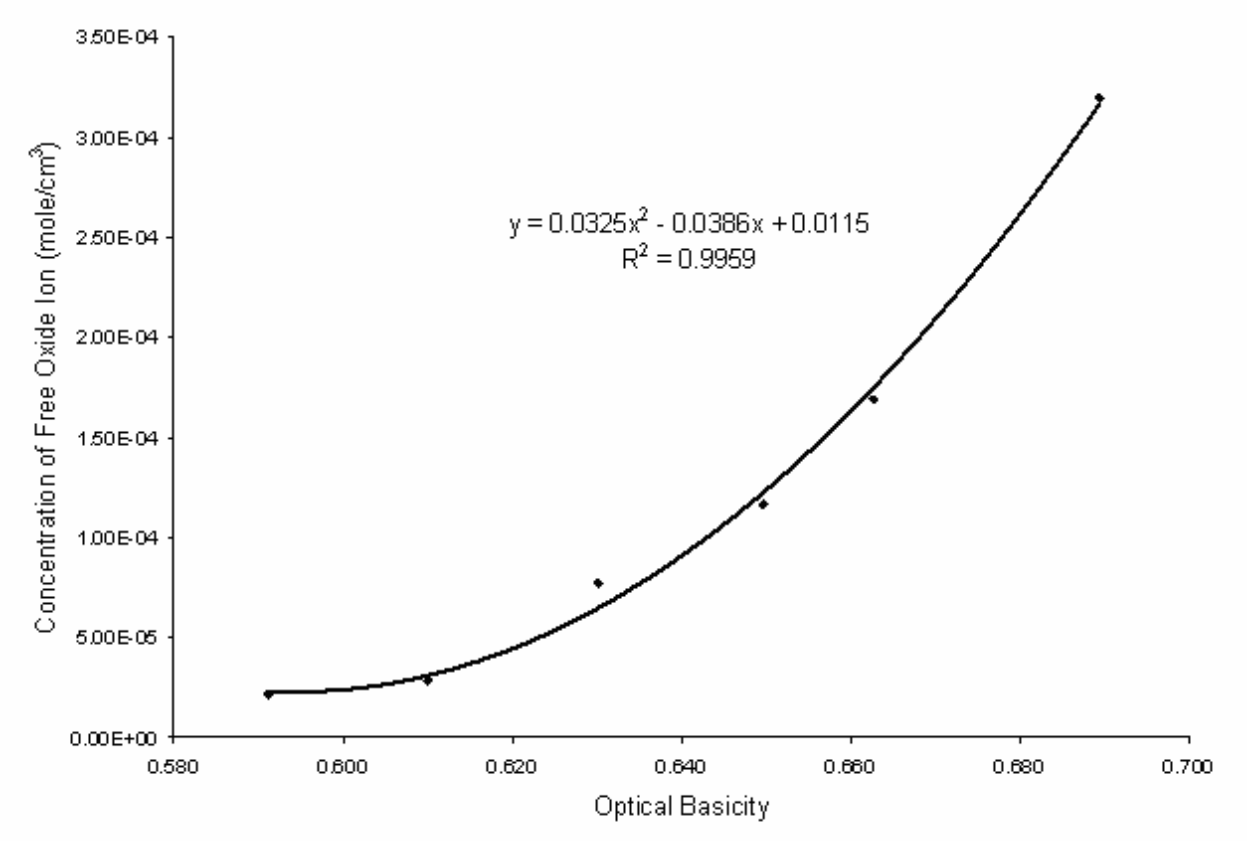

Figure 5.4 $C_{O^{2-}}$ as a function of Λ in the range of 0.60< Λ<0.70. Data points listed in Table 5.3.

Fig. 5.4 illustrates that the free oxide concentration increased with the square of the optical basicity, $C^*_{O^{2-}} \propto \Lambda^2$. From Fig. 5.2 (and Fig. 5.3, but for a different system at only 1000°C), the current density was linearly proportional to the optical basicity, $j \propto \Lambda$. The current density was therefore dependent on the square root of the free oxide ion concentration, $j \propto \sqrt{C^*_{O^{2-}}}$.

Since the parameters j and $\sqrt{C^*_{O^{2-}}}$ are proportional to one another, ratios of $j(\Lambda)$ and $\sqrt{C^*_{O^{2-}}}(\Lambda)$ should have similar values. Table 5.5 lists the calculated values for j (equations listed in Table 5.2) and $C^*_{O^{2-}}$ (equation from best fit curve in Fig. 5.4) at optical basicity points of 0.60, 0.65, and 0.70 on iridium, rhodium, and platinum electrodes. When ratios are compared for Λ = 0.70 and 0.60 and Λ = 0.65 and 0.60, the proportionality $j \propto \sqrt{C^*_{O^{2-}}}$ is undoubtedly confirmed. Except for the ratio $j_{0.70}/j_{0.60}$ calculated for the rhodium working electrode, all ratios listed in Table 5.4 were consistent. Not only were the relationships for the current density and free oxide concentration consistent, but also the ratios for current densities of the three platinum group elements were comparable, suggesting the mechanism of the reaction was the same regardless of the electrode material.

Table 5.5 Calculated Values for j and $C^*_{O^{2-}}$ as Predicted from Best Fit Lines of Figs. 5.2 and 5.3

Working Electrode	Λ	j (A/cm^2)	$C^*_{O^{2-}}$ (mol/cm^3)	$\frac{j_{0.70}}{j_{0.60}}$	$\sqrt{\frac{C^*_{O^{2-},0.70}}{C^*_{O^{2-},0.60}}}$	$\frac{j_{0.65}}{j_{0.60}}$	$\sqrt{\frac{C^*_{O^{2-},0.65}}{C^*_{O^{2-},0.60}}}$
Iridium	0.60	0.224	4.00×10^{-5}	3.0	3.2	2.0	1.9
	0.65	0.451	14.1×10^{-5}				
	0.70	0.678	40.5×10^{-5}				
Rhodium	0.60	0.208	4.00×10^{-5}	2.7	3.2	1.8	1.9
	0.65	0.382	14.1×10^{-5}				
	0.70	0.555	40.5×10^{-5}				
Platinum	0.60	0.177	4.00×10^{-5}	3.0	3.2	2.0	1.9
	0.65	0.358	14.1×10^{-5}				
	0.70	0.539	40.5×10^{-5}				

The current density appeared to be related to the square root of the concentration of the free oxide ion. Recall that the scan rate had no effect on the oxygen evolution current. It was assumed that even if there was another interfacial phenomenon such as Langmuir adsorption, the Butler-Volmer equation was applicable[92]. (See also 1.4 A FUNDAMENTAL ELECTROCHEMICAL EQUATION.) It was tempting to use these relationships as a backdoor approach to determine α_f, the transfer coefficient for the anodic reaction,

$2O^{2-} \xrightarrow{f} O_2 + 4e^-$.

The Butler-Volmer equation can be expressed in terms of current density, j, instead of current, i,

$j = Fk^0 C_{O^{2-}}^{*\alpha_f} C_{O_2(melt)}^{*\alpha_b} \left(e^{\alpha_f F\eta/RT} - e^{-\alpha_b F\eta/RT} \right)$.

All the parameters in the equation were fixed except for $C_{O^{2-}}^{*\alpha_f}$ as the electrode material (k^0), furnace atmosphere ($C_{O_2(melt)}^{*}$), temperature (T), and overpotential (η) were constant. At an overpotential of about 1.2V, the term $e^{-\alpha_b F\eta/RT}$ became trivial. Since $j \propto \sqrt{C_{O^{2-}}^{*}}$, it was apparent that α_f was on the order of 0.5. A forward transfer coefficient of 0.5 was reported by Emi, Sakuraya, and Sanbongi[46] from Tafel slopes in CaO-SiO_2 melts at 1480°C and 1590°C under an argon atmosphere. However, unlike the conclusion presented in this thesis that charge transfer limited the electrochemical reaction over a very wide range of potentials, they stated that mass transfer became rate limiting in as little as 10msec from decay curves obtained using a potentiostatic double pulse method.

The effect of adjusting the partial pressure of oxygen above the headspace in the furnace was not examined with any of the five aluminosilicate electrolytes in this thesis. By systematically changing the partial pressure of oxygen above the melt and allowing sufficient time to equilibrate, the physically dissolved concentration of oxygen molecules would have shifted in accordance with Bunsen's Law, $C_{O_2(melt)}^{*} = k(T) p_{O_2(g)}$[58]. If holding all other parameters in the Butler-Volmer equation constant, $j \propto p_{O_2(g)}^{\alpha_b}$, since $C_{O_2(melt)}^{*}$ is directly proportional to $p_{O_2(g)}$. Perhaps a value for α_b could have been determined for the reduction of oxygen molecules to free oxide ions,

$2O^{2-} \xleftarrow[b]{} O_2 + 4e^-$.

Suito and Ohtani[48] performed galvanostatic polarization measurements at 1350°C in binary alkali silicate melts and found that the exchange current density, j_0, increased with $p_{O_2(g)}$. Table 5.6 lists j_0 as a function of composition and partial pressure of oxygen for each of the binary silicates. When the values for j_0 of a fixed melt composition were plotted against $\sqrt{p_{O_2(g)}}$, in many cases, a linear relationship with high correlation was obtained (Fig. 5.5). Since $j \propto j_0 \propto p_{O_2(g)}^{\alpha_b}$ and $j_0 \propto \sqrt{p_{O_2(g)}}$, α_b was assigned a value of 0.5.

Table 5.6 Exchange Current Density (A/cm^2) as a Function of Composition and Partial Pressure of Oxygen (Adapted from Suito and Ohtani[48])

	p_{O_2} **(atm)**	**3:2**	**1:1**	**2:3**	**1:2**
Li_2O-SiO_2	1	0.185	0.180	0.160	0.135
	0.21	0.150	0.150	0.120	0.130
	0.03	0.130	0.120	0.105	0.110
Na_2O-SiO_2	1	0.505	0.240	0.170	0.135
	0.21	0.310	0.200	0.140	0.155
	0.03	0.230	0.145	0.135	0.125
K_2O-SiO_2	1	–	0.290	0.240	0.230
	0.21	–	0.290	0.225	0.230
	0.03	–	0.155	0.140	0.150

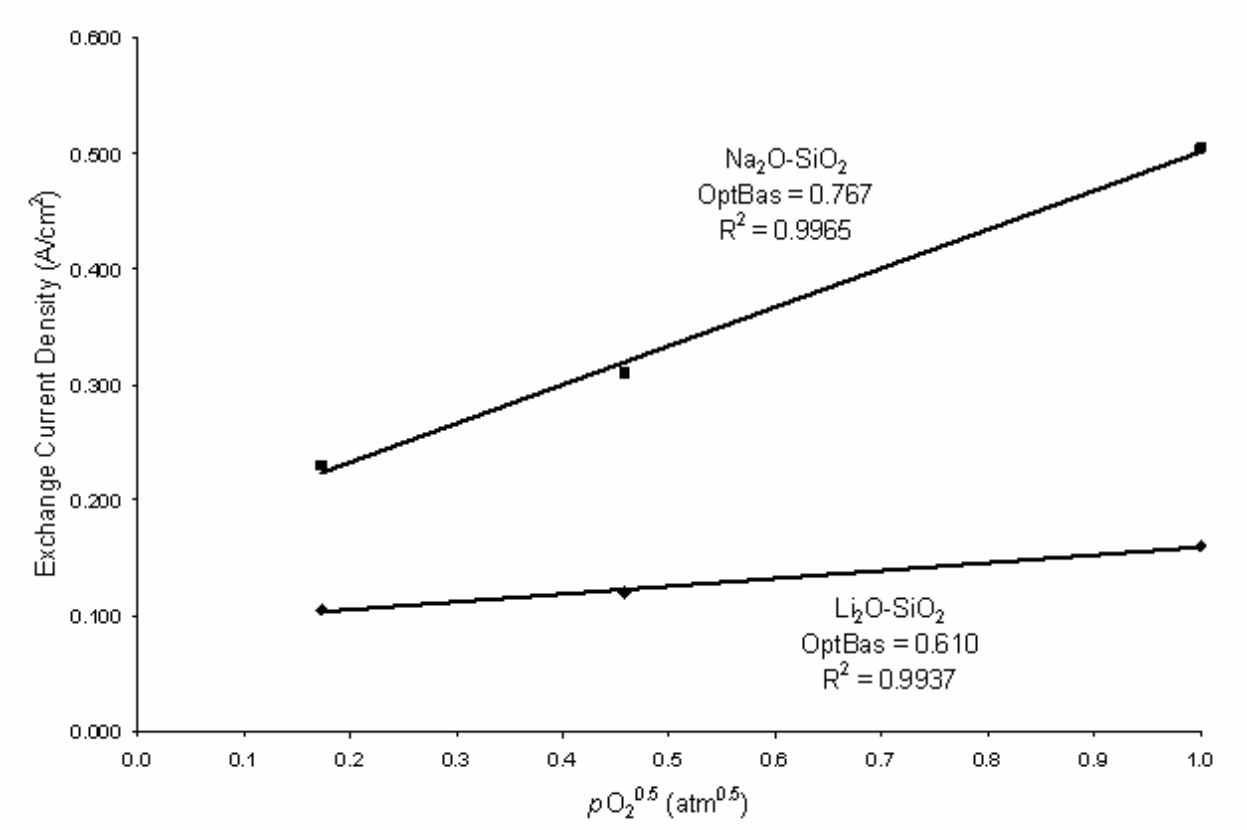

Figure 5.5 j_0 plotted against $\sqrt{p_{O_2(g)}}$ to estimate α_b. Data points listed in Table 5.6. The $3Na_2O{:}2SiO_2$ and $2Li_2O{:}3SiO_2$ melts were plotted to illustrate the trend over a wide range of optical basicity values.

The transfer coefficients, α_f and α_b have been determined to be 0.5 from the relationships of current density with the optical basicity (and therefore the concentration of free oxide ion) and exchange current density with the partial pressure of oxygen. The values of transfer coefficients should have been corroborated from Tafel slopes; however, when attempts were made to fit the data from CVs out to 2.0V vs. Mo|MoO_2, no conclusions could be drawn for α because the plots were nonlinear. Also complicating this treatment was the anodic current occurring prior to oxygen evolution due to the formation of metastable oxide films on iridium and rhodium.

The following two equations are useful to describe the mechanisms of multi-electron, multi-step reactions[47]:

$$\alpha_f = \frac{\gamma_f}{\nu} + r\beta$$

$$\alpha_b = \frac{n - \gamma_b}{\nu} - r\beta$$

In these equations, γ is the number of electrons transferred prior to the rate determining step, υ is the number of occurrences of the rate determining step, r is number of electrons transferred at the rate determining step, β is the symmetry coefficient, n is the number of electrons for the overall reaction, and f and b denote forward and back reactions. Assuming the values for α_f and α_b were 0.5, and that the activation barrier of the rate determining step was symmetric ($\beta = 0.5$), the following values were suggested[47]: $\gamma_f = 1$, $r = 0$, $\upsilon = 2$, $\gamma_b = 1$, $n = 2$. A value of $r = 0$ could make sense if two monoatomic oxygen or two O^- species chemically bonded at the rate determining step. However, $n = 2$ did not support the overall reaction $2O^{2-} \rightarrow O_2(g) + 4e^-$. Proper determination of the mechanism for oxygen evolution and reduction would require carefully constructed experiments to extract values for α_f and α_b. Then, by calculating values for γ_f, r, υ, γ_b, and n, the exact model for oxygen evolution and reduction could be inferred, along with all species involved including but not limited to O^{2-}, $O^-(ads)$, $O_2^{2-}(ads)$, $O_2^-(ads)$, $O(ads)$, and $O_2(g)$.

While a crude estimate for enhancing the current density of the anodic reaction has led to values for α_f and α_b of 0.5, it was clear that more needs to be done in this area if an exact mechanism is desired. Despite the disparity of $n = 2$ when an overall reaction suggested $n = 4$, the correlation of current density with $C^*_{O^{2-}}$ and p_{O_2} is strong and will certainly impact the operation of the molten oxide electrolysis cell.

Aside from the relationship of exchange current density with the partial pressure of oxygen, the data in Table 5.6 also qualitatively supported the concept that the most basic network modifiers contributed the most free oxide ions to the melt. From Table 1.2, $\Lambda_{K_2O} > \Lambda_{Na_2O} > \Lambda_{Li_2O}$. The optical basicity of the silicate melt has been correlated to a higher concentration of free oxide ions, and thus a higher exchange current density. In Table 5.6, for the same molar ratio of

M_2O:SiO_2, the highest values for j_0 were reported for K_2O-SiO_2, followed by Na_2O-SiO_2 and Li_2O-SiO_2.

5.3 Behavior of the Free Oxide Ion in the Electrolyte

Undoubtedly, the free oxide ion is the anionic species that participates in electrochemical reactions at the anode. Several authors have drawn this conclusion, but little evidence has been provided to support this claim[27,44,45,48]. Perhaps they believed the idea was too elementary or obvious. Or, in many cases, since they were not posed with the task of enhancing the current density under electrolysis conditions, they never had reason to question the matter further. Whatever the lack of an authoritative basis may have been, the arguments presented in the previous section provided a strong case connecting the current density with the free oxide ion concentration.

A semi-quantitative connection between the anodic current and the concentration of the free oxide ion was found in only one reference. Interestingly, LaFage and Taxil[27] suggested that the product $j\tau^{1/2}$ could be useful as an index of the basicity in soda-lime-silicate glasses. The Sand equation has a linear dependence on concentration (assuming that the diffusion coefficient is independent of concentration)[27],

$$j\tau^{1/2} = \frac{\pi^{1/2} nFC^*_{O^{2-}} D^{1/2}}{2}.$$

Straight lines were obtained for their melts at 1100°C under an air atmosphere, but they went no further to elaborate on the idea that the current was functionally dependent on the free oxide ion concentration.

Several authors performing feasibility studies of molten oxide electrolysis from lunar regolith, notably from the same university, were of the school of thought that the free oxide ion concentration was too low (10^{-5} mol/L = 10^{-8} mol/cm^3) in molten silicates to sustain electrolytic current[8,10,65]. Not only was $C^*_{O^{2-}}$ low and assumed to be buffered over a wide range of compositions, but the formation of new O^{2-} from silicate polymer chains was thought to be a kinetically slow process. In stark contrast to these claims, the free oxide ion concentration was

found to range from 5 x 10^{-5} to 4 x 10^{-4} mol/cm^3 (3 to 4 orders of magnitude greater and spanning 1 order of magnitude in range) in melts of similar composition at comparable temperatures. Additionally, from NMR studies, the chemical exchanges among different forms of oxygen in molten silicates have been found to be very rapid[45].

The following concepts elucidate the nature of the free oxide ion in the melt under electrolysis conditions:

- The free oxide ion exists as a discrete entity in molten silicates, throughout the bulk and in the vicinity of the anode. It is expected to be the most easily available source of oxygen anions at the anode since it is not covalently bound to network formers.

- As the free oxide ions are consumed at the anode, a chemical potential gradient is established from the bulk electrolyte to the electrode with a higher concentration of O^{2-} in the bulk. O^{2-} ions diffuse down this gradient at sufficiently high rates (no mass transfer effects have been witnessed in this work) resulting in a slight polymerization of the bulk electrolyte as exchanges of the form $2(Si_nO_{3n+1})^{-2n-2} \Rightarrow (Si_{2n}O_{6n+1})^{-4n-2} + O^{2-}$ occur.

- Concomitantly, as cations from network formers such as Si^{4+} and tetrahedrally coordinated Fe^{3+} are consumed at the cathode, the melt in the vicinity of the cathode becomes enriched with excess oxygen, depolymerizing the silicate structure. Perhaps these cathodic reactions can be depicted as the following:

  $SiO_4^{4-}(melt) + 4e^- \Rightarrow Si(l) + 4O^{2-}(melt)$

  $FeO_2^-(melt) + 3e^- \Rightarrow Fe(l) + 2O^{2-}(melt)$.

  Reactions of network modifying cations which are present in the melt to charge balance the negative polyanionic clusters likely do not involve free oxide ions:

  $Fe^{2+}(melt) + 2e^- \Rightarrow Fe(l)$.

  Since network modifiers have high values for Λ_{oxide} (Table 1.2), consumption of their cations at the cathode should effectively decrease Λ_{melt}. When comparing a melt containing FeO

with an electrolyte free of FeO with the same molar ratios of CaO-MgO-Al_2O_3-SiO_2, it is apparent that the melt free of FeO will have the lower Λ_{melt} and hence the lower free oxide ion concentration. This is consistent with O^{2-} being consumed at the anode but not being regenerated at the cathode.

Since network formers have low values for Λ_{oxide}, consumption of their cations at the cathode should effectively increase Λ_{melt}. If SiO_4^{4-} clusters are considered, more free oxide ions are generated at the cathode than are consumed at the anode per Si^{4+} (4 vs. 2). This increases the free oxide ion concentration.

- Reactions at both polarized electrodes send a ripple across the electrolyte, otherwise the anodic reaction would be deprived of free oxide ions. Thermodynamically, the equilibrium distribution of anionic species is desired by the bulk electrolyte. The exchanges of oxygen throughout the melt are rapid (as suggested by NMR[39]) to attain the equilibrium distribution of O^{2-}, SiO_4^{4-}, $Si_2O_7^{6-}$, $Si_3O_{10}^{8-}$, etc. This equilibrium is predominantly established by the composition of the electrolyte with more basic melts possessing a higher proportion of free oxide ion, orthosilicate units, and pyrosilicate units as opposed to acidic melts containing fewer free oxide ions, longer chains, and ring structures.

There is some evidence supporting these ideas from constant current electrolysis experiments performed in S1A+10wt%FeO. Fig 5.6 is a plot of the voltage of an iridium anode separated from a molybdenum cathode by 1.75in (4.45cm) at 2.0A and 1575°C. The voltages reported are vs. Mo|MoO_2 positioned 0.875in (2.22cm) from the anode with no *iR* compensation. First, the voltage is oscillating, indicative of gaseous oxygen evolution. Second, the potential of the electrode increased very slowly with time. Referring back to Fig. 5.1, to maintain the same current density with decreasing Λ_{melt}, the potential must increase. This is witnessed qualitatively in Fig 5.6.

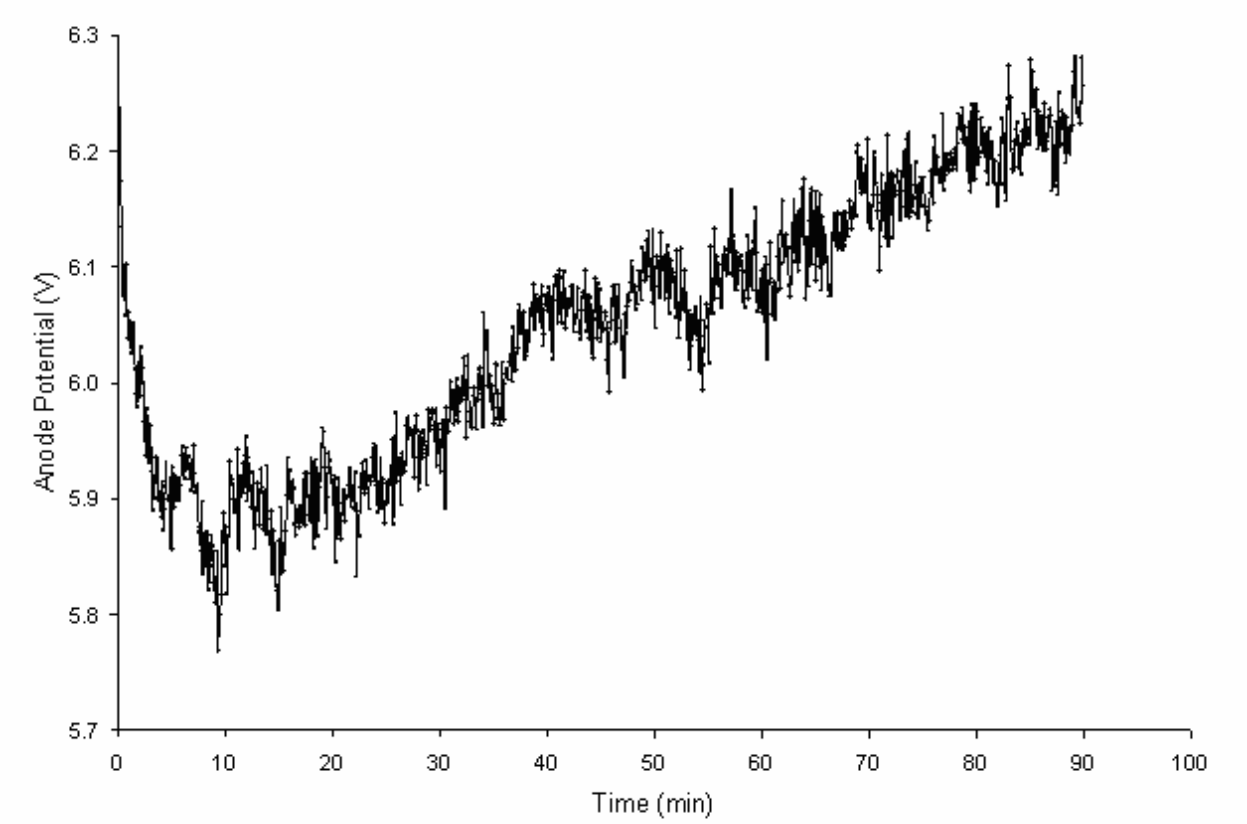

Figure 5.6 Potential of the anode vs. Mo|MoO_2 during constant current electrolysis at 2.0A. Anode: Ir Cathode: Mo RE: Mo|MoO_2 Melt: S1A+10wt%FeO

A high current efficiency of 90% was suggested by Simnad, Derge, and George[93] in binary melts of FeO-SiO_2 under flowing argon at iron oxide concentrations <70wt%. Assuming this electrolyte behaved similarly, the amount of oxygen gas evolved during electrolysis of 2.0A for 90min would have been 0.025mol. The total volume of the electrolyte was only about 65cm^3. Assuming the FeO behaved similarly to CaO, a melt with an optical basicity of 0.626 would merely contain 0.0047mol of O^{2-} initially (Fig. 5.4). Either the current efficiency was extremely low or the free oxide concentration in the bulk electrolyte was replenished from cathodic reactions involving either FeO_2^- or SiO_4^{4-}. Quite interestingly, for CaO-Al_2O_3-SiO_2 and MgO-Al_2O_3-SiO_2 melts under air at 1550°C with iron oxide concentrations of 5wt% and Al/(Al+Si) = 0.334, for NBO/T approximately equal to 1.1, trends in Fe^{2+}/Fe^{3+} approached 0.5[60]. S1A+10wt%FeO was very near these values of Al/(Al+Si) and NBO/T. If the cathodic reactions can be described by

$$2\left(FeO_2^-(melt) + 3e^- \Rightarrow Fe(l) + 2O^{2-}(melt)\right)$$

$$Fe^{2+}(melt) + 2e^- \Rightarrow Fe(l),$$

and if the anodic reaction for the equivalent number of electrons can be represented as

$$2\left(2O^{2-}(melt) \Rightarrow O_2(gas) + 4e^-\right),$$

the free oxide concentration remains constant. Hence, the potential at the anode remains essentially constant. The slight increase in the potential (Fig. 5.6) was likely due to a higher proportion of Fe^{2+} in the melt. Another consideration was that the resistance of the electrolyte increased slightly with the removal of network modifying Fe^{2+}.

5.4 Implications for Scale-Up

5.4.1 Recommendation for Inert Anode

The data presented in Table 5.1 and Fig. 5.2 suggested that iridium would be the best candidate to utilize as an inert anode, while rhodium and platinum were comparable. The trend lines indicated the current density achieved on iridium was highest; iridium was the most active anode material. Even if one contended that the trend lines in Fig. 5.2 were not statistically differentiable, iridium would still be the best candidate for future development. Iridium has the highest melting temperature at 2446°C (2719K), followed by rhodium at 1964°C (2237K) and platinum at 1768°C (2041K). Iridium should therefore exhibit the best creep resistance and mechanical stability at the cell operating temperature forecasted to be around 1600°C (1873K) because it has the highest homologous temperature, T_{cell}/T_{mp}.

Iridium also possesses the lowest vapor pressure of the candidate anodes[94,95]. Future work will determine whether the value is acceptable as any losses of the platinum group metals will be costly due to their very high prices. Another drawback to using iridium is its scarcity. Production tends to fall short of industrial requirements despite many of its superior properties[96].

As to why iridium possessed the best current density (Fig. 5.2), the answer remains unclear. Without additional tests to extract k^0 and the true surface area (which is a function of surface roughness at 1575°C), the reason for $j_{Ir} > j_{Rh} \sim j_{Pt}$ cannot be determined. From the data presented

in Fig. 5.2, iridium performed best in terms of current generated per change in geometric surface area. Since the anode shape and depth of immersion will define the macroscopic contact area of the anode/electrolyte interface, this metric is satisfactory to the engineer designing the molten oxide electrolysis cell. With expensive materials in highly corrosive melts, minimizing the amount of interfacial contact area while maintaining the requisite level of operation is sensible and "good enough". But to the fundamental electrochemist, discerning whether the higher performance of iridium is due to a better catalytic property or rougher surface is important. Monitoring the surface roughness in aqueous electrochemistry prior to testing in molten silicates is trivial because the morphology will surely be reconstructed at 1575°C to minimize surface energy. The operating temperature of the molten oxide electrolysis cell would enhance diffusion along the surface of the grains, most likely yielding a very smooth surface. If iridium, rhodium, and platinum had comparable surface roughness, then k^0 of iridium would be highest. However, it may very well be possible that $k^0_{Ir} < k^0_{Pt}$ but roughness(Ir) > roughness(Pt), or vise versa. Unless there was a way to quench the working electrode from 1575°C with no change in morphology or monitor its surface *in-situ* to determine the roughness and therefore the true surface area, only the metal with the greatest product of k^0 *and* surface roughness can be concluded as best barring other operational issues such as volatility, solubility, and cost.

5.4.2 Increase the Optical Basicity of the Electrolyte

As described previously in 5.1 Current Density as a Function of Optical Basicity, increasing the optical basicity of the melt greatly influenced the performance of the anode. Referring back to Fig. 5.1, up to 2.0V vs. Mo|MoO_2, the anodic current density trajectories were divergent over the range of electrolytes. The process engineer can interpret this plot in several ways. The foreseeable design of the molten oxide electrolysis cell will utilize constant current. Melts of higher optical basicity will require less overvoltage for the same current density, i.e., the same throughput can be achieved with higher power efficiency. It is doubtful that a constant potential configuration would be built; however, if the overpotential at the anode was held constant, the same power consumption would lead to a higher output. In both scenarios, the efficiency of the molten oxide electrolysis cell would be enhanced in melts of greater optical basicity.

Increasing the concentration of network modifying oxides (hence increasing the optical basicity) would also decrease the resistivity of the electrolyte[97]. The potential drop across the electrodes amounts to a decrease in power efficiency and is influenced by the anode/cathode separation distance and resistivity of the melt. Since the anode/cathode separation distance must be large enough to prevent the interaction of gaseous oxygen and molten metal, decreasing the melt resistivity is the only tunable parameter once the interelectode spacing has reached its lower limit. This trend can be shown qualitatively from considerations of the uncompensated resistances of 0.5mm diameter iridium working electrodes immersed around 13mm to have surface areas around $0.2cm^2$ (Fig. 5.7). The distance between the working and reference electrodes was roughly 0.875in (2.22cm) in each experiment. Since the geometry was fixed, R_u was an indicator for the melt resistivity.

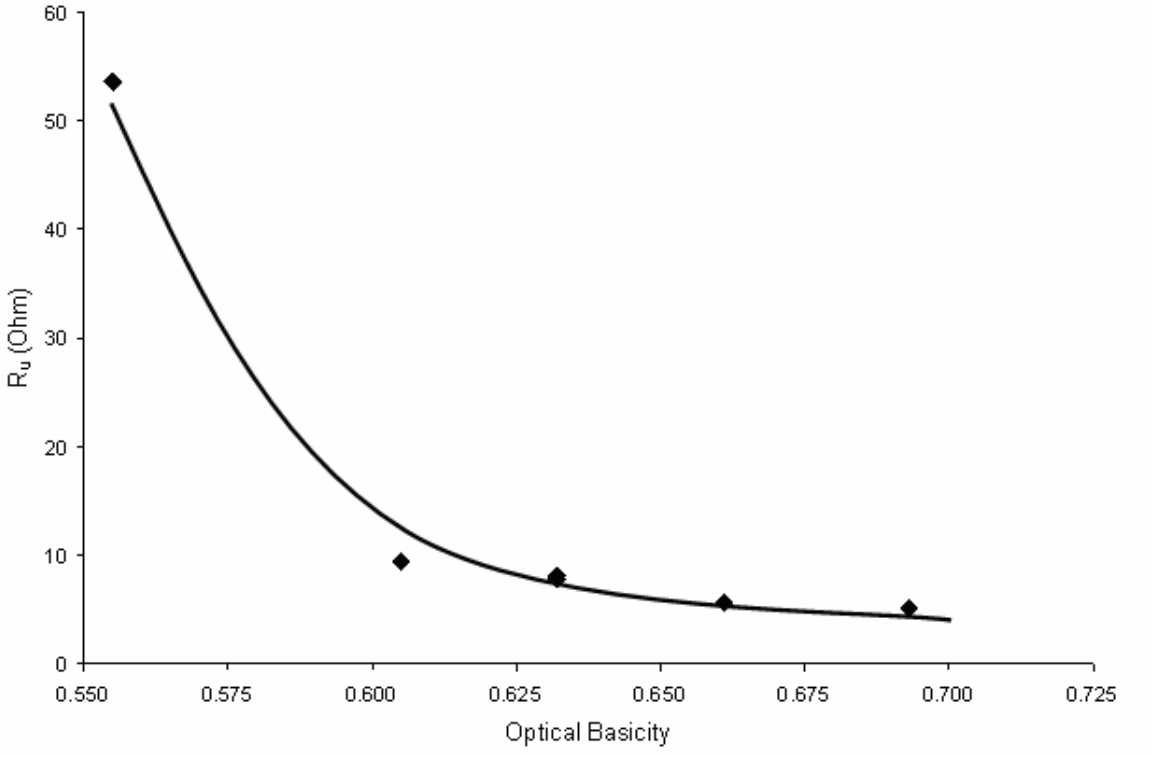

Figure 5.7 Trend on melt resistivity (as indicated by R_u) plotted against optical basicity. Line drawn freehandedly and merely intended to guide the eye.
WE: 0.5mm Ir CE: Mo RE: Mo|MoO_2 WE/RE separation distance: 0.875in (2.22cm)

Important relationships that were not monitored in this thesis were how the optical basicity and atmosphere above the electrolyte influenced the redox states of iron. A higher optical basicity is

anticipated to favor Fe^{3+}[58]. This is important for several reasons. First, if the iron exists predominantly as either Fe^{2+} or Fe^{3+}, the likelihood of cell shorting is greatly minimized. The current will be predominantly transferred by ions as opposed to semicondution or polaron hopping[33]. Second, if the majority of the iron in the electrolyte was already present as Fe^{3+}, the following reactions would be greatly diminished:

$$Fe^{2+}(melt) \Rightarrow Fe^{3+}(melt) + e^{-}$$

$$Fe^{2+}(melt) + \tfrac{1}{2} O_2 \Rightarrow Fe^{3+}(melt) + O^{2-}(melt).$$

Limiting these reactions will maintain high current efficiency of the electrolysis cell.

Increasing the optical basicity is appealing for a variety of reasons, but one must not get too carried away with adding basic constituents like CaO and MgO, or else the system will not be molten at 1575°C. Increasing the operating temperature is undesirable because it would further decrease the already narrow field of candidates for the inert anode, and it would more rapidly degrade the components of the electrolysis cell. Also, since the source of energy for maintaining the cell operating temperature is the Joule heating of the electrolysis current, there may be a lower bound on electrolyte resistivity or else the Joule heating might be insufficient.

In 5.2 RELATIONSHIPS OF j WITH $C^{*}_{O^{2-}}$ AND p_{O_2}, the exchange current density was found to increase with increasing p_{O_2}. This observation would be trivial once the molten oxide cell is operational because p_{O_2} would increase from 0.21 and approach 1.

5.5 SUMMARY

Adjusting the optical basicity of the electrolyte greatly enhanced the current density on the anode. The underlying reason was found to be the increase in the concentration of the free oxide ion. The current density scaled as $j \propto \sqrt{C^{*}_{O^{2-}}}$ and $j \propto \sqrt{p_{O_2(g)}}$, but since the partial pressure of oxygen is expected to be high in a functional molten oxide electrolysis cell, altering the electrolyte composition would be the more effective means at achieving a higher current density.

The free oxide ion was present in large enough quantities to sustain electrolytic current. A scheme including reactions at the anode, cathode, and bulk electrolyte was proposed in which the free oxide ion concentration varied with the composition of the melt, a value that slowly decreases with depletion of network modifiers and slowly increases with depletion of network formers.

Iridium was the best anode because it provided the greatest current density. When other properties like its low volatility and high mechanical stability at elevated temperatures were considered, iridium stood out as a superior candidate for an inert anode.

Increasing the optical basicity of the melt would impact the power efficiency as a lower overpotential would be required to achieve the same current density in a melt of higher basicity. The electrolyte resistivity would also be lower for a more basic melt, further enhancing the power efficiency. Since the redox states of multivalent ions are impacted by the basicity of the electrolyte, it may also be possible to minimize oxygen solubility and redox looping, thus improving the current efficiency of the electrolysis cell.

CHAPTER 6: FUTURE CONSIDERATIONS

Over the duration of the past sixteen months of designing and conducting experiments, surveying a wealth of literature across many fields, and interpreting results, many interesting conclusions have been drawn. For each result, positive or negative, meaningful or inconsequential, new questions arose. The following questions are posed with some remarks or references for the next round of research.

Could a ceramic material function as an inert anode? (Refer to 2.4.1.2 CERAMICS)

> Had it not been for the difficulty of obtaining or fabricating fully dense ceramics, SnO_2 and Cr_2O_3 would have been considered for study. Yttria stabilized ZrO_2 (YSZ) closed one end tubes (McDanel) were purchased as was silver (Alfa Aesar), but a working electrode was never constructed. The YSZ would have served as an oxygen ion conductor. Since silver oxides are unstable at elevated temperatures[86] and silver has melting point of 962°C, gaseous oxygen would have bubbled from this anode. In the presence of iron oxide containing melts, YSZ was predicted to degrade[77], so pursuing this design may have been a futile endeavor.

Could a reference electrode be developed to withstand highly oxidizing atmospheres as well as be stable in the presence of electrolytes containing iron oxide? (Refer to 2.4.3 REFERENCE ELECTRODE)

> A new reference electrode may simply be a quasi-reference electrode composed of platinum or iridium. This would surely withstand oxygen rich atmospheres. Possibly, the ceramic shroud of the $Mo|MoO_2$ electrode could be positioned such that the molybdenum surface is not exposed to the gases in the furnace tube. Or, by depositing a $MoSi_2$ intermetallic phase on the exposed surface of the molybdenum rod above the melt line, a passivating layer of SiO_2 would protect the Mo from oxidation.

Rather than a vertical crucible furnace, could a different furnace be used? (Refer to 3.3 FURNACE ASSEMBLY and 2.3 FURNACE TUBE AND CAP CONSTRUCTION)

The furnace utilized in these experiments was a vertical crucible furnace. While this design was good for maintaining atmospheres of inert gases, large batches were required, expensive alumina crucibles were single-use, and the heating and cooling times were very slow to avoid thermally stressing the alumina furnace tubes. If studies are pursued to determine the oxygen solubility in the melt, solubility of anode materials under polarization, and redox ratios of transition metal ions, perhaps an elevator hearth furnace should be used. Since the molten oxide electrolysis cell will operate in oxygen-rich atmospheres, the results would accurately represent the behavior in practice.

Could the nature of the passivation peaks on iridium and rhodium be ascertained by the Point Defect Model[88] as proposed in 4.2.2 IDENTIFICATION OF PHASES FORMED?

The current density has been shown to vary linearly with the optical basicity for CaO-MgO-Al_2O_3-SiO_2 melts. Are comparable values for j obtained in electrolytes comprised of different constituent oxides but with the same Λ_{melt}? (Refer to 5.1 CURRENT DENSITY AS A FUNCTION OF OPTICAL BASICITY and APPENDIX B)

A Li_2O-Al_2O_3-SiO_2 (19.362-15.068-65.570 wt%) melt decomposed the alumina crucible rapidly because alumina was highly soluble. Also a white, powdery residue was found under the furnace cap owing to the volatility of alkali metal oxides. The answer to this question is important because it would bolster the notion that the optical basicity gives the global concentration of the free oxide ion; thus the current density at a fixed overpotential could serve as a direct measurement of $C^*_{O^{2-}}$. It would not alter the proposed usage of CaO-MgO-Al_2O_3-SiO_2 melts in the molten oxide electrolysis cell.

Could XPS measurements be performed on CaO-MgO-Al_2O_3-SiO_2 melts to quantify $C^*_{O^{2-}}$? (Refer to 5.2 RELATIONSHIPS OF j WITH $C^*_{O^{2-}}$ AND p_{O_2})

Because the electrolyte compositions used were primarily CaO and SiO_2 and the optical basicity gave the proportion of free oxide ions[57], it was assumed that the trend of $C^*_{O^{2-}}$ vs.

Λ_{melt} (Fig. 5.4) was applicable to CaO-MgO-Al_2O_3-SiO_2 systems. Rather than use this approximation, a direct measurement would have been preferable.

The values for α_f and α_b were suggested to be 0.5. However, these values did not possess a corresponding mechanism that fit the reaction $2O^{2-} \rightarrow O_2(g) + 4e^-$. Could Tafel plots be constructed to determine the oxygen evolution reaction sequence as well as determine the rate limiting step? (Refer to 5.2 RELATIONSHIPS OF j WITH $C^*_{O^{2-}}$ AND p_{O_2})

This information is desirable to someone interested with fundamental electrochemistry. It is to be noted that determination of these parameters may enhance the performance of the inert anode if the surface of the anode can be altered to hasten the rate limiting step. However, since the temperature of the molten oxide electrolysis is so high, any surface modifications to catalyze the oxygen evolution reaction are unlikely to last, either by degradation or diffusion into the bulk of the anode. This may in fact be a futile effort for enhancing the current density.

Could the electrolyte be separated into an anolyte and catholyte to interrogate the behavior of the free oxide ion? (Refer to 5.3 BEHAVIOR OF THE FREE OXIDE ION IN THE ELECTROLYTE)

It was suggested that the free oxide ion concentration was replenished by polymerization reactions and reduction of network forming cations such as Si^{4+}. If a cation conducting refractory material was stable at elevated temperatures, perhaps the electrolysis cell could be separated into an anolyte and catholyte. After constant current electrolysis, the solidified silicates could be analyzed for their composition and free oxide concentration.

What are the effects of adding iron oxide to the electrolyte? (Refer to 5.3 BEHAVIOR OF THE FREE OXIDE ION IN THE ELECTROLYTE and 5.4.2 INCREASE THE OPTICAL BASICITY OF THE ELECTROLYTE)

Except for an electrolysis experiment performed in S1A+10wt%FeO, all of the melt compositions considered were free of transition metal oxides. The addition of transition metal oxides (especially iron oxide in the context of steelmaking) may pose challenges for implementation and optimization of molten oxide electrolysis cells. The behavior of iron oxide in melts used in this thesis has yet to be determined.

Simnad, Derge, and George[93] suggested a high current efficiency of 90% in binary melts of FeO-SiO_2 at FeO concentrations <70wt%. Since the atmosphere was depleted of oxygen except for the small quantity generated during electrolysis, the Fe^{3+} content in the bulk electrolyte was expected to be very low. Hence, shorting via semiconduction and/or polaron hopping due to multivalent states was greatly diminished[33]. However, if the oxygen content of the headspace in the furnace tube was high and allowed to equilibrate with the molten silicate, the Fe^{3+} content of the melt would have been much higher. Determination of the Fe^{3+}/Fe^{2+} ratio as functions of optical basicity, p_{O_2}, and iron oxide loading is suggested if shorting occurs. The equilibrium concentration of Fe^{3+}/Fe^{2+} in the melt should also be determined in the presence of liquid iron. These ratios can be determined using Mössbauer spectroscopy, colorimetric wet chemical techniques, or possibly by square-wave voltammetry[27,60].

The molten oxide electrolysis cell will operate under highly oxidizing conditions due to both the oxygen rich atmosphere and the proposed high basicity melt. Yang and Belton[98] have determined the Fe^{3+}/Fe^{2+} ratios for slags of similar composition to the electrolytes studied in this thesis over a range of basicity and p_{O_2} values. Fe^{3+} is highly favored at high basicity and p_{O_2}. Furthermore, iron ore is predominantly ferric in nature. Compared with cathodic reduction of Fe^{2+} in acidic melts of low basicity, Fe^{3+} would require an additional electron. But the gains in voltage efficiency and throughput far outweigh the decrease in iron deposited per electron. Actually, if detrimental effects of redox looping and oxygen solubility at the anode are mitigated and factored, the current efficiency may be greater to run in a cell containing predominantly Fe^{3+}.

Iridium has been chosen as the inert anode candidate for future development. Iridium has a low volatility but a very high price. How can the composition of the inert anode be altered to minimize the iridium content and volatile losses? (Refer to 5.4.1 RECOMMENDATION FOR INERT ANODE)

Alloying with a metal of significantly lower cost may be a viable option, especially if the alloy resists oxidation or spalling. A thick anode containing a large fraction of the iridium within its core is not an effective use of the iridium. Perhaps the inert anode would exhibit

great enough strength to be fabricated as a thin-walled tube with an end cap. If not, maybe the iridium alloy can be plated on a refractory metal substrate. The extremely high operating temperatures would require a barrier to the interdiffusion of the iridium and the refractory metal substrate.

One idea for minimizing volatile losses of iridium is the incorporation of a diffusion barrier on the surface. Perhaps a readily oxidizable element whose stable oxide possesses a matching biaxial modulus can be incorporated into the alloy. Above the melt line, the iridium would be jacketed by the diffusion barrier, but where the anode is in contact with the molten electrolyte, the oxide phase would dissolve into the melt. Assuming its expansion coefficient is comparable to iridium, an ideal candidate would be alumina. Alumina would not contaminate the electrolyte or the pool of molten metal at the cathode. The alloy composition adjacent to the molten electrolyte would be depleted of aluminum, but since iridium is the electroactive material, there would be no detraction in the performance of the anode.

What is the best means to determine the current efficiency?

If the cathodic product is separable from the electrolyte and crucible, its mass and composition would give the total electrons required to reduce the given amount of metal. Since the current and duration are known, the current efficiency is simply calculated. However, one would have to wait until the furnace was cool to analyze the product, thus limiting the researcher to one heating/cooling cycle per experiment in the vertical crucible furnace.

Perhaps oxygen evolution could be a better reaction to study. The very fact that oxygen is fugitive can be an advantage. An inlet stream of inert gas would be purged until the oxygen concentration was zero at the outlet. While the current is passed, oxygen evolves from the anode. After a transient period dependent on the flow rate of the inlet gas and the volume of the furnace tube, the concentration of oxygen in the outlet stream achieves a steady state value. Since the applied current is known, the concentration of oxygen can be determined

assuming 100% current efficiency. Deviation from this concentration can be used to infer the current efficiency. One must be cautious in melts containing transition metal oxides as the atmosphere in the headspace of the furnace tube may alter the redox ratio with time as the headspace becomes saturated with oxygen. As the redox values change, so does the chemical solubility of oxygen and possibly even the conduction mechanism of the melt.

CHAPTER 7: CONCLUDING REMARKS

Molten oxide electrolysis is one of four breakthrough technologies that may drastically reduce greenhouse gas emissions associated with steelmaking[7]. Not only would it replace the contemporary blast furnace, a capital intensive structure that is the primary source of carbon dioxide in modern steelmaking, but the byproduct could be pure oxygen gas, a highly valued commodity. Additionally, a molten oxide electrolysis cell would not displace the physical plant already in place with contemporary steel mills; it is simply a new means of generating hot metal. It should be viewed as a green technology because of its environmental benefits and opportunities for the steel industry to generate profit beyond iron derived products.

Molten oxide electrolysis has been considered by NASA for in-situ resource utilization. Oxygen could be generated from the regolith of planets and moons for respiration and propellant, and metals such as iron and silicon could be used for structural and functional materials[8-10]. It has even been considered for the remediation of chemical waste[11].

Though its conception dates back to the beginning of the 20th century[12], only a scant amount of literature has been published on topics related to molten oxide electrolysis. Much stems not from electrowinning metals but from oxygen production for space exploration[8-10]. Unfortunately, the old literature established a bad precedent as only a narrow range of compositions for the electrolyte was considered. Furthermore, the fields of molten silicate science and electrochemistry are both required not only for understanding the behavior of the system under electrolysis conditions, but also for properly constructing experiments to extract information.

The work presented in this thesis aimed to overcome the shortfalls of the previous notions of how molten oxide electrolysis would operate. The system as a whole was approached. Although the initial motivation was to develop the inert anode, this was put aside in favor of understanding how the electrolyte influenced the anodic current. It was believed that the development of an inert anode for a system with poor efficiency was of little benefit, particularly if the inert anode could not function over a range of electrolyte compositions.

It has been concluded that the basicity of the electrolyte should be as high as possible, primarily to influence the oxygen evolution current, but also to reduce the resistivity and maximize the ferric content of the melt. All of these factor into enhancing the efficiency of the molten oxide electrolysis cell.

Iridium has been determined as the best candidate for future development of the inert anode. Rhodium and platinum did not have as high a current density, and rhenium, a refractory metal, completely volatilized under anodic polarization. All the platinum group metals are exceptionally expensive, but if the corrosion and volatility are negligible, the inert anode could always be reclaimed. Iridium offers a unique combination of properties, but its cost and scarcity may be prohibitive unless designs beyond monolithic bodies of pure iridium are pursued.

Despite the rousing enhancements molten oxide electrolysis may offer to a variety of applications as disparate as steel production and space exploration, a functional electrolysis cell has yet to be developed. However, the findings reported in this thesis shed new light. Experiments were constructed to accurately monitor the behavior of electrode materials and determine the influence of the electrolyte composition on the performance of the cell. The approach to the system was unique as were many of the results. A candidate for the inert anode, an absolute necessity for green steelmaking and oxygen generation, was determined. And while speculative, many of the proposed mechanisms were supported by thermodynamic data and observations drawn from other fields.

The implementation of a molten oxide electrolysis cell poses many operational and materials related challenges, especially with regard to the inert anode. Ultimately, these hurdles must be overcome because the sustainability of our environment and the enabling resource of the civilized world are intimately linked. The author's outlook is optimistic that the conclusions drawn from this thesis will be of great benefit for advancing molten oxide electrolysis from a lab-scale novelty to a full-fledged means of green steelmaking and exploration of the cosmos.

APPENDIX A

Table A.1 Components to Construct Furnace Cap (see Figs. 2.1 and 2.2)

Component Description	Supplier	Part Number	Material
Ultra-Torr Fitting, NPT-¼" x ¼" Tube	Swagelok	SS-4-UT-1-4BT	Stainless Steel
Hollow Hex Plug, Male NPT-¼"	Swagelok	SS-4-HP	Stainless Steel
Adapter, NPT-¼" x NPT-¼"	McMaster Carr	48805K36	Stainless Steel
¼" Barbed Fitting x NPT-¼"	McMaster Carr	53505K64	Stainless Steel
6 ¾" Blank Flange	MDC Vacuum	F675000	Stainless Steel
6 ¾" x 5" Flange	MDC Vacuum	F675500	Stainless Steel
Gasket, 6 ¾" Flange	MDC Vacuum	GK-500	Copper
Hex Cap Bolts, 5/16"–24 x 2 ¼"	MDC Vacuum	BA-300	Steel
-425 O-ring	Grainger	1WKX9	Silicone
Cooling Lines, ¼" Diameter	Grainger	3P669	Copper
¼" Barbed Fitting x ¼" Tube	Swagelok	B-4-HC-1-400	Brass

APPENDIX B

Table B.1 Listing of Electrolyte Compositions in Mole Percent (see also Table 2.1)

Figure[87]	Melting Point°C	FeO	Li_2O	CaO	MgO	Al_2O_3	SiO_2	Λ_{melt}
442	1050	-	20.000	46.667	-	-	33.333	0.740
443	932	-	23.451	-	14.903	-	61.646	0.583
449	1026	-	30.904	-	-	8.524	60.572	0.588
449	1033	-	33.333	-	-	-	66.667	0.584
450	975	-	28.357	-	-	4.595	67.047	0.573
453	1026	-	34.337	-	-	7.831	57.831	0.599
598	1320	-	-	30.304	11.244	-	58.452	0.601
598	1379	-	-	50.295	8.397	-	41.308	0.683
598	1357	-	-	27.650	27.858	-	44.493	0.637
598	1350	-	-	34.442	17.799	-	47.759	0.637
630	1335	-	-	59.064	-	33.222	7.713	0.725
682	1205	66.667	-	-	-	-	33.333	0.740
682	1177	72.808	-	-	-	-	27.192	0.778
682	1178	58.122	-	-	-	-	41.878	0.693
696	1083	44.361	-	-	-	9.513	46.126	0.640
864	1203	26.957	-	36.521	-	-	36.522	0.722
864	1208	33.333	-	33.333	-	-	33.334	0.740
869	1070	36.318	-	6.734	-	6.734	50.214	0.632
869	1108	47.515	-	6.872	-	6.872	38.742	0.682
870	1118	35.663	-	26.264	-	5.904	32.169	0.718
870	1125	21.449	-	32.352	-	6.924	39.275	0.679
871	1178	23.626	-	38.187	-	3.669	34.518	0.716
874	1250	53.986	-	27.049	-	5.441	13.524	0.834
875	1215	16.368	-	41.815	-	4.539	37.277	0.698
882	1230	-	-	12.651	15.045	9.634	62.670	0.560
882	1235	-	-	29.294	14.848	9.244	46.613	0.619
899	1222	-	-	11.053	13.989	11.054	63.905	0.555
900	1236	-	-	32.808	8.935	8.258	49.999	0.616
909	1270	-	-	23.101	18.775	9.391	48.733	0.606
916	1234	-	-	33.994	11.991	10.011	44.004	0.632
2246	1295	16.688	-	20.828	20.827	-	41.656	0.662
2652	1310	-	-	38.124	4.733	14.286	42.858	0.634
2652	1330	-	-	28.980	13.877	14.286	42.857	0.622
2654	1430	-	-	41.949	18.041	10.016	29.995	0.686
2661	1420	-	-	43.690	17.235	11.768	27.307	0.693
5451	1330	-	13.333	-	10.000	23.333	53.334	0.572

REFERENCES

[1] "Nucor's Environmentally Friendly Pig Iron" <http://www.nucor.com/enviropages/articles/Environmentally_Friendly_Pig_Iron_Project.htm> Accessed: August 20, 2007

[2] "USGS Mineral Commodity Summaries: Iron and Steel 2007" <http://minerals.usgs.gov/minerals/pubs/commodity/iron_&_steel/festemcs07.pdf> Accessed: November 26, 2007

[3] Y. Kim and E. Worrell, "International Comparison of CO_2 Emission Trends in the Iron and Steel Industry," *Energy Policy*, **30** [10] 827-38 (2002)

[4] "AISI | Steel Industry Reaches New Milestone in Energy Efficiency – Again!" <http://www.steel.org/AM/Template.cfm?Section=2006&TEMPLATE=/CM/ContentDisplay.cfm&CONTENTID=16356> Accessed: August 20, 2007

[5] "USGS Minerals Yearbook: Recycling – Metals 2004" <http://minerals.usgs.gov/minerals/pubs/commodity/recycle/recycmyb04.pdf> Accessed: August 20, 2007

[6] "AISI | AISI Creates Energy Reduction Strategy for Steelmaking" <http://www.steel.org/AM/Template.cfm?Section=2006&TEMPLATE=/CM/ContentDisplay.cfm&CONTENTID=13456> Accessed: August 20, 2007

[7] "AISI | CO_2 Breakthrough Fact Sheets" <http://www.steel.org/AM/Template.cfm?Section=Fact_Sheets2&TEMPLATE=/CM/HTMLDisplay.cfm&CONTENTID=18071> Accessed: August 20, 2007

[8] R.O. Colson and L.A. Haskin, "Producing Oxygen by Silicate Melt Electrolysis", in *Resources of Near-Earth Space*. Edited by J.S. Lewis, M.S. Matthews, and M.L. Guerrieri. U. Arizona Press, 1993, 109-27

[9] D. Khetpal, A.C. Ducret, and D.R. Sadoway, "From Oxygen Generation to Metals Production: In Situ Resource Utilization by Molten Oxide Electrolysis," NASA Conference Publication, 2003-212339 [2002 Microgravity Materials Science Conference] 548-55 (2003)

[10] L.A. Haskin, R.O. Colson, D.J. Lindstrom, R.H. Lewis, and K.W. Semkow, "Electrolytic Smelting of Lunar Rock for Oxygen, Iron, and Silicon", in *The Second Conference on Lunar Bases and Space Activities of the 21st Century: papers from a conference sponsored by Lyndon B. Johnson Space Center and the Lunar and Planetary Institute, Houston, Texas, and held in Houston, Texas, April 5-7, 1988*. Edited by W.W. Mendell. National Aeronautics and Space Administration, Office of Management, Scientific and Technical Information Program, 1992, 411-22

[11] D.R. Sadoway, "New Opportunities for Metals Extraction and Waste Treatment by Electrochemical Processing in Molten Salts," *J. Mater. Res.*, **10** [3] 487-92 (1995)

[12] R.H. Aiken, Process of Making Iron from the Ore, US 816142, 1906

[13] "TRP 9956: Technical Feasibility Study of Steelmaking by Molten Oxide Electrolysis" <http://www.steel.org/AM/Template.cfm?Section=Fact_Sheets2&CONTENTID=18069&TEMPLATE=/CM/ContentDisplay.cfm> Accessed: August 21, 2007

[14] D.R. Sadoway, "Inert Anodes for the Hall-Heroult Cell: The Ultimate Materials Challenge," *JOM*, **53** [5] 34-5 (2001)

[15] A.J. Bard and L.R. Faulkner, *Electrochemical Methods: Fundamentals and Applications*. John Wiley, New York, 2001

[16] A. Carton, C. Rapin, R. Podor, and P. Berthod, "Corrosion of Chromium in Glass Melts," *J. Electrochem. Soc.*, **153** [3] B121-B7 (2006)

[17] J. Di Martino, C. Rapin, P. Berthod, R. Podor, and P. Steinmetz, "Corrosion of Metals and Alloys in Molten Glasses. Part 1: Glass Electrochemical Properties and Pure Metal (Fe, Co, Ni, Cr) Behaviours," *Corros. Sci.*, **46** [8] 1849-64 (2004)

[18] J. Di Martino, C. Rapin, P. Berthod, R. Podor, and P. Steinmetz, "Corrosion of Metals and Alloys in Molten Glasses. Part 2: Nickel and Cobalt High Chromium Superalloys Behaviour and Protection," *Corros. Sci.*, **46** [8] 1865-81 (2004)

[19] A. Littner, B.G. Allemand, M. Francois, and M. Vilasi, "Molten Glass Corrosion Resistance of $Mo_xRu_ySi_z$ Compounds at 1350 Degrees C in an Alkali Borosilicate Glass," *Corros. Sci.*, **48** [6] 1426-36 (2006)

[20] S.K. Sundaram and R.F. Speyer, "Electrochemical Corrosion and Protection of Molybdenum and Molybdenum Disilicide in a Molten Soda-Lime Silicate Glass Environment," *J. Am. Ceram. Soc.*, **79** [7] 1851-6 (1996)

[21] M.W. Medlin, K.D. Sienerth, and H.D. Schreiber, "Electrochemical Determination of Reduction Potentials in Glass-Forming Melts," *J. Non-Cryst. Solids*, **240** [1-3] 193-201 (1998)

[22] O. Claussen and C. Russel, "Thermodynamics of Various Polyvalent Main Group Elements in a Borosilicate Glass Melt," *J. Non-Cryst. Solids*, **209** [3] 292-8 (1997)

[23] J. De Strycker, S. Gerlach, G. von der Gonna, and C. Russel, "Voltammetric Studies of Fe^{2+}/Fe^{3+} Redox Equilibria in Some $Na_2O \cdot CaO \cdot Al_2O_3 \cdot SiO_2$ Liquids," *J. Non-Cryst. Solids*, **272** [2-3] 131-8 (2000)

[24] J. De Strycker, P. Westbroek, and E. Temmerman, "Development of a Platinum Rotating Disc Electrode for Dynamic Electrochemical Measurements in Glass Melts," *J. Non-Cryst. Solids*, **289** [1-3] 106-12 (2001)

[25] J. De Strycker, P. Westbroek, and E. Temmerman, "Electrochemical Behaviour and Detection of Co(II) in Molten Glass by Cyclic and Square Wave Voltammetry," *Electrochemistry Comm.*, **4** [1] 41-6 (2002)

[26] J. De Strycker, P. Westbroek, and E. Temmerman, "Electrochemical Behaviour of Iron in Molten Enamel by Means of Cyclic, Square Wave, and Hydrodynamic Voltammetry," *J. Electroanal. Chem.*, **565** [2] 149-58 (2004)

[27] B. Lafage and P. Taxil, "Analysis of Molten Industrial Silicates by Electrochemical Techniques," *J. Appl. Electrochem.*, **19** [5] 729-35 (1989)

[28] H. Schirmer and C. Russel, "Square-Wave Voltammetry and Impedance Spectroscopy in Iron-Doped Melts of the System $Li_2O/Al_2O_3/SiO_2$," *J. Non-Cryst. Solids*, **352** [38-39] 4069-75 (2006)

[29] K. Takahashi and Y. Miura, "Electrochemical Studies on Diffusion and Redox Behavior of Various Metal Ions in Some Molten Glasses," *J. Non-Cryst. Solids*, **38-39** [2] 527-32 (1980)

[30] J.Y. Tilquin, P. Duveiller, J. Glibert, and P. Claes, "Effect of Basicity on Redox Equilibria in Sodium Silicate Melts: An In-Situ Electrochemical Investigation," *J. Non-Cryst. Solids*, **211** [1-2] 95-104 (1997)

[31] J.Y. Tilquin, J. Glibert, and P. Claes, "Qualitative and Quantitative Electrochemical Studies of Multivalent Elements in Molten Oxide Glasses," *Electrochim. Acta*, **38** [4] 479-86 (1993)

[32] G. von der Gonna and C. Russel, "Voltammetric Studies on Redox Equilibria of Various Polyvalent Elements in $CaO/BaO/Al_2O_3/SiO_2$ Melts," *J. Non-Cryst. Solids*, **288** [1-3] 175-83 (2001)

[33] C.-A.F. Yen, "Electrical Conductivity in the $FeO{\cdot}Fe_2O_3$-Al_2O_3-SiO_2 System". Ph.D. Thesis in Materials Science and Engineering from MIT, 1977

[34] C. Russel and G. Sprachmann, "Electrochemical Methods for Investigations in Molten Glass, Illustrated at Iron-Doped and Arsenic-Doped Soda Lime Silica Glass Melts," *J. Non-Cryst. Solids*, **127** [2] 197-206 (1991)

[35] K. Ueda and S. Doi, "Interdiffusivity of FeO-CaO in FeO-CaO-SiO_2 Melts by Means of Electrochemical Method," *Mater. Trans., JIM*, **59** [2] 164-8 (1995)

[36] J. Vondrak, D. Rohanova, B. Klapste, and J. Velicka, “Voltammetric Measurement of the Pt Electrode Capacity and the Determination of the Polyvalent Ions Diffusion Coefficients in the Glass Melt,” *Ceram.-Silikáty*, **47** [2] 51-5 (2003)

[37] K. Frolov, C. Journeau, P. Piluso, and M. Duclot, “Electrochemical Determination of Oxidic Melt Diffusion Coefficients,” *Intl. J. Thermophys.*, **26** [4] 1181-92 (2005)

[38] G. von der Gonna and C. Russel, “A Square-Wave Voltammetric Study on the Diffusivities of Polyvalent Elements in $CaO/BaO/Al_2O_3/SiO_2$ Glass Melts,” *J. Non-Cryst. Solids*, **306** [3] 263-70 (2002)

[39] R.A. Osteryoung and J.J. O'Dea, “Square Wave Voltammetry”, in *Electroanalytical Chemistry, Vol. 14*. Edited by A.J. Bard. Marcel Dekker, New York, 1986, 209-308

[40] T. Morita, H. Yamashita, and T. Maekawa, "Cr^{6+}/Cr^{3+} Equilibrium in Mixed-Alkali Borate Melts," *Nippon Seramikkusu Kyokai Gakujutsu Ronbunshi-J. Ceram. Soc. Jpn.*, **102** [5] 419-23 (1994)

[41] K. Suzumura, K. Kawamura, and T. Yokokawa, “Voltammetric Studies on the Redox Behavior of Cr, Mn, Cu, Sb and As Ions in Na_2O-B_2O_3 Melts,” *J. Chem. Soc., Faraday Trans.*, **87** [2] 307-12 (1991)

[42] A. Ghosh and T.B. King, “Kinetics of Oxygen Evolution at a Platinum Anode in Lithium Silicate Melts,” *Trans. Met. Soc. AIME*, **245** 145-52 (1969)

[43] J.O.M. Bockris, J.A. Kitchener, and A.E. Davies, “Electric Transport in Liquid Silicates,” *Trans. Faraday Soc.*, **48** 536-48 (1952)

[44] M. Maric, M.P. Brungs, and M. Skyllaskazacos, “Anodic Voltammetric Behavior of a Platinum Electrode in Molten Sodium Disilicate Glass Containing Fe_2O_3,” *J. Non-Cryst. Solids*, **105** [1-2] 7-16 (1988)

[45] J.Y. Tilquin, J. Glibert, and P. Claes, “Anodic Polarization in Molten Silicates,” *J. Non-Cryst. Solids*, **188** [3] 266-74 (1995)

[46] T. Emi, T. Sakuraya, and K. Sanbongi, “Kinetics of Oxygen Electrode Reaction at the Interface of Slag/Metal Boundaries,” *Met.-Slag-Gas React. Processes*, [Pap. Int. Symp.], 87-97 (1975)

[47] J.O.M. Bockris, A.K.N. Reddy, and M. Gamboa-Aldeco, *Modern Electrochemistry, 2A: Fundamentals of Electrodics, 2nd Ed*. Kluwer Academic/Plenum, New York, 2000

[48] H. Suito and M. Ohtani, “Galvanostatic Polarization Measurements on a Solid Platinum-Alkali Silicate Melts,” *Trans. Iron Steel Inst. Jpn.*, **17** [1] 37-45 (1977)

[49] M. Kawakami and K.S. Goto, "Potentiostatic Polarization Measurements on Solid Platinum - Molten PbO-GeO_2, PbO-SiO_2, and Na_2O-SiO_2 Interfaces," *Metall. Trans.*, **4** [4] 1097-101 (1973)

[50] C.B. Alcock and G.W. Hooper, "Thermodynamics of Gaseous Oxides of the Platinum Group Metals," *Proc. R. Soc. Lond., Ser. A, Math. Phys. Sci.*, A254 551-61 (1960)

[51] J.K. Higgins, "Reaction at the Platinum Molten Glass Interface under Alternating-Current Electrolysis Conditions," *Glass Technol.*, **21** [3] 145-55 (1980)

[52] J.K. Higgins, "Anodic Polarization and Electrode-Potentials at Platinum-Electrodes in Molten Silicate, Borate, and Phosphate-Glasses," *Glass Technol.*, **23** [4] 180-6 (1982)

[53] J.K. Higgins, "Studies of Platinum and Molybdenum Electrodes in Molten Silicates, Berates, and Phosphates," *J. Electrochem. Soc.*, **140** [12] 3436-48 (1993)

[54] J.K. Higgins, "Anodic Polarization at Platinum-Electrodes in Molten Silicate Glass," *Glass Technol.*, **23** [2] 90-100 (1982)

[55] Y. Miura and K. Takahashi, "Electrode Reactions of Various Electrically Conducting Materials in Some Molten Glasses," *J. Non-Cryst. Solids*, **38-39** [1] 347-52 (1980)

[56] A. Warczok, G. Riveros, T. Utigard, and M. Artigas, "Electrolysis of Liquid Fayalite Slags," *Can. Metall. Q.*, **44** [4] 563-70 (2005)

[57] *Slag Atlas, 2nd Edition*. Edited by VDEh. Verlag Stahleisen, Dusseldorf, 1995

[58] *Electrochemistry of Glasses and Glass Melts, Including Glass Electrodes*. Edited by H. Bach, F.G.K. Baucke, and D. Krause. Springer-Verlag, Berlin, 2001

[59] Y. Waseda and J.M. Toguri, *The Structure and Properties of Oxide Melts: Application of Basic Science to Metallurgical Processing*. World Scientific, Singapore, 1998

[60] B.O. Mysen, *Structure and Properties of Silicate Melts*. Elsevier, New York, 1988

[61] G. Meszaros, Research Scientist, U.S. Steel, personal communication, 2007

[62] J.H. Park and P.C.H. Rhee, "Ionic Properties of Oxygen in Slag," *J. Non-Cryst. Solids*, **282** [1] 7-14 (2001)

[63] J.A. Duffy, "A Review of Optical Basicity and Its Applications to Oxidic Systems," *Geochim. Cosmochim. Acta*, **57** [16] 3961-70 (1993)

[64] J.A. Duffy, M.D. Ingram, and I.D. Sommerville, "Acid-Base Properties of Molten Oxides and Metallurgical Slags," *J. Chem. Soc., Faraday Trans. 1: Phys. Chem. Condensed Phases*, **74** [6] 1410-19 (1978)

[65] K.W. Semkow and L.A. Haskin, "Concentrations and Behavior of Oxygen and Oxide Ion in Melts of Composition $CaO \cdot MgO \cdot XSiO_2$," *Geochim. Cosmochim. Acta*, **49** [9] 1897-908 (1985)

[66] "Fluke 1550B MegOhmMeter" <http://us.fluke.com/usen/products/specifications.htm?cs_id=32084(FlukeProducts)&category=INSUL(FlukeProducts)> Accessed: November 16, 2007

[67] J.N. Hryn and M.J. Pellin, "A Dynamic Inert Metal Anode," *Light Metals* (Warrendale, Pennsylvania), 377-81 (1999)

[68] T. Akai, J. Nishii, M. Yamashita, and H. Yamanaka, "Chemical Behavior of Platinum-Group Metals in Oxide Glasses," *J. Non-Cryst. Solids*, **222** 304-9 (1997)

[69] P. Dable, M. Allibert, and J.C. Poignet, "Solubility of Platinum and Rhodium in Lime-Alumima-Silica Melts at 1700 K," *J. Am. Ceram. Soc.*, **84** [5] 1097-107 (2001)

[70] G.D. Smith and E. Zysk, "Volume 13, Corrosion → Corrosion of the Noble Metals → Platinum" in ASM Handbooks Online, ASM International (2002) Accessed: August 31, 2007

[71] J.B. Lambert, "Volume 2, Properties and Selection: Nonferrous Alloys and Special-Purpose Materials → Refractory Metals and Alloys" in ASM Handbooks Online, ASM International (2002) Accessed: August 31, 2007

[72] J. Hlaváč, *The Technology of Glass and Ceramics: An Introduction*. Elsevier, New York, 1983

[73] "Engineered Materials Handbook → Traditional Applications for Ceramics → Refractories" in ASM Handbooks Online, ASM International (2002) Accessed: August 31, 2007

[74] *Ceramic Innovations in the 20th Century*. Edited by J.B. Wachtman. American Ceramic Society, Westerville, OH 1999

[75] D.M. Smyth, "Electrical Conductivity of Ceramic Materials", in *Advanced Ceramics*. Edited by S. Saito. Oxford University Press, Oxford, 1988, 147-64

[76] *Fine Ceramics*. Edited by S. Saito. Elsevier, New York, 1988

[77] P.P. Budnikov, *The Technology of Ceramics and Refractories*. Mass. Inst. Tech., Cambridge, 1964

[78] F.V. Tooley, *The Handbook of Glass Manufacture, 3rd Ed., Vol. 1*. Ashlee, New York, 1984

[79] J. Staněk, *Electric Melting of Glass*. Elsevier, New York, 1977

[80] C. Moore and R.I. Marshall, *Steelmaking*. Institute of Metals, London, 1991

[81] F. Baucke, T. Pfeiffer, S. Biedenbender, G. Roeth, and R.D. Werner, Reference Electrode for Electrochemical Determination of Oxygen Pressure in Ionic Melts, EP 94-110689 635718, 1995

[82] E.T. Turkdogan, "Theoretical Concept on Slag-Oxygen Sensors to Measure Oxide Activities Related to FeO, SiO_2, and CaO Contents of Steelmaking Slags," *Ironmaking Steelmaking*, **27** [1] 32-6 (2000)

[83] A. Sirk, Post-Doctoral Associate, personal communication, 2007

[84] S.W. Zhang, H.R. Rezaie, H. Sarpoolaky, and W.E. Lee, "Alumina Dissolution into Silicate Slag," *J. Am. Ceram. Soc.*, **83** [4] 897-903 (2000)

[85] M. Guo, P.T. Jones, S. Parada, E. Boydens, J.V. Dyck, B. Blanpain, and P. Wollants, "Degradation Mechanisms of Magnesia-Chromite Refractories by High-Alumina Stainless Steel Slags under Vacuum Conditions," *J. Eur. Ceram. Soc.*, **26** [16] 3831-43 (2006)

[86] HSC Chemistry, Vers. 5.11, Outokumpu

[87] *Phase Diagrams for Ceramists, Vols. 1-14*. American Ceramic Society, Westerville, OH, 2005

[88] D.D. Macdonald, "On the Existence of Our Metals-Based Civilization I. Phase-Space Analysis," *J. Electrochem. Soc.*, **153** [7] B213-B224 (2006)

[89] Factsage, Vers. 5.5, Thermfact & GTT-Technologies

[90] D.D. Macdonald, Distinguished Professor of Materials Science and Engineering & Director of the Center for Electrochemical Science and Technology, Penn State University, personal communication, 2007

[91] N. Jarrett, W.B. Frank, and R. Keller, "Advances in the Smelting of Aluminum," *Metall. Treatises*, 137-57 (1981)

[92] A.C. Co, "Oxygen Reduction Kinetics and Mechanism in High Temperature Solid Oxide Fuel Cells". Ph.D. Thesis in Chemistry from U. Calgary, 2005

[93] M.T. Simnad, G. Derge, and I. George, "Ionic Nature of Liquid Iron-Silicate Slags," *J. Metals, Trans. AIME*, **200** 1386-90 (1954)

[94] "Miscellaneous Data → Element → Pgm Vapour Press.Pt.Ir" in The PGM Database available online at http://www.platinummetalsreview.com/jmpgm/index.jsp, Johnson Matthey Accessed: November 2, 2007

[95] "Miscellaneous Data → Element → Pgm Vapor Press.Rh.Ru&Os" in The PGM Database available online at http://www.platinummetalsreview.com/jmpgm/index.jsp, Johnson Matthey Accessed: November 2, 2007

[96] "Metals Data → Iridium" in The PGM Database available online at http://www.platinummetalsreview.com/jmpgm/index.jsp, Johnson Matthey Accessed: November 2, 2007

[97] J.O.M. Bockris, J.A. Kitchener, S. Ignatowicz, and J.W. Tomlinson, "Electric Conductance in Liquid Silicates," *Trans. Faraday Soc.*, **48** 75-91 (1952)

[98] L.X. Yang and G.R. Belton, "Iron Redox Equilibria in $CaO-Al_2O_3-SiO_2$ and $MgO-CaO-Al_2O_3-SiO_2$ Slags," *Metall. Mater. Trans., B, Process Metall. Mater. Proc. Sci.*, **29** [4] 837-45 (1998)